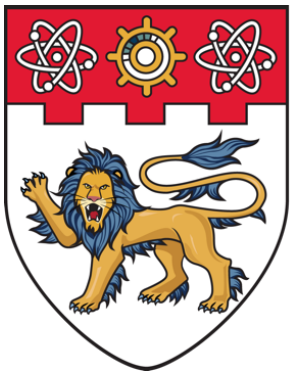

NANYANG TECHNOLOGICAL UNIVERSITY
SINGAPORE

SMART SURFACES USING FUNCTIONAL POLYMER BRUSHES PREPARED VIA ORGANOCATALYZED LIVING RADICAL POLYMERIZATION

SIM XUAN MING

SCHOOL OF CHEMISTRY, CHEMICAL ENGINEERING AND BIOTECHNOLOGY

2023

SMART SURFACES USING FUNCTIONAL POLYMER BRUSHES PREPARED VIA ORGANOCATALYZED LIVING RADICAL POLYMERIZATION

SIM XUAN MING

SCHOOL OF CHEMISTRY, CHEMICAL ENGINEERING AND BIOTECHNOLOGY

A thesis submitted to the Nanyang Technological University in partial fulfilment of the requirement for the degree of Doctor of Philosophy

2023

Statement of Originality

I hereby certify that the work embodied in this thesis is the result of original research done by me except where otherwise stated in this thesis. The thesis work has not been submitted for a degree or professional qualification to any other university or institution. I declare that this thesis is written by myself and is free of plagiarism and of sufficient grammatical clarity to be examined. I confirm that the investigations were conducted in accord with the ethics policies and integrity standards of Nanyang Technological University and that the research data are presented honestly and without prejudice.

13 August 2023

Date

Sim Xuan Ming

Supervisor Declaration Statement

I have reviewed the content and presentation style of this thesis and declare it of sufficient grammatical clarity to be examined. To the best of my knowledge, the thesis is free of plagiarism and the research and writing are those of the candidate's except as acknowledged in the Author Attribution Statement. I confirm that the investigations were conducted in accord with the ethics policies and integrity standards of Nanyang Technological University and that the research data are presented honestly and without prejudice.

13 Aug 2023

. . . . . .
Date

. . . . . .
Professor Atsushi Goto

Authorship Attribution Statement

This thesis contains material from 2 paper(s) published in the following peer-reviewed journal(s) in which I am listed as an author.

Chapter 2 is published as Sim, X. M.; Wang, C.-G.; Liu, X.; Goto, A. Multistimuli Responsive Reversible Cross-Linking–Decross-Linking of Concentrated Polymer Brushes. *ACS Appl. Mater. Interfaces* **2020**, *12*, 28711–28719. DOI: 10.1021/acsami.0c07508.

The contributions of the co-authors are as follows:

- Professor A. Goto provided the initial project.
- I performed all the laboratory work and analysis at the Division of Chemistry and Biological Chemistry, School of Chemistry, Chemical Engineering and Biotechnology, Singapore.
- Dr. C.-G. Wang performed the laboratory work (for C_8F_{17}-alkyne) at the Division of Chemistry and Biological Chemistry, School of Chemistry, Chemical Engineering and Biotechnology, Singapore.
- Professor A. Goto, Dr. C.-G. Wang, and Dr. Xu. Liu provided guidance in the interpretation of the experimental data.
- I and Dr. C.-G. Wang prepared the manuscript drafts. Professor A. Goto edited and finalized the manuscript.

Chapter 3 is published as Sim, X. M.; Chen, C.; Goto, A. Polymer Coupling via Hetero-Disulfide Exchange and Its Applications to Rewritable Polymer Brushes. *ACS Appl. Mater. Interfaces* **2021**, *13*, 24183–24193. DOI: 10.1021/acsami.1c07195.

The contributions of the co-authors are as follows:

- Professor A. Goto provided the initial project.
- I performed all the laboratory work and analysis at the Division of Chemistry and Biological Chemistry, School of Chemistry, Chemical Engineering and Biotechnology, Singapore.

- Professor A. Goto and Dr. C. Chen provided guidance in the interpretation of the experimental data.
- I prepared the manuscript drafts. Professor A. Goto edited and finalized the manuscript.

13 August 2023

. . . . . .

Date

. . . . . .

Sim Xuan Ming

Abstract

This thesis aims to synthesize functional polymer brushes prepared via organocatalyzed living (reversible-deactivation) radical polymerization to create smart surfaces i.e., multi-stimuli responsive reversibly crosslinking/decrosslinking polymer brushes, rewritable polymer brushes on surfaces, and aggregation-induced emission (AIE)-bearing polymer brushes to recognize sizes of external molecules.

Chapter 1 describes the introduction and literature reviews of living radical polymerization and the general approaches for the preparation of well-defined chain-end functionalized polymers via living/controlled polymerization techniques. The concepts of polymer brushes on surfaces, click reaction, Diels–Alder reaction, and aggregation-induced emission, along with the motivation and aim of each chapter are presented.

Chapter 2 presents the synthesis of a reversible crosslinking/decrosslinking polymer brush via the Diels–Alder (DA) and retro-Diels–Alder (rDA) reactions. A bismaleimide crosslinker was used to crosslink poly(furfuryl methacrylate) (PFMA) brushes at 70 °C via the DA reaction to form a crosslinked PFMA brush. Subsequently, the crosslinked PFMA brushes underwent decrosslinking via the rDA reaction at 110 °C, creating a thermal-responsive crosslinked PFMA brush. The surface wettability of the brushes is reversibly tailored by the reversible crosslinking/decrosslinking processes. Disulfide-containing bismaleimide provides another crosslinking/decrosslinking pathway of the crosslinked PFMA brush by reversible oxidation/reduction. Binary and striped patterned brushes were obtained from the disulfide-containing crosslinked PFMA brushes using a photo-induced reduction. Reversibility, multi-stimuli responsiveness and metal-free polymerization approach are appealing aspects in the present work that may find application in adsorption/desorption interfaces, rewritable interfaces, and sensing interfaces.

Chapter 3 presents the facile yet quantitative post-polymerization modification of polymer-iodide (Polymer-I) using $HSCH_2CH_2SH$ to obtain thiol-terminated polymers (Polymer-SH) at room temperature. Polymer-SH is also modified to obtain pyridyl disulfide-terminated polymers (Polymer-SS-Py). The hetero-disulfide exchange between Polymer-SH and Polymer-SS-Py generated a polymer possessing a disulfide bond (Polymer-SS-Polymer). SH-functionalization polymer chains were grafted to a Py-SS-functionalized solid substrate to obtain a polymer disulfide brush layer on the solid surface via the hetero-disulfide exchange (writing). A reducing agent is used to cleave the disulfide bond and the brush polymers are detached from the surface (erasing). Other SH-functionalized polymer chains can then be attached (rewriting) to the solid substrate, demonstrating a rewritable smart surface. Such rewritable smart surfaces may be exploited for rewritable microarray technologies and sensing interfaces.

Chapter 4 presents the syntheses of an AIE-bearing fluorescent polymer brush, i.e., poly(4-(1,2,2-triphenylvinyl)phenyl methacrylate) polymer brush. The polymer brush was fabricated in patterned manners with different graft density domains and served as a conceptually new molecular size analyzer of external molecules in the oligomeric molecular regions. The sizes of external molecules are recognized via changes in the photoemission of the polymer brushes. Different graft density domains selectively capture external molecules of different sizes. Small external molecules can enter the highly-density polymer brush domain on the surface, concomitantly inducing the AIE side groups in the polymer brush chains to aggregate to give a more intense AIE. On the other hand, large external molecules cannot enter (are excluded from) the highly-density polymer brush domain on the surface, giving a relatively less intense AIE. The graft density of the brushes determines the size exclusion (molecular weight) threshold of the external molecules. Using AIE polymer brushes with different graft density domains, the present work distinguished external molecules with molecular weights of 300 and

1000 by the change in the AIE emission of the polymer brushes. The present technique can tune the graft density in a wide range and may be used to analyze a wide range of molecular sizes.

Chapter 5 presents the conclusion of the thesis, offering the novelty, significance, and key achievements highlighted in the preceding chapters, as well as providing insights on potential practical applications that can be exploited in the future.

Acknowledgements

Firstly, I would like to express my deepest gratitude to my supervisor, Professor Atsushi Goto, for this valuable opportunity. Professor Atsushi Goto has been extremely helpful in rendering support and guidance in both tangible and intangible ways; he has always been the most affable, approachable and is always able to offer feasible advice on seemingly intractable problems in my research. I avail myself of this opportunity to thank Professor Atsushi Goto, who gave me free rein as far as my research was concerned and who built my self-confidence and independence by allowing me high levels of autonomy. I am honored to be one of the recipients of Professor Atsushi Goto's philanthropic scholarship and am beholden to Professor Atsushi Goto for the vast knowledge and experience conferred upon me during my years of Ph.D. study and research which will prove useful to my future endeavors.

Secondly, it is my pleasant duty to extend my sincere acknowledgement to my thesis advisory committees, Associate Professor Yeow Kok Lee, Edwin, Assistant Professor Shingo Ito and Associate Professor Naohiko Yoshikai (ex-thesis advisory committee) for providing new perspectives and offering valuable and constructive insights and advice to enhance my critical thinking and problem-solving skills.

Thirdly, I am highly indebted to Dr. Wang Chen-Gang, Dr. Gordon Ge Yicen, Dr. Chen Chen and Dr. Wu Xiaolu for their excellent guidance. Their teachings, patience and understanding are paramount in providing a comprehensive and all-rounded research experience.

Fourthly, I am extending my heartfelt thanks to my respected PhD students, Post Doctorates and colleagues for their constructive advice and continuous support as mentioned below: -

S/N	Post Doctorates	PhD Students	Colleagues
1	Chang Jun Jie	Zheng Yichao	Amerlyn Chong Ming Liing
2	Le Hong Tho		Tay Xiu Ting
3	Han Shuaiyuan		Chew Ye Qiu

A special shoutout to Le Hong Tho, Zheng Yichao and Tay Xiu Ting for their selfless assistance and sincere support, as well as for their generous encouragement and sage advice that buoyed me throughout my PhD studies.

Lastly, to my parents, Shen Guan Ting and Wong Wei Cheng, who have made me who I am today, I love you. I address my sincere appreciation and profound gratitude to my loved ones, Sim Jun Xia, Sim Zhi Yu, Sim Zheng Xian, Rocky Sim, Krystal Shen and Teddy Shen for their unremitting emotional and physical support and understanding throughout all my life and academic endeavors. Finally, I wish to express my deepest recognition to my fellow friends who stood by me through good and bad times.

Thank you for being there and then.

Table of Contents

Chapter 1 Introduction

Radical Polymerization has been a runaway success for the production of synthetic polymers worldwide since its development in the 1910s. At present, conventional radical polymerization amounts annually to about 100 million tons of plastic materials and 4.6 million tons of synthetic rubber.[1] Yet, conventional radical polymerization is difficult to yield well-defined polymers with controlled molecular weight, low dispersity, sophisticated chain architecture, and site-specific functionality.[2]

1.1. Controlled Radical Polymerization

Controlled radical polymerization (CRP), also termed living radical polymerization or reversible-deactivation radical polymerization provides such control, leading to an unprecedented development of well-defined polymeric architectures including but not limited to linear, branched, and crosslinked architectures.[2] CRP has been applied in numerous high-value markets e.g., dispersants, rheology and surface modifiers and so on.[3]

Scheme 1.1. Reversible activation process: general scheme.

Based on the notion of reversible activation of a dormant species (Polymer-X, where X is a capping agent) to the propagating radical (Polymer•), CRP comprises a sufficiently large number of the activation-deactivation cycles for low dispersity ($Đ = M_w/M_n$, where M_w and M_n are the weight- and number-average molecular weights, respectively (**Scheme 1.1**).[4-6]

Several CRP i.e., Nitroxide-mediated Polymerization (NMP)[7,8], Atom Transfer Radical Polymerization (ATRP)[9-12] and Reversible Addition–Fragmentation chain Transfer (RAFT) polymerization,[13-17] employing different capping agents have been developed.

1.1.1. Nitroxide Mediated Polymerization (NMP)

Scheme 1.2. Reversible activation of NMP.

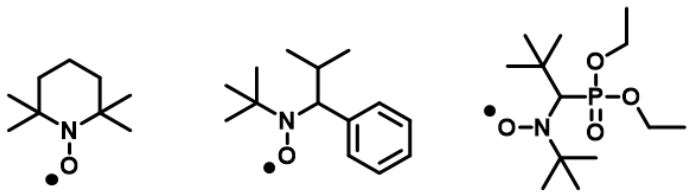

Figure 1.1. Various capping agents of NMP.

NMP was pioneered by Solomon, Rizzardo and Cacioli in 1985.[18] Their pioneering work, first published as a patent, received scant attention until 1993 when Georges et al. reported the synthesis of high molecular weight polystyrene homopolymers with low dispersity via NMP of styrene mediated by 2,2,6,6-tetramethylpiperidinyl-1-oxy (TEMPO) as a capping agent (**Scheme 1.2**).[7]

Subsequently, several new nitroxides such as *N*-*tert*-butyl-*N'*-(1-diethylphosphono-2,2'-dimethylpropyl)nitroxide (SG1)[19,20] and 2,2,5-trimethyl-4-phenyl-3-azahexane-3-oxyl

(TIPNO)[21,22] (**Figure 1.1**) were developed, which extended the range of polymerizable monomers via NMP to include styrene, acrylates, and 1,3-dienes.[23]

1.1.2. Atom Transfer Radical Polymerization (ATRP)

Scheme 1.3. Reversible activation of ATRP.

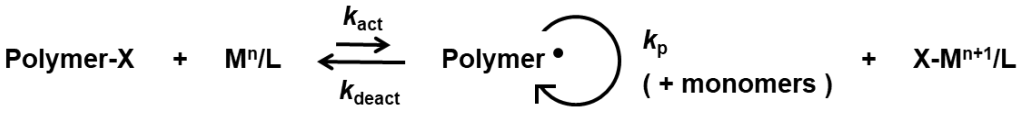

ATRP was independently developed by Sawamoto et al.[24] and Matyjaszewski et al.[9] in 1995. ATRP is a catalytic process mechanistically mediated by a redox-active transition metal complex (M^n) able to homolytically abstract a halogen (X = Cl, Br) atom from Polymer-X to yield Polymer• that induces a large number of activation-deactivation cycles (**Scheme 1.3**).

ATRP enables the polymerization of a range of monomers such as methacrylates, acrylates, styrene, and acrylamides.[10,25,26] Photo-induced ATRP using iridium complexes[27] and more recently, organic photoredox catalysts such as 10-phenylphenothiazine (PTH)[28] has also been established in fabricating well-defined polymer with low dispersity and high chain-end fidelity.

1.1.3. Reversible Addition–Fragmentation chain Transfer (RAFT) polymerization

Scheme 1.4. Reversible activation of RAFT polymerization, where P_n• and P_m• are propagating polymer chains.

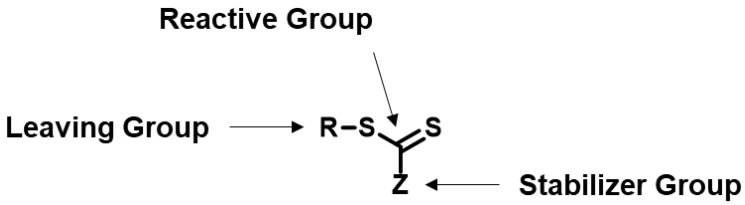

Figure 1.2. RAFT agent: general structure.

RAFT polymerization, first reported in 1998 by Moad, Rizzard and Thang et al. is a CRP technique that relies on a degenerative chain transfer between Polymer• and a RAFT agent that functions as a dormant species (**Scheme 1.4**).[13,29]

Commonly used RAFT agents (R-X, where X = SC(=S)Z) include a good homolytic leaving R-group with respect to the propagating radical, and a capping agent (X = SC(=S)Z) consisting of a stabilizing Z-group such as dithiocarbamates (Z = NR_1R_2), dithioesters (Z = alkyl or aryl), trithiocarbonates (Z = SR_1) and xanthates (Z = OR_1) (**Figure 1.2**). A diverse range of RAFT agents renders RAFT polymerization possible to a vast spectrum of monomer

classes through careful selection of reagents and experimental conditions.[30-33] Accordingly, RAFT polymerization in homogenous, heterogenous and continuous flow reactors was reported.[34,35]

1.1.4. Reversible Complexation Mediated Polymerization (RCMP)

Despite the widespread use of these methodologies, the use of toxic transition metal catalysts in ATRP may limit its practical applicability for biomedical materials.[36-38] Polymers produced by RAFT polymerization can have an odour due to the presence of sulfur.[39] NMP is amenable to a relatively limited range of monomers.[40] Therefore, an alternative method without using metals or sulfur is desired.

Scheme 1.5. Reversible activation of RCMP.

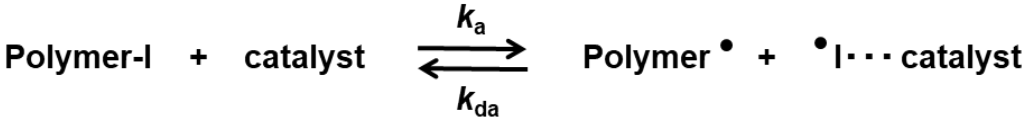

Our research group has pioneered an organocatalyzed controlled radical polymerization, termed reversible complexation mediated polymerization (RCMP), utilizing an alkyl iodide (R−I) initiator and organocatalysts such as quaternary ammonium iodide and tertiary amines.[41] Mechanistically, the coordination of a dormant species (Polymer−I) to the organocatalyst yield a transient Polymer···I···catalyst complex via halogen bonding, which generates Polymer• reversibly (**Scheme 1.5**).

RCMP is a metal-free and sulfur-free technique. RCMP also does not need a special capping agent.[41] The employed catalysts are relatively inexpensive, nontoxic, simple to use and

compatible with a wide scope of functional monomers.[41] Low-molar-mass R–I initiators are generally employed to achieve a sufficiently fast initiation to effectively generate radicals that undergo fast addition to monomer.[42] Rate of polymerization increases in the order of primary < secondary < tertiary R–I initiators and is proportional to the stability of the generated radicals.[42] Hence, sterically hindered tertiary R–I initiators are generally employed because of the weakened carbon–iodine bond and the increased radical stability afforded by hyperconjugation and/or resonance to achieve well defined, low dispersity polymers.[42] Photo-induced RCMP has also been developed to enable the preparation of polymer brushes through photolithography.[43,44]

1.2. Chain-end Functionalized Polymer

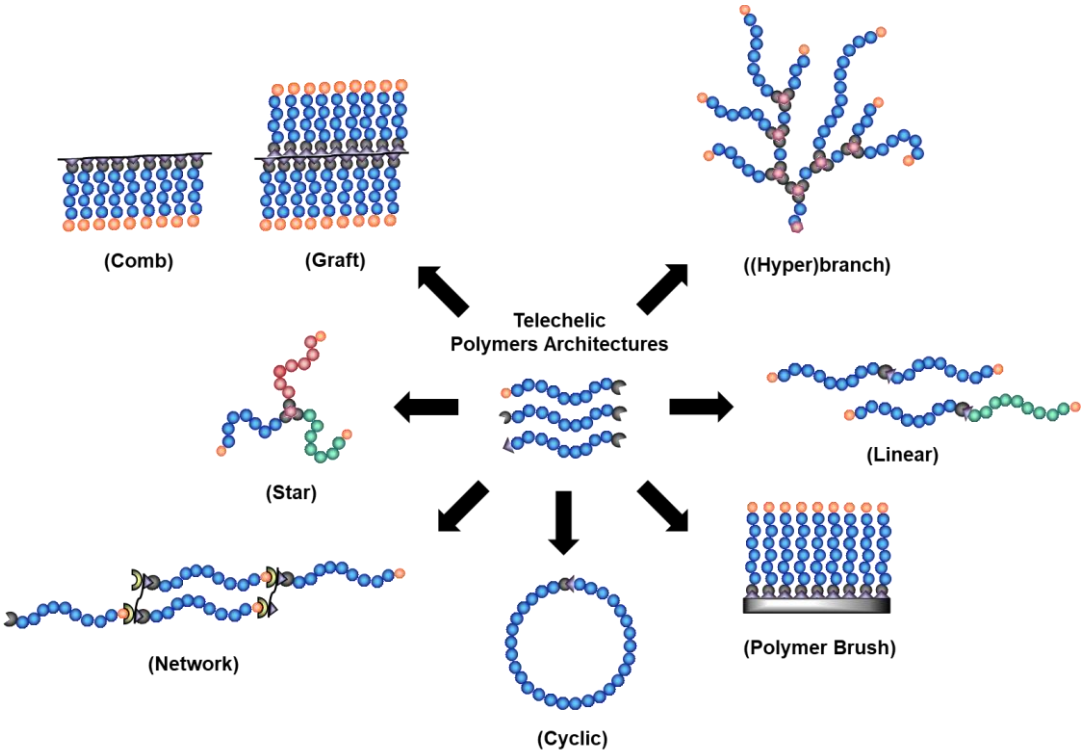

Figure 1.3. Macromolecular architectures prepared via end-functionalized precursors.

Recent advances in CRP offer control over chain-end functionalities, which make the synthesis of various macromolecular architectures e.g., branched polymers, polymer networks, cyclic, and block copolymers possible via radical routes (**Figure 1.3**).[45-48] Chain-end functionalized polymers can be coupled to complementary functionalities on solid substrates to form tethered polymer chains.[49]

Various methods were put forth for the modification of polymeric chain ends synthesized via CRP.[45,50] Functionality can be integrated into the initiating segment of the respective CRP initiators, furnishing an α-functional polymer.[45] Correspondingly, functionality can be incorporated into the terminating segment of the respective CRP initiators, affording an ω-functional polymer (**Scheme 1.6**).[45] Examples of functional groups include OH, CO_2H, NH_2, acetal, alkyne and even complex functionality such as fullerene was reported.[45,51]

Scheme 1.6. Syntheses approaches: general scheme.

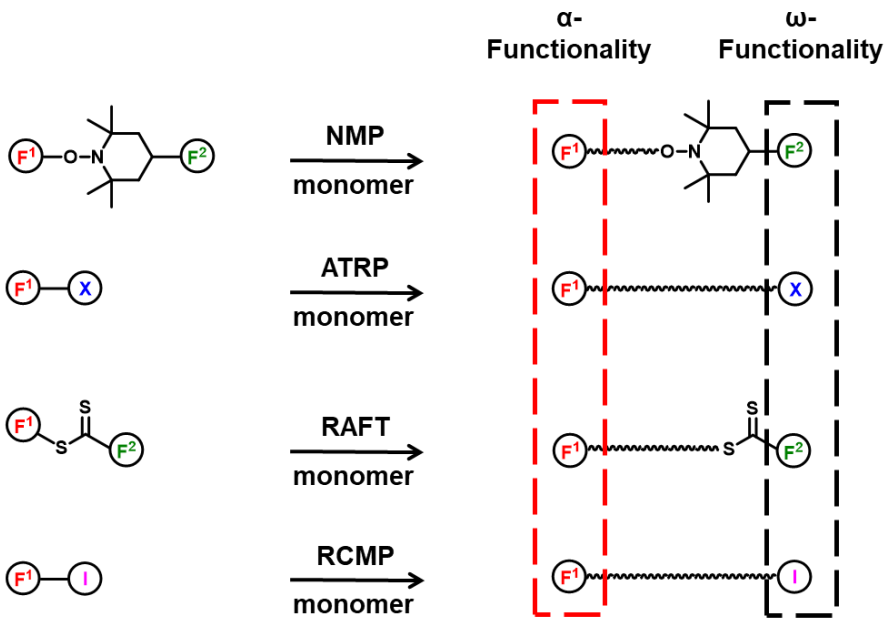

Alternatively, functionalization can be achieved via post-modification of the propagating chain end. Among the CRP methods discussed thus far, polymers synthesized via ATRP and RCMP contain terminal halogens that are highly receptive to various nucleophilic substitutions and chemical reactions for the introduction of other functionalities. An assortment of post-polymerization transformations is reported in the literature.[45,50,52-54] For example, primary amines functionalities were introduced into the terminating segment of the propagating chain end via post-modification, generating amino-end functionalized polymers. Coessens et al. prepared amino end-functionalized poly(methacrylate) and poly(*n*-butyl acrylate) through the reduction of the azido-terminated chain end via the Staudinger process and the subsequent hydrolysis of the resultant iminophosphorane chain end.[55] Monge et al. prepared an amino end-functionalized poly(tert-butyl acrylate)s through the modification of a halogen chain end via the Grabriel reaction.[56] Post-polymerization modification of polymers synthesized via NMP and RAFT processes, likewise, have been extensively studied,[57-59] but have rarely been utilized because of the limited reactivities of nitroxides and dithioesters.[45]

1.3. Polymer Brush

Surface-tethered macromolecules, known as polymer brushes, are a densely ordered arrangement of polymer chains bound to the solid surfaces at one end.[60] Polymer brushes, acting as highly regular ultra-thin films at the interface, are stable in biological environments and are effective in modulating the physical and chemical properties of solid substrates.[61,62] Colloid stabilization, anti-fouling and control of wetting properties are exemplars of the applications of polymer brushes.[63-68]

Polymer chains may be tethered to surfaces either via “grafting-to” or “grafting-from” approaches,[60] each offering its benefits and inherent shortcomings. In the former, pre-

synthesized end-functionalized polymers are attached to the solid surfaces either by physisorption or chemisorption (covalent bonding) (**Figure 1.4b**).[62] However, a grafting-to approach often suffers from low grafting densities and film thickness as steric repulsion between an existing attached polymer layer and the free polymer molecules limits and restricts the diffusion of further chains to reach the reactive sites on the surface as the thickness of the polymer film (i.e., polymer chain length) increases.[60,62] Consequently, these limitations push forward the use of the ‘‘grafting from’’ technique as the preferred method for the fabrication of concentrated polymer brushes.

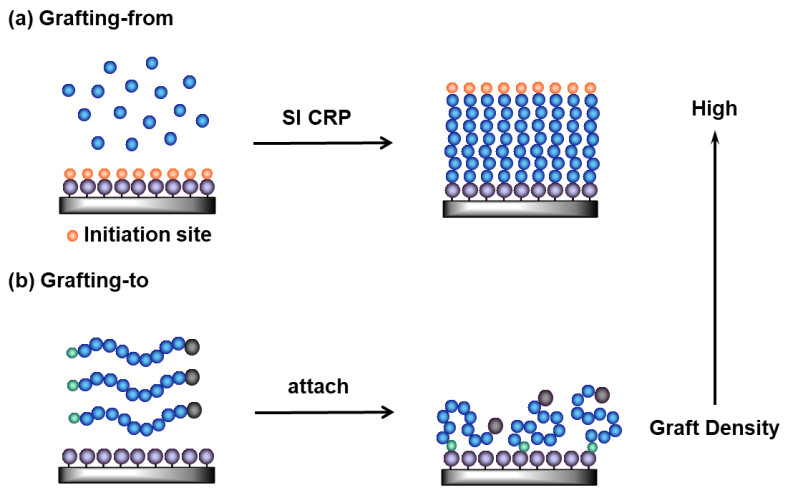

Figure 1.4. Syntheses of polymer brushes via (a) grafting-from and (b) grafting-to approaches.

The grafting-from method termed surface-initiated polymerization uses an immobilized initiator or chain-transfer agent (CTA) layer on the surface whereby successive in situ polymerization generates concentrated polymer brushes with high grafting density that are covalently bonded to the solid substrate (**Figure 1.4a**).[62] Concentrated polymer brushes with high surface occupancy can be easily fabricated using numerous surface-initiated living

polymerization techniques (e.g., ionic polymerization and ring-opening metathesis polymerization) yet, more often than not surface-initiated controlled radical polymerization (SI CRP) has been employed for the facile preparation of polymer brushes on various solid surfaces suchlike metal, silicon and organic substrate[69,70] for its versatility in both aqueous and organic solvents, amenability to various monomer functionalities and simple experimental design.

1.4. Crosslinked Polymer Brush

Crosslinked polymer brushes (polymer brush gels) possess the characteristics of both polymer brushes and gels. Polymer brush gels have shown remarkable stability[71], solvent resistance[72], anti-corrosion[73] and durability[74] and have recently found uses in biomedical applications, tissue engineering and anti-fouling coating.[75]

Brushes can be crosslinked by heating, photoirradiation, pH, irradiation of radioactive rays and so on.[76] The preparation of crosslinking can be principally classified into two general synthetic methods: chemical crosslinking and physical crosslinking approaches.[76]

Chemical crosslinking is a chemical process by which polymer chains are linked together via chemical bonding yielding large and increasingly complex polymer networks. Chemical crosslinking can be further categorized into two synthetic methods: (a) Pre- and (b) post-crosslinking.

Pre-crosslinking leveraging on monomer having multiple polymerizable functionalities e.g., divinylbenzene whereby the successive in situ polymerization generates the corresponding crosslinked polymer brush.[76] Post-crosslinking, on the other hand, involves a chemical reaction between reactive pendant groups in the polymer chains and the crosslinkers, giving the desired

polymer networks.[76] Common crosslinking reagents are bifunctional compounds with reactive groups that selectively binds to the functional groups present in the target macromolecules.[77]

Unlike chemical crosslinking, physical crosslinking is achieved via non-covalent interactions e.g., halogen bonding, ionic interactions, hydrogen bond and so on.[76] Physical crosslinking are labile and can be reversibly dissociated and recombined on various kinds of external stimuli such as heating/cooling.[76]

1.5. Patterned Polymer Brush

Patterned polymer brushes are useful in many application domains where specific dimensions of brush coverage are needed. Patterned polymer brushes have continued to find applications in light-emitting diodes (LEDs), organic electronics, biomaterials and optical materials.[78-80]

The recent development of lithography techniques has enabled the facile fabrication of patterns on surfaces to a few tens of nanometers.[80] Generally, patterned polymer brushes may be prepared either via "bottom-up" or "top-down" approaches:[32] (a) "bottom-up" approach in which the immobilized initiator or CTA monolayers on the surface are pre-patterned prior to surface-initiated polymerization and (b) "top-down" approach in which a homogeneous polymer brush is destructively patterned by lithography-based methods through the application of a locally confined mechanical force or photoirradiation using a photo mask (**Figure 1.5**).[80]

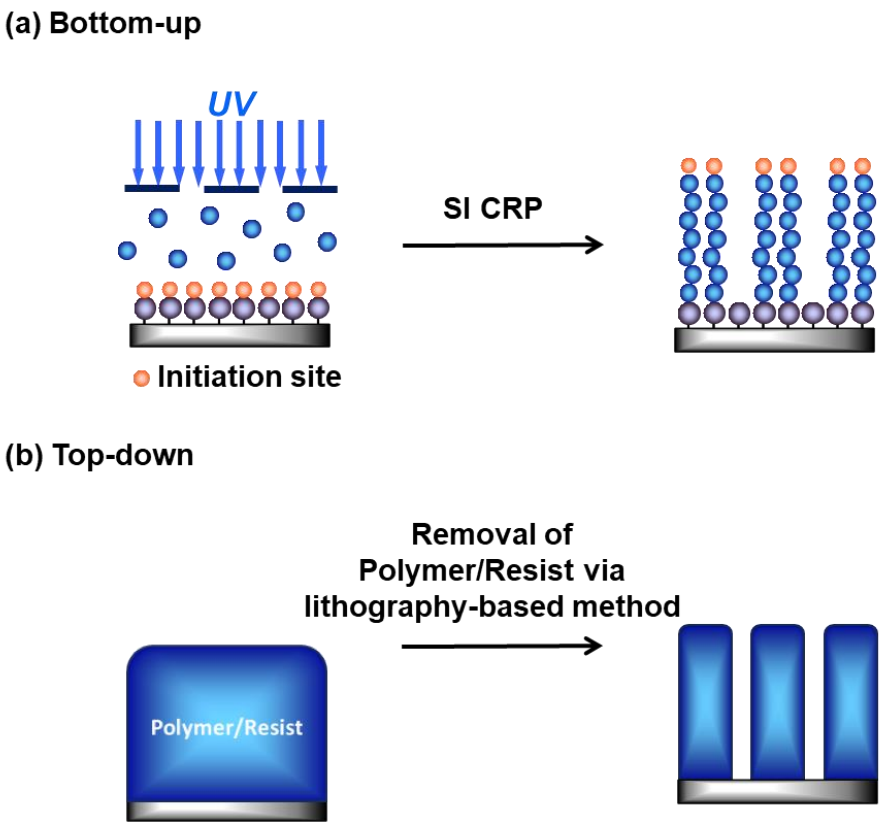

Figure 1.5. Syntheses of patterned polymer brushes via (a) bottom-up and (b) top-down approaches.

Alternatively, post-modification of the chain end can be used to prepare chain-end patterned polymer brushes. Recently, our group has published two papers validating the approach via a photo-selective chain-end modification of Polymer-I to fabricate chain-end patterned polymer brushes on surfaces.[81,82]

1.6. Click Reaction and Diels–Alder Reaction

Polymers bearing "clickable" groups, e.g., azide, alkynyl, vinyl, and thiol, at the chain end or side chains can be connected with other polymers via click reactions, which can modulate the polymer properties such as glass transition temperature (T_g), lower or upper critical solution

temperature (LCST or UCST).[83] Block copolymers obtainable at the chain end connection can also form self-assemblies and undergo morphology transition by varying the temperature.[83]

Diels–Alder (DA) reaction – among the most prevalent members of "click" chemistry – involves a concerted [4 + 2] pericyclic reaction of a diene (e.g., furan and its derivatives) and a dienophile (e.g., maleimide and its derivatives) to yield a cyclohexene adduct (**Scheme 1.7**).[84-88]

Scheme 1.7. Diels–Alder reaction: general scheme.

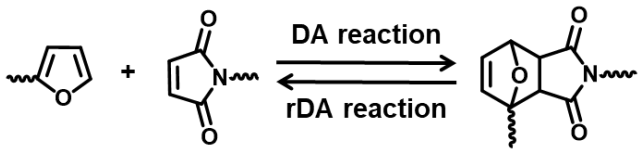

The DA adduct (DA product) can revert to the original reactants by heating (retro-Diels–Alder, rDA).[89,90] The thermal reversibility of the DA and rDA reactions inspired the creation of a thermally responsive surface via reversible crosslinking.[87,91,92]

Reversibly crosslinked polymer brushes can tune the mechanical, biological, and physiochemical properties of the solid surface and may display potential applications for biomedical interface engineering and so on.[93-95] Yet, only a few examples have been reported.

1.7. Aggregation-Induced Emission

Luminescent materials are utilized in molecular sensing, information encoding, biological imaging, and so forth.[96–98] Their emission is often impeded by the aggregation-caused

quenching (ACQ) effect whereby the luminogens partially or completely quenched their fluorescence in the aggregated state.[97] In 2001, Tang et al. pioneered a class of aggregation-induced emission (AIE)-type luminogens (AIEgens) that exhibited enhanced photoemission in the aggregated states, a phenomenon opposite to ACQ.[99–103] The restriction of intramolecular rotation in the aggregates suppresses the thermal decay of the excited luminogens, resulting in enhanced photoemission.

Incorporation of AIEgens into polymer brushes may impart luminescence because these surface-grafted materials can be prepared at sufficiently high grafting density such that the AIEgens will be efficiently aggregated, resulting in enhanced fluorescence signals that endow them with potential applications in sensing.[104,105]

1.8. Aim in Chapter 2

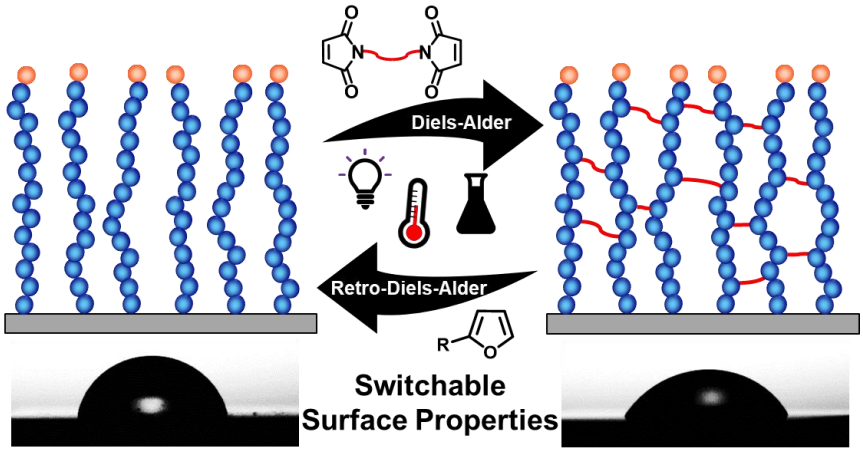

Figure 1.6. Multi-stimuli responsive reversibly crosslinked polymer brushes on solid surfaces.

The motivation to synthesise reversibly crosslinked polymer brushes stems from the desire to harness the characteristics inherent to both polymer brushes and gels. Polymer brushes offer tailored surface properties to the solid substrates, while crosslinked polymer brushes provide stability and durability, as described in the previous section. Reversible crosslinked polymer brushes, which undergo crosslinking and decrosslinking via external stimuli, present an opportunity to create surfaces that can be dynamically modified in terms of their physiochemical properties e.g., wettability, through crosslinking and decrosslinking processes. While reversibly crosslinked polymer brushes are interesting materials, their challenging synthetic approach has led to only a few examples being reported. In Chapter 2, we exploited the intrinsic thermal reversibility of the Diels–Alder (DA) and retro-Diels–Alder (rDA) reactions to create a thermally responsive surface via reversible crosslinking. We prepared a furan-bearing polymer brush through surface-initiated RCMP. The furan moieties of the polymer brush chains can undergo the DA reaction with a bismaleimide crosslinker to generate

crosslinked polymer brushes. The crosslinked polymer brushes were decrosslinked via a rDA reaction at an elevated temperature, reverting the original uniform uncrosslinked polymer brushes. Through judicious selection and incorporation of a suitable functional bismaleimide crosslinker in the reversible DA reaction, we seek to create a multi-stimuli responsive reversible crosslinked polymer brush capable to respond to a wide range of external stimuli. This can potentially introduce additional responsiveness to the polymer brushes beyond thermal stimulus, offering an alternative approach to tailor the surface wettability through crosslinking/decrosslinking processes.

Chapter 2 aims to synthesise reversible crosslinked polymer brushes and multi-stimuli responsive reversible crosslinked polymer brushes. In Chapter 2, we prepared a furan-bearing polymer i.e., poly(furfuryl methacrylate) (PFMA) brushes through surface-initiated RCMP. PFMA polymer brushes were crosslinked with a bismaleimides crosslinker that selectively binds to the furan moieties at 70 °C via the DA reaction yielding a crosslinked PFMA brush. The crosslinked PFMA brush gels underwent decrosslinking via the rDA reaction at 110 °C, yielding a temperature-responsive reversible crosslinking/decrosslinking of PFMA brush gels (**Figure 1.6**).

Additionally, in the present study, we made use of a disulfide-bearing bismaleimide crosslinker to give a disulfide (S−S) bond between the PFMA chains. The S−S bond is cleaved through a thermal or photo stimulus and regenerated via an oxidative stimulus, providing the PFMA brush gels with another pathway for reversible crosslinking/decrosslinking (**Figure 1.6**). The utilization of the DA/rDA reactions and the reversible S–S bond formation/cleavage enabled a multi-stimuli-responsive reversible crosslinking/decrosslinking of PFMA brush gels for tuning the surface wettability (**Figure 1.6**).

1.9. Aim in Chapter 3

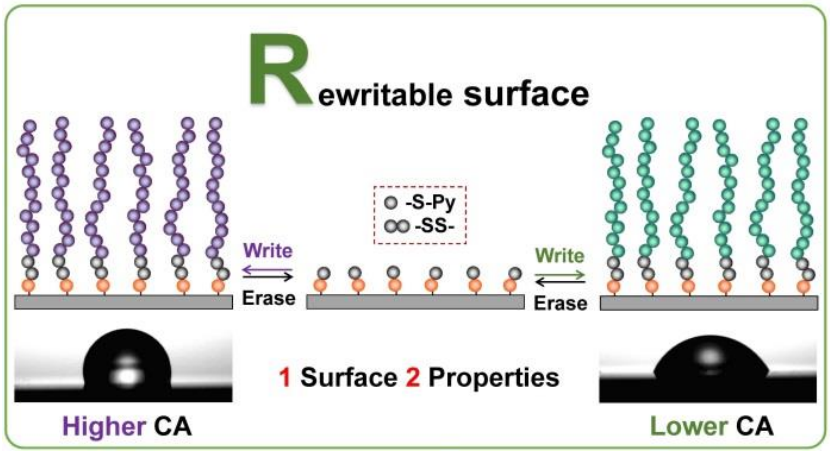

Figure 1.7. Rewritable polymer brushes via hetero-disulfide exchange.

A reaction of poly(acrylates)-bromide (Polymer-Br) with a thiol (R-SH) to generate Polymer-S-R was previously utilized for the chain-end transformation of Polymer-Br prepared by ATRP. However, relatively long reaction times (approximately 12 h) are required for a complete conversion of Polymer-Br to Polymer-S-R.[106]

In Chapter 3, we exploited their method and used polymer-iodide (Polymer-I) as a precursor to synthesize thiol-terminated polymers (Polymer-SH). Polymer-I has a weaker carbon-iodine bond and would be more reactive than Polymer-Br. Hence, the reaction is expected to proceed faster. An interesting application of Polymer-SH that I was motivated to seek in Chapter 3 is to create writable, erasable, and rewritable polymer brushes on surfaces (**Figure 1.7**). The hetero-disulfide exchange of Polymer-SH and a pyridyl disulfide-terminated polymer (Polymer-SS-Py) generates a polymer possessing a disulfide bond (Polymer-SS-Polymer). Polymer-SS-Polymer is cleavable by the treatment with reducing agents such as dithiothreitol (DTT) to regenerate the original Polymer-SH. We may use this reversible

reaction to attach Polymer-SH on the Polymer-SS-Py brush surface to form a Polymer-SS-Polymer brush surface (writing process) and detach Polymer-SH from the Polymer-SS-Polymer brush surface (erasing process).

Chapter 3 aims to synthesize rewritable polymer brush surfaces through polymer coupling via hetero-disulfide exchange (**Figure 1.7**). Our research group previously reported post-polymerization modification of the iodide chain end of Polymer-I (not grafted polymer brush but non-grafted polymer) via substitution reactions using primary amines (R-NH_2) and cysteamine (R-SH) to generate polymers with functional R chain ends (Polymer-NH-R or Polymer-S-R) with R = phenyl, alkyl, $Si(OEt)_3$, SH, OH, and NH_2 groups, for example.[54,81,82]

In Chapter 3, we used a simple substitution reaction and converted Polymer-I to Polymer-SH and attached (grafted) Polymer-SH to the (Py-SS)-immobilized surface via the hetero-disulfide exchange of the surface Py-S-group with Polymer-SH, generating a polymer brush on the surface (writing process) via a disulfide (-SS-) bond. A reductant is used to cleave the -SS- bond detaching the brushes from the surface (erasing process). The hetero-disulfide exchange with another Polymer-SH, subsequently, generates another polymer brush on the surface (rewriting process). Tuning of the surface wettability is achieved during the process of writing, erasing, and rewriting through grafting hydrophilic, hydrophobic, and super-hydrophobic polymers (Polymer-SH) on the surface.

1.10. Aim in Chapter 4

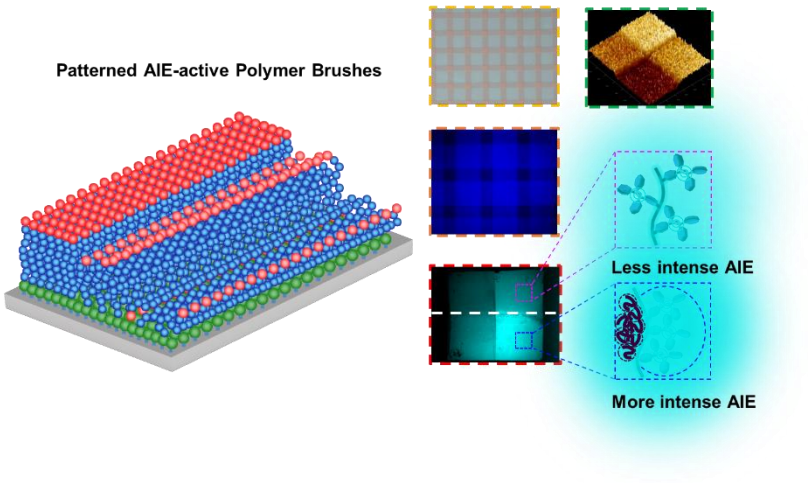

Figure 1.8. Size recognition of external molecules on polymer brushes using aggregation-induced emission.

As mentioned, AIEgens exhibit weak photoemission in the non-aggregated states and strong photoemission in the aggregated states. This property inspired us to create AIEgens-bearing polymer brushes on surfaces with different graft densities so as to modulate their photoemission intensities. The obtained patterned brushes function as a conceptually novel AIE-based molecular size analyzer. The concept is centered on a size exclusion effect influenced by graft density; namely, graft density is the determinant for the size exclusion threshold of the external molecules. High-density brush chains are extended perpendicular to the surface owing to the steric hindrance imposed by the neighboring brush chains. For this reason, external molecules whose sizes exceed the distance between the graft chains are unable to diffuse into the brush layer (size exclusion). On the other hand, the flexibility of low-density brush chains allows external molecules to enter the brush layer. An interesting application of using AIEgens-bearing polymer brushes that I was motivated to seek in Chapter 4 is to

recognize the sizes of external molecules through the size exclusion effect and detect their capture via the changes in the photoemission intensities of the brush. This surface can analyze sizes of external molecules from the emission intensity of the polymer brushes and may serve as a (potentially simpler and faster) alternative to size exclusion chromatography.

Chapter 4 aims to study the size recognition of external molecules on polymer brushes using aggregation-induced emission. Our research group previously developed a technique to obtain patterned polymer brushes via RCMP. Alkyl iodide (R–I) initiators were uniformly immobilized on the surfaces. The surfaces were subsequently subjected to middle/near-UV irradiation (250−385 nm) using photo masks to decompose the initiator in the irradiated areas and fabricate pre-patterns of the initiator in a short time (≤ 10 min).[107]

In Chapter 4, we varied the UV irradiation time to modulate the initiator densities. We obtained pre-patterns of the initiator with different initiator densities using photo masks. AIEgens-bearing polymer brushes comprising different graft densities were fabricated via surface-initiated RCMP of an AIE monomer i.e., 4-(1,2,2-triphenylvinyl)phenyl methacrylate (**Figure 1.8**). We immersed a half area of the obtained patterned brushes in polyethylene glycol (PEG, M_n = 300), while the other half remained non-immersed and measured the disparity in the photoemission intensities between the immersed and non-immersed areas using a fluorescence stereomicroscope. The same experiment was conducted using a higher molecular weight PEG (M_n = 1000).

The smaller-size PEG (M_n = 300) can easily diffuse into the high-density polymer brush layers. PEG is hydrophilic (amphiphilic), whereas the fluorescent side group in the AIE-bearing polymer brush chains are aromatic and hydrophobic. The immiscibility between the hydrophilic PEG and the hydrophobic fluorescent side group in the polymer brush chains leads to the aggregation of the latter in the presence of PEG. This aggregation would result in a more

intense AIE (**Figure 1.8**). As mentioned, larger-size PEG is unable to diffuse into the high-density polymer brush layers, owing to the size exclusion effect, resulting in a less intense AIE (**Figure 1.8**). From the change and no change in the emission intensities, we can recognize the sizes of external molecules.

Reference(s)

(1) Braun, D. *Int. J. Polym. Sci.* **2009**, 1–10.

(2) Matyjaszewski, K.; Spanswick, *J. Mater. Today* **2005**, *8*, 26–33.

(3) Destarac, M. *Polym. Chem.* **2018**, *9*, 4947–4967.

(4) Fukuda, T. *J. Polym. Sci. A. Polym. Chem.* **2004**, *42*, 4743–4755.

(5) Goto, A.; Fukuda, T. *Prog. Polym. Sci.* **2004**, *29*, 329–385.

(6) Fukuda, T.; Goto, A. In *Polymer Science: A Comprehensive Reference*; Matyjaszewski, K., Möller, M., Eds.; Elsevier: Amsterdam, The Netherlands, **2012**, pp. 120–157.

(7) Georges, M. K. et al. *Macromolecules* **1993**, *26*, 2987–2988.

(8) Hawker, C. J. et al. *Chem. Rev.* **2001**, *101*, 3661–3688.

(9) Wang, J.-S.; Matyjaszewski, K. *J. Am. Chem. Soc.* **1995**, *117*, 5614–5615.

(10) Matyjaszewski, K.; Xia, J. *Chem. Rev*. **2001**, *101*, 2921–2990.

(11) Tsarevsky, N. V.; Matyjaszewski, K. *Chem. Rev*. **2007**, *107*, 2270–2299.

(12) Matyjaszewski, K.; Tsarevsky, N. V. *Nat. Chem*. **2009**, *1*, 276.

(13) Chiefari, J. et al. *Macromolecules* **1998**, *31*, 5559–5562.

(14) Moad, G. et al. *Aust. J. Chem*. **2005**, *58*, 379–410.

(15) Lowe, A. B.; McCormick, C. L. *Prog. Polym. Sci*. **2007**, *32*, 283–351.

(16) Barner, L. et al. *Macromol. Rapid Commun*. **2007**, *28*, 539–559.

(17) Vogt, A. P. et al. *Aust. J. Chem*. **2007**, *60*, 396–399.

(18) Nesvadba, P. In *Fundamentals of Controlled/Living Radical Polymerization*; Moad et al. Royal Society of Chemistry, **2013**, pp. 112–167.

(19) Grimaldi, S. et al. *Macromolecules* **2000**, *33*, 1141–1147.

(20) Charleux, B. et al. *Macromolecules* **2005**, *38*, 5485–5492.

(21) Benoit, D. et al. *J. Am. Chem. Soc*. **1999**, *121*, 3904–3920.

(22) Benoit, D. et al. *Macromolecules* **2000**, *33*, 363–370.

(23) Odian, G. Principles of Polymerization. John Wiley & Sons: Hoboken, New Jersey, **2004**, pp. 326.

(24) Kato, M. et al. *Macromolecules* **1995**, *28*, 1721–1723.

(25) Matyjaszewski, K. *Macromolecules* **2012**, *45*, 4015–4039.

(26) Siegwart, D. J. et al. *Prog. Polym. Sci*. **2012**, *37*, 18–37.

(27) Treat, N. J. et al. *J. Am. Chem. Soc*. **2014**, *136*, 16096–16101.

(28) Fors, B. P.; Hawker, C. J. *Angew. Chem. Int. Ed*. **2012**, *51*, 8850–8853.

(29) Braunecker, W. A.; Matyjaszewski, K. *Prog. Polym. Sci.* **2007**, *32*, 93–146.

(30) Schmidt, B. V. K. J. Novel Macromolecular Architectures via a Combination of Cyclodextrin Host/Guest Complexation and RAFT Polymerization. Springer International Publishing, **2014**, pp. 8.

(31) Moad, G. et al. *Aust. J. Chem*. **2006**, *59*, 669–692.

(32) Boyer, C. et al. *J. Polym. Sci. A Polym. Chem*. **2011**, *49*, 551–595.

(33) Keddie, D. J. et al. *Macromolecules* **2012**, *45*, 5321–5342.

(34) Perrier, S.; Takolpuckdee, P. *J. Polym. Sci. A Polym. Chem.* **2005**, *43*, 5347–5393.

(35) Moad, G. In Controlled Radical Polymerization: Mechanisms. American Chemical Society, **2015**, pp. 211–246.

(36) Thakur, V. K. Cellulose-Based Graft Copolymers: Structure and Chemistry. CRC Press: Boca Raton, FL, **2015**, pp. 108.

(37) Puglia, D. et al. Multifunctional Polymeric Nanocomposites Based on Cellulosic Reinforcements. Elsevier: Oxford, United Kingdom, **2016**, pp. 85.

(38) Macchione, M. A. et al. *Polymers* **2018**, *10*, 527.

(39) Nicholson, J. The Chemistry of Polymers. Royal Society of Chemistry: Cambridge, **2017**, pp. 41.

(40) Grubbs, R. B. *Polym. Rev*. **2011**, *51*, 104–137.

(41) Goto, A. et al. *J. Am. Chem. Soc*. **2013**. *135*, 11131−11139.

(42) Lei, L. et al. *Macromolecules* **2014**, *47*, 6610−6618.

(43) Ohtsuki, A. et al. *J. Am. Chem. Soc*. **2015**. *137*, 5610−5617.

(44) Wang, C.-G. et al. *Angew. Chem. Int. Ed*. **2018**, *57*, 13504−13508.

(45) Tasdelen, M. A. et al. *Prog. Polym. Sci*. **2011**, *36*, 455–567.

(46) Yagci, Y.; Tasdelen, M. A. *Prog. Polym. Sci*. **2006**, *31*, 1133–1170.

(47) Jakubowski, W.; Matyjaszewski, K. *Macromol. Symp*. **2006**, *240*, 213–223.

(48) Golas, P. L.; Matyjaszewski, K. *Chem. Soc. Rev.* **2010**, *39*, 1338–1354.

(49) Escorihuela, J. et al. *Adv. Mater. Interfaces* **2015**, *2*, 1500135.

(50) Lunn, D. J. et al. *Polym. Sci. A Polym. Chem*. **2017**, *55*, 2903–2914.

(51) Klaikherd, A. et al. *J. Am. Chem. Soc*. **2009**, *131*, 4830–4838.

(52) Coessens, V.; Matyjaszewski, K. *Macromol. Rapid Commun*. **1999**, *20*, 127–134.

(53) Zhang, H. et al. *Polymers* **2004**, *45*, 1455–1466.

(54) Chen, C. et al. *Macromolecules* **2016**, *49*, 9425–9440.

(55) Coessens, V. et al. *Polym. Bull.* **1998**, *40*, 135–142.

(56) Monge, S. et al. *Macromol. Rapid Commun.* **2007**, *28*, 2272–2276.

(57) Moad, G. et al. *Polymers* **2005**, *46*, 8458–8468.

(58) Postma, A. et al. *Macromolecules* **2006**, *39*, 5293–5306.

(59) Dietrich, M. et al. *Polym. Chem.* **2010**, *1*, 634–644.

(60) Padeste, C.; Neuhaus, S. Functional Polymer Structures. Polymer Micro- and Nanografting. 1st Ed. Elsevier: Oxford, United Kingdom, **2015**, pp. 1–10.

(61) Murray, M.-Y. Comprehensive Biotechnology. 3rd Ed. Elsevier: Amsterdam, **2019**, pp. 477.

(62) Ayres, N. *Polym. Chem.* **2010**, *1*, 769–777.

(63) Zhao, B.; Brittain, W. J. *Prog. Polym. Sci.* **2000**, *25*, 677–710.

(64) Azzaroni, O. *J. Polym. Sci. A Polym. Chem.* **2012**, *50*, 3225–3258.

(65) Dunderdale, G. J. et al. *ACS Appl. Mater. Interfaces* **2015**, *7*, 12220–12229.

(66) Chen, W.-L. et al. *Macromolecules* **2017**, *50*, 4089–4113.

(67) Das, S. et al. *Ind. Eng. Chem. Res.* **2018**, *57*, 2727–2745.

(68) Feng, C.; Huang, X. *Acc. Chem. Res.* **2018**, *51*, 2314–2323.

(69) Baskaran, D. et al. *Angew. Chem. Int. Ed.* **2004**, *43*, 2138–2142.

(70) Zoppe, J. O. et al. *Chem. Rev.* **2017**, *117*, 1105–1318.

(71) Dehghani, E. S. et al. *Eur. Polym. J.* **2018**, *99*, 415–421.

(72) Yang, T. et al. *RSC Adv.* **2018**, *8*, 15740–15753.

(73) Demirci, S. *Polymers* **2018**, *10*, 956.

(74) Yamazawa, Y. et al. *J. Mater. Chem. B.* **2019**, *7*, 4280–4291.

(75) Dehghani, E. S. et al. *Langmuir* **2016**, *32*, 10317–10327.

(76) Oyama, T. In Encyclopedia of Polymeric Nanomaterials: Kobayashi, S.; Müllen, K. Springer: Berlin, Heidelberg, **2014**, pp. 1–11.

(77) Balaguer, M. P. et al. *J. Agric. Food Chem.* **2011**, *59*, 13212–13220.

(78) Shimoda, T. et al. *MRS Bull.* **2003**, *28*, 821–827.

(79) Menard, E. et al. *Chem. Rev.* **2007**, *107*, 1117–1160.

(80) Nie, Z.; Kumacheva, E. *Nat. Mater.* **2008**, *7*, 277–290.

(81) Chen, C. et al. *Chem. Commun.* **2018**, *54*, 13738–13741.

(82) Chen, C. et al. *Polym. Chem.* **2019**, *10*, 5913–5919.

(83) Zhuang, J. et al. *Chem. Soc. Rev.* **2013**, *42*, 7421–7435.

(84) Barner-Kowollik, C. et al. *Angew. Chem. Int. Ed.* **2011**, *50*, 60–62.

(85) Hizal, G. et al. *J. Polym. Sci. A Polym. Chem.* **2011**, *49*, 4103–4120.

(86) Tasdelen, M. A. *Polym Chem.* **2011**, *2*, 2133–2145.

(87) Gandini, A. *Prog. Polym. Sci.* **2013**, *38*, 1–29.

(88) Tasdelen, M. A. et al. *Prog. Polym. Sci*. **2016**, *52*, 19–78.

(89) Carruthers, W. Cycloaddition Reactions in Organic Synthesis. Pergamon Press: Oxford, **1990**.

(90) Gheneim, R. et al. *Macromolecules*. **2002**, *35*, 7246–7253.

(91) Olabisi, O.; Adewale, K. Handbook of Thermoplastics. 2nd Ed. CRC Press, Taylor & Francis Group: Boca Raton, **2016**, pp. 497.

(92) Dirlam, P. T. et al. *Langmuir*. **2010**, *26*, 3942–3948.

(93) Loveless, D. M. et al. *Angew. Chem. Int. Ed.* **2006**, *45*, 7812–7814.

(94) Dehghani, E. S. et al. *Macromolecules* **2017**, *50*, 2495–2503.

(95) Mocny, P.; Klok, H.-A. *Macromolecules* **2020**, *53*, 731–740.

(96) Zhou, J. et al. *Chem. Rev.* **2015**, *115*, 395–465.

(97) Ostroverkhova, O. *Chem. Rev.* **2016**, *116*, 13279–13412.

(98) Gao, R. et al. *Chem. Soc. Rev.* **2021**, *50*, 5564–5589.

(99) Luo, J. et al. *Chem. Commun.* **2001**, 1740–1741.

(100) Hu, R. et al. *Prog. Polym. Sci.* **2020**, *100*, 101176.

(101) Cai, X.; Liu, B. *Angew. Chem., Int. Ed.* **2020**, *59*, 9868–9886.

(102) Fan, M. et al. *Appl. Phys. Rev.* **2021**, *8*, 041328.

(103) Chua, M. H. et al. *ACS Nano* **2023**, *17*, 1845–1878.

(104) Chen, Y. et al. *Biosens. Bioelectron.* **2018**, *111*, 124–130.

(105) Huo, Z. et al. *J. Colloid Interface Sci.* **2021**, *600*, 421–429.

(106) Anastasaki, A. et al. *Polym. Chem.* **2017**, *8*, 689–697.

(107) Wang, C.-G. et al. *ACS Appl. Mater. Interfaces* **2019**, *11*, 14478–14484.

Chapter 2 Reversible Crosslinking-decrosslinking of Multi-stimuli Responsive Concentrated Polymer Brushes

2.1. Abstract: Poly(furfuryl methacrylate) (PFMA) brushes were crosslinked using bismaleimide crosslinkers via the Diels-Alder (DA) reaction at 70 °C, generating crosslinked PFMA brushes (PFMA brush gels). The crosslinked PFMA brushes were decrosslinked at 110 °C via the retro-Diels-Alder (rDA) reaction, offering the temperature-responsive reversible PFMA brush gels. The wettability of the brush was tunable by crosslinking and decrosslinking. The use of a disulfide containing bismaleimide as a crosslinker gave the S-S bond at the crosslinking point. The S-S bond was cleaved upon thermal or photo stimulus and regenerated through oxidative stimulus, offering another reversible decrosslinking/crosslinking pathway of the PFMA brush gel. The use of photo stimulus together with photomasks further offered patterned brushes with the crosslinked and decrosslinked domains. The combination of the DA/rDA reactions and the reversible S-S bond cleavage provided multi-stimuli-responsive brush gels for switching the surface properties in unique manners. The reversible crosslinking, multi-responsiveness, access to patterned structures, and metal-free synthetic procedure are attractive features in the present approach for creating smart functional surfaces.

KEYWORDS: *polymer brush, polymerization, stimuli-responsive crosslinking and decrosslinking, surface patterning, functional surface*

2.2. Introduction

Stimulus-responsive smart surfaces, which change the surface properties triggered by external thermal, acidic/basic, chemical, electrical or optical stimulus, are finding extensive

applications on biomolecular adsorption/desorption, molecular sensing, self-cleaning, and so forth.[1–4] The fabrication of polymer brushes on surfaces is an effective approach for surface modification.[5–9] Stimulus-responsive polymer brushes offer smart surfaces bearing switchable functions and morphologies upon stimulus.[10,11]

Surface-initiated living (or reversible-deactivation) radical polymerization, in which the polymer chains grow from the initiators bound on a solid surface, is a useful method to fabricate well-defined polymer brushes.[6,12–14] Our research group developed an organocatalyzed living radical polymerization, termed reversible complexation mediated polymerization (RCMP), using an alkyl iodide (R−I) as an initiator and an organic molecule as a catalyst.[15–22] Mechanistically, polymer-iodide dormant species (polymer−I) is supposed to coordinate a catalyst (A^+I^-) via a halogen bonding to form a complex (polymer−I···catalyst), which reversibly generates a propagating radical (polymer$^\bullet$) (**Scheme 2.1a**). RCMP is amenable to a wide range of monomers and can afford concentrated polymer brushes with high graft density (σ) and surface occupancy ($\sigma^* \geq 10\%$).[23,24] The high surface occupancy propels the polymer chains towards extension, leading to unique properties such as high elasticity, ultra-low friction, and super-antifouling against proteins and microorganisms.[25] Such properties of concentrated polymer brushes are different from those of semi-diluted or diluted brushes prepared by conventional radical polymerization or grafting-to methods.

Scheme 2.1. (a) Reversible Activation in Reversible Complexation-Mediated Polymerization (RCMP); (b) Reversible Diels-Alder Reaction between Furan and Maleimide Moieties.

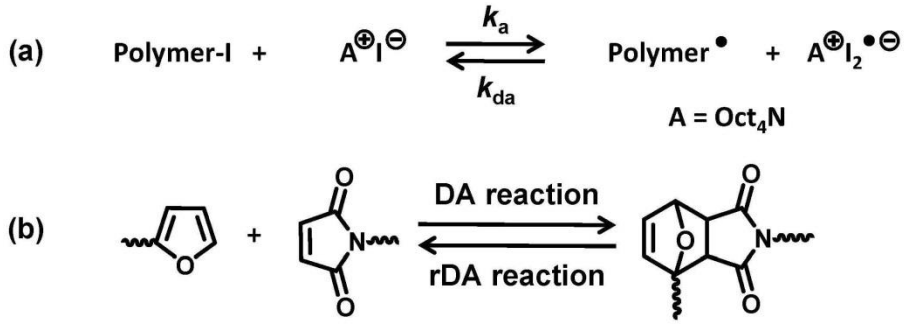

Crosslinked polymer brushes, also known as polymer brush gels, exhibit the properties of both polymer brushes and gels and find unique biomedical applications on interface lubrication, tissue engineering, and anti-fouling coating.[26–31] In comparison to uncrosslinked polymer brushes, polymer brush gels display superior mechanical strength, solvent resistance, anti-corrosion, and durability, exhibiting applications on surface lubrication and interfacial catalysis.[32–37] Reversibly crosslinked polymer brushes, which are crosslinked and decrosslinked via external stimuli, can offer a useful approach for controlling the mechanical, biological, and physicochemical surface properties and may find potential applications on electrolyte materials and biomedical interface engineering.[36,38,39] Whereas reversibly crosslinked polymer brushes are interesting materials, only scarce examples have been reported.

The Diels–Alder (DA) reaction is an effective "click" reaction used in organic synthesis and polymer chemisty.[40–44] In the DA reaction, a [4+2] cycloaddition reaction occurs between an electron-rich conjugated diene (e.g., furan and its derivatives) and an electron-poor alkene (e.g., maleimide and its derivatives) to form a six-membered ring structure (**Scheme 2.1b**). An attractive feature of the DA reaction is its thermal reversibility. Upon heating, the six-

membered ring structure undergoes a retro-Diels-Alder (rDA) reaction to yield the original diene and alkene. The DA and rDA reactions have widely been used for the preparation and functionalization of polymer materials.[41–43,45] Several examples have also been reported to utilize the DA reaction in polymer brush applications.[46–51]

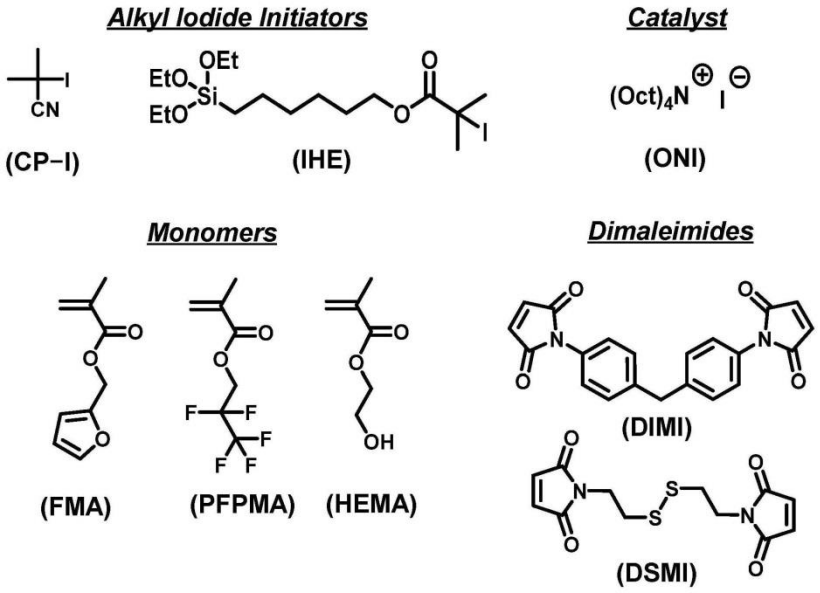

Figure 2.1. Structures of alkyl iodides, a catalyst, monomers, and dimaleimides used in this work.

Scheme 2.2. Schematic Illustration of Synthesis of PFMA Brush and Reversible Crosslinking and Decrosslinking of PFMA Brush via DA and rDA reactions.

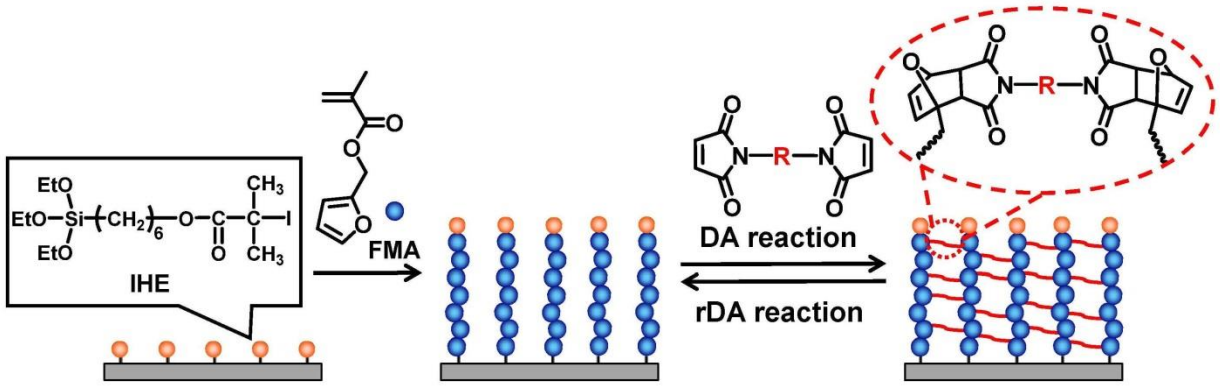

The unique reversibility of the DA and rDA reactions inspired us to create stimuli-responsive surfaces via crosslinking and decrosslinking of polymer brushes. In the present work, we used a furan-containing monomer, i.e., furfuryl methacrylate (FMA, **Figure 2.1**) and prepared concentrated poly(furfuryl methacrylate) (PFMA) brushes by means of surface-initiated RCMP. The PFMA brushes exhibited two different hydrophobicities (contact angles) switched via the crosslinking (DA) (70 °C) and decrosslinking (rDA) (110 °C) reactions with a bismaleimide crosslinker, i.e., 4,4'-bismaleimidodiphenylmethane (DIMI, **Figure 2.1**) (**Scheme 2.2**). The modulation of the hydrophobicity was repeatable over many cycles.

Furthermore, in the present work, we used bis(2-maleimidoethyl) disulfide (DSMI, **Figure 2.1**) as a bismaleimide crosslinker to introduce disulfide (S-S) bridges between the PFMA brush chains. The S-S bonds can be cleaved (dissociate) upon thermal (40 °C) or photo (UV) stimulus and be regenerated through oxidation. Such reversible generation of the S-S bonds provides an alternative method to switch surface properties via crosslinking and decrosslinking. The photo-responsive decrosslinking enabled spatial control in the crosslinked/decrosslinked areas using photomasks, yielding patterned brush surfaces with dual properties. In the present

work, we combined the DA/rDA reactions and the S-S dissociation/regeneration to demonstrate wider applications. The reversible crosslinking, multi-responsiveness, high graft density, and metal-free preparation of the brush gels are attractive features in the present approach for creating functional surfaces.

2.3. Results and Discussion

2.3.1. DA and rDA Reactions of FMA and PFMA in Solution. Before studying the polymer brushes, we studied the DA reaction between the FMA monomer (0.56 M, 20 eq) and DIMI (0.028 M, 1 eq) in DMSO-d_6 at 60 °C (in solution). After 8 h, ^{1}H *NMR* spectroscopy (**Chapter 2.6, Figure S2.2**) showed the disappearance of the *maleimide (DIMI) (a signal* at 7.16 ppm for CH=CH) and the generation of the DA adduct (signals at 6.55, 5.25, and 3.25−3.18 ppm for the [2+4] cycloaddition moiety), suggesting the successful DA reaction between FMA and DIMI. Instead of the FMA monomer, we also studied the PFMA polymer (M_n = 24000 and $Đ$ = 1.35 (PMMA-calibrated GPC values)). PFMA (49.75wt%, monomer unit = 2.8 M, 210 eq) was reacted with DIMI (0.5wt%, 0.013 M, 1 eq) in DMF (49.75wt%) at 70 °C (**Figure 2.2a**). PFMA was converted to the crosslinked PFMA gel after 14 h, confirming the occurrence of the DA crosslinking of PFMA with DIMI. The crosslinked PFMA gel was decrosslinked at 110 °C via a rDA reaction. In the decrosslinking, the FMA monomer was added to trap the released DIMI. The above obtained crosslinked PFMA gel swollen in DMF (50wt%), the FMA monomer (2.5wt%, 25 eq to DIMI), and additional DMF (47.5wt%) were heated at 110 °C for 24 h. After the decrosslinking, the gel was reverted to a liquid state (**Figure 2.2a**). **Figure 2.2b** shows the GPC chromatograms of the original PFMA (black line) and the decrosslinked PFMA (red line), suggesting that a large fraction of the decrosslinked PFMA was reverted to the original PFMA. A shoulder peak was observed on the high-molecular-

weight side for the decrosslinked PFMA and was attributed to the remaining coupled PFMA chains, which were not able to completely be eliminated after heating at 110 °C for 24 h. The M_n value (28000) of the decrosslinked PFMA was relatively close to that (24000) of the original PFMA, suggesting, with respect to the number average, a large fraction of the polymer was reverted to the original PFMA. These results indicate that the DA and rDA reactions between PFMA and DIMI were highly effective for the reversible crosslinking of PFMA. It should be noted that the full (100%) decrosslinking via the rDA reaction was difficult to achieve. For the polymer brushes described below, after the rDA reaction, the brushes might still be partially crosslinked to small degrees. In a strict sense, the reversible crosslinking-decrosslinking via the DA and rDA reactions described below is viewed as nearly reversible crosslinking-decrosslinking.

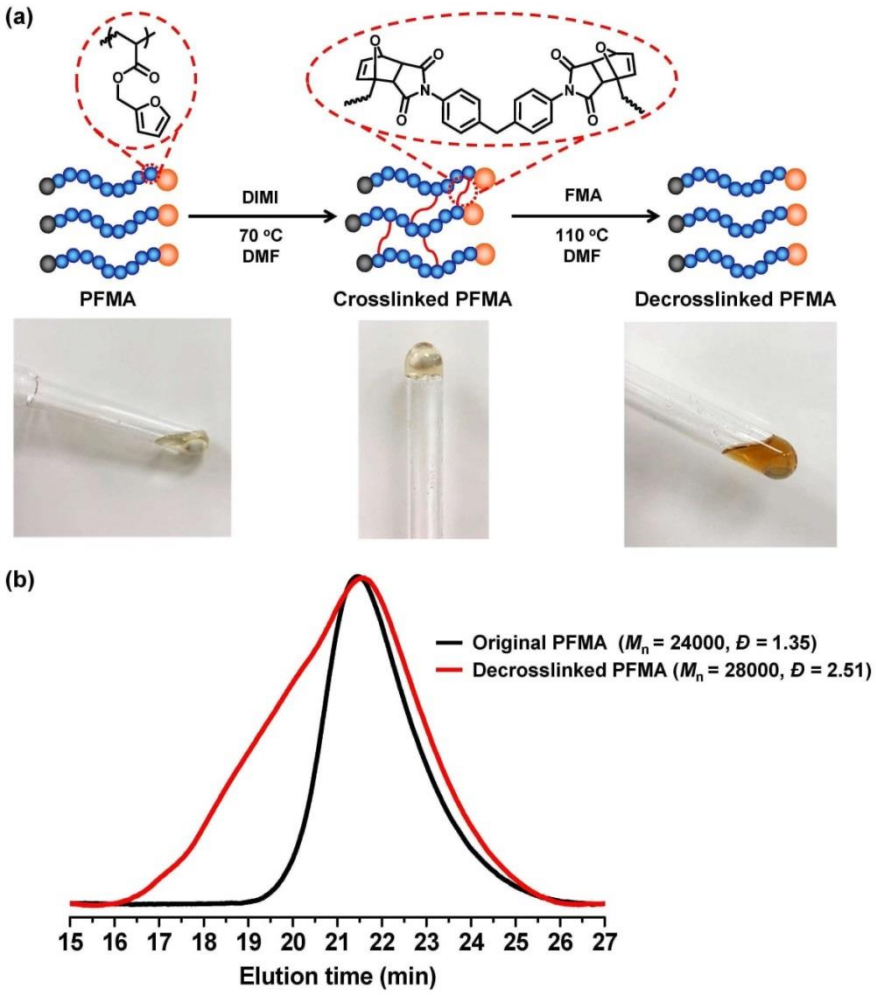

Figure 2.2. (a) Schematic illustration and images of the uncrosslinked, crosslinked, and decrosslinked PFMA. (b) GPC chromatograms of original (uncrosslinked) PFMA (black line) and decrosslinked PFMA (red line).

Table 2.1. Synthesis of Concentrated PFMA and Copolymer Brushes.[a]

Entry	M_1[b]	M_2[c]	$[M_1]_0/[M_2]_0/[CP{-}I]_0/[ONI]_0$ (mM)[d]	Conv of M_1/M_2 (%)[e]	M_n[f] ($M_{n,theo}$[g])	$Đ$[f]	DP[h]	h (nm)	σ (chains/nm^2)	σ^* (%)
1	FMA	−	8000/0/8/64	13/−	21000 (21000)	1.35	130	10	0.35	31
2	FMA	PFPMA	4000/4000/8/64	7/14	21000 (21000)	1.41	105	7	0.25[i]	27
3	FMA	HEMA	4000/4000/8/64	6/9	23000 (11000)	1.49	75	5	0.16	27

[a]Polymerizations were performed at 60 °C for 6 h (entry 1), 8 h (entry 2) and 24 h (entry 3). [b]FMA monomer. [c]Comonomer. [d]The target DP at a full (100%) monomer conversion was 1000. [e]Monomer conversion determined with ^{1}H NMR. [f]PMMA-calibrated THF-GPC values of the free polymers for entries 1 and 2. PMMA-calibrated DMF-GPC value of the free polymer for entry 3. [g]Theoretical M_n calculated with $[M_1]_0$, $[M_2]_0$, $[CP{-}I]_0$, and monomer conversion. [h]Estimated DP values according to DP = ($[monomer]_0/[CP{-}I]_0$)×(monomer conversion). [i]Assuming the density of PFPMA (polymer) is the same as that of PFMA (monomer) (= 1.26 g/mL).

2.3.2. Synthesis of Polymer Brushes. Table 2.1 (entry 1) shows the synthetic result of the homo-PFMA brush. An alkyl iodide initiator IHE (**Figure 2.1**) was immobilized on a silicon-wafer (**Scheme 2.2**). The IHE-immobilized wafer was heated in a mixture of FMA (8000 mM, 1000 eq), CP−I (**Figure 2.1**, 8 mM, 1 eq) as a non-immobilized (free) alkyl iodide initiator, and ONI (**Figure 2.1**, 64 mM, 8 eq) as a catalyst at 60 °C for 6 h, yielding the PFMA brush (**Scheme 2.2**). The free initiator (CP−I) was added because its addition can improve the control over M_n and dispersity, and the M_n and $Đ$ values of the free polymer generated from the free initiator are in good agreement with those of the graft polymer in many cases. The obtained free PFMA had M_n = 21000 and $Đ$ = 1.35 (PMMA-calibrated GPC values). The dry thickness (h) of the PFMA brush was 10 nm. Because the M_n value determined with GPC was not an absolute value, we estimated the DP of the polymer from the $[monomer]_0/[CP{-}I]_0$ ratio multiplied by the monomer conversion (DP = ($[monomer]_0/[CP{-}I]_0$)×(monomer conversion)). Using this DP value and assuming an identical M_n value for the graft and free polymers, the σ and σ* values were calculated to 0.35 chains/nm^2 and 31%, respectively.

Random copolymerizations of FMA with hydrophobic 2,2,3,3,3-pentafluoropropyl methacrylate (PFPMA) and hydrophilic 2-hydroxyethyl methacrylate (HEMA) yielded PFMA-

r-PPFPMA and PFMA-*r*-PHEMA random copolymer brushes with higher hydrophobicity and higher hydrophilicity, respectively (**Table 2.1**, entries 2 and 3), where PPFPMA is poly(2,2,3,3,3-pentafluoropropyl methacrylate) and PHEMA is poly(2-hydroxyethyl methacrylate). The M_n and $Đ$ values of the obtained free copolymers were 21000−23000 and 1.41−1.49, respectively (PMMA-calibrated GPC values). The graft densities were high (σ = 0.16−0.25 chains/nm^2 and σ^* = 27%) and located in a concentrated brush regime ($\sigma^* \geq 10\%$). In the present work, we intentionally stopped the polymerizations at low monomer conversions (6−13%) of FMA to prevent the self-crosslinking reaction of the FMA units.[52]

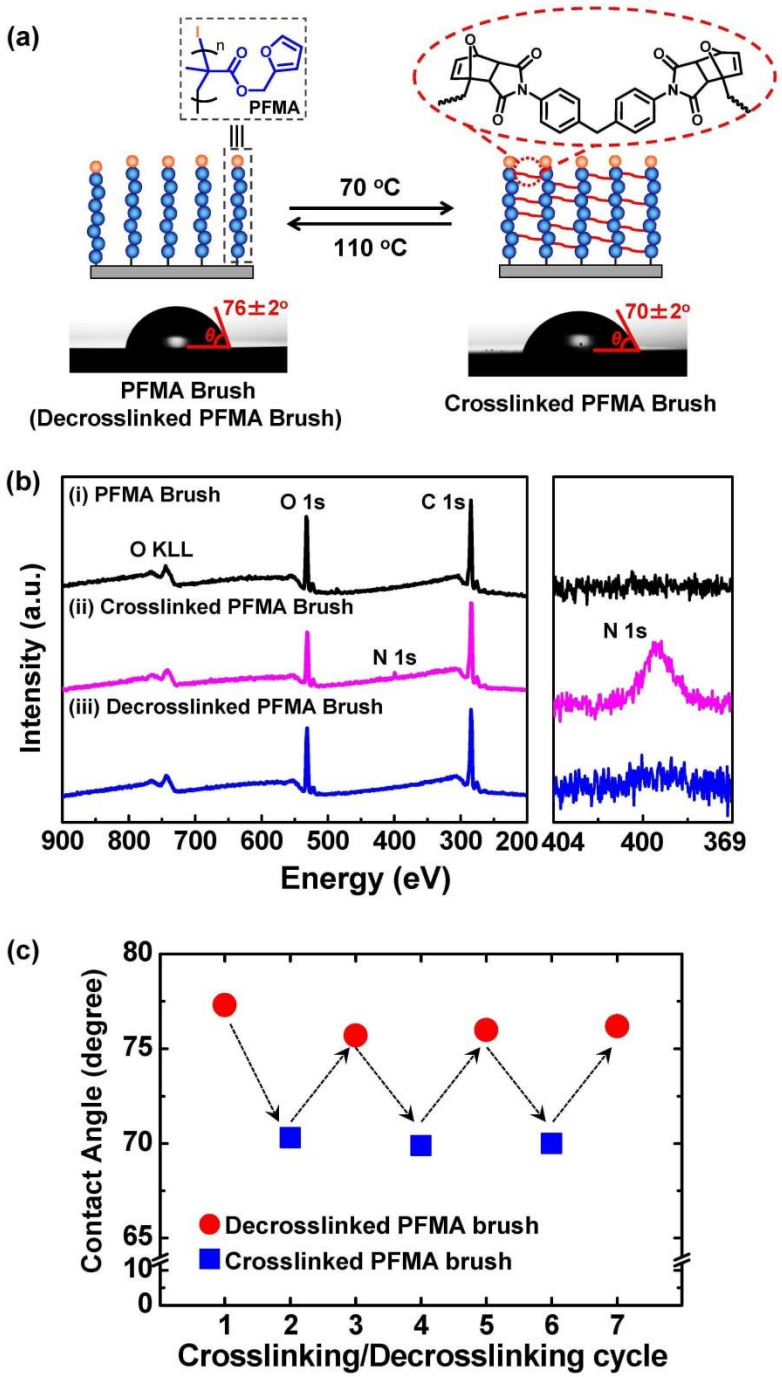

Figure 2.3. (a) Reversible crosslinking (70 °C) and decrosslinking (110 °C) of PFMA brush via DA and rDA reactions using DIMI crosslinker and WCA analysis. The WCA analysis (76°) for PFMA brush (left) is not for the original PFMA brush but for the decrosslinked PFMA brush generated from the crosslinked PFMA brush. (b) XPS survey and high-resolution N 1s spectra of PFMA brushes. (c) Change in WCA by crosslinking and decrosslinking of PFMA brush in a cycled manner.

2.3.3. Reversible Thermal Crosslinking and Decrosslinking of PFMA Brushes. The obtained brushes were crosslinked with DIMI via the DA reaction (**Figure 2.3a**). The wafer with the homo-PFMA brush (**Table 2.1**, entry 1) was immersed in a DMF solution with DIMI (1wt%) and heated at 70 °C to crosslink the brush chains. **Figures 2.3b** shows the X-ray photoelectron spectroscopy (XPS) analysis of the uncrosslinked PFMA and crosslinked PFMA brushes. In the spectrum of the crosslinked PFMA brush, the nitrogen 1s electron signal (399 eV) originated from DIMI was clearly observed, while no nitrogen signal was detected for the uncrosslinked PFMA brush. We also investigated the swelling behaviors of the uncrosslinked and crosslinked PFMA brushes. In the dry state, the uncrosslinked and crosslinked brushes similarly had 10 nm in thickness. If all FMA units are crosslinked through DIMI (crosslinker), the dry thickness should increase from 10 nm (no crosslinking) to 21 nm (full crosslinking), considering the molecular weights of FMA and DIMI. The observed similar thickness (10 ± 1 nm) suggests that the extent of crosslinking is < 9% (= 1 nm/(21–10 nm)). This relatively small value (< 9%) would be reasonable because the studied polymer brush is a concentrated one (σ^* = 31%) and the conformation of the polymer chains (hence the gel thickness) is fixed at even a small extent of crosslinking. After swelling in toluene, the thicknesses of the uncrosslinked and crosslinked brushes increased to 19 nm and 12 nm, respectively. The smaller increase for the crosslinked brush is reasonable, because the brush chains cannot freely extend due to the crosslinking among the chains. Thus, the XPS and swelling analyses show the occurrence of the crosslinking DA reaction between the PFMA brush chains and DIMI.

Table 2.2. Contact Angles (CA) and Apparent Solid-Vapor Surface Tensions (γ_S) of Polymer Brushes.

Entry	Polymer Brush[a]	Uncrosslinked			Crosslinked		
		CA (°) (Water)	CA(°) (CH_2I_2)	γ_S (mJ/m^2)	CA (°) (Water)	CA(°) (CH_2I_2)	γ_S (mJ/m^2)
1	PFMA	77	31	44.4	70	16	50.0
2	PFMA-*r*-PPFPMA	90	53	32.7	85	43	38.2
3	PFMA-*r*-PHEMA	65	34	46.8	54	27	53.6

[a]The synthetic conditions and characterization of the polymer brushes are given in **Table 2.1**.

The static water contact angle (WCA) of the uncrosslinked PFMA brush was 77° and that of the crosslinked PFMA brush was 70° (**Figure 2.3a** and **Table 2.2**, entry 1). In the field of polymer brushes, a decreased WCA by crosslinking was first experimentally observed in poly(acrylamide) brush systems by Schönherr and Spencer[53] and later on in other systems.[27] A brush polymer anchors on the solid substrate at one chain end and can bridge to the liquid-vapor interface at the other chain end during the WCA analysis. Leermakers et al. suggested that the bridging of the polymer chain to the liquid-vapor interface can generate surface pressure (internal pressure inside the brush) and hence increase the WCA.[54] Schönherr and Spencer suggested that the lateral cross-linking of polymer brush chains can decrease the chain conformational freedom, hence inhibiting the bridging effect and decreasing the WCA.[53] We observed the decrease in the WCA after the DA reaction (**Figure 2.3a** and **Table 2.2**, entry 1), which supports the formation of the crosslinked polymer brush. However, it should be noted that DIMI (used as a crosslinker) is slightly more hydrophilic (due to the presence of imide) than PFMA and that the incorporation of DIMI in the brush layer might also contribute to the decrease in the WCA.

Exploiting the reversibility of the DA reaction, the crosslinked PFMA brush was decrosslinked with the addition of the FMA monomer (as a trap of DIMI) at 110 °C via the rDA reaction. After the rDA reaction, the WCA was restored to 76° (**Figure 2.3a**). The XPS

spectrum of the decrosslinked PFMA brush showed no nitrogen 1s signal of DIMI (**Figure 2.3b**), meaning the successful decrosslinking. 2-Furyl methyl ketone, which is a furan derivative obtainable from plant biomass, was also able to use as a trap of DIMI in the rDA reaction. The DA and rDA reactions of PFMA and DIMI were reversible and repeatable for several cycles. **Figure 2.3c** shows that the WCA was consistently sustained at approximate 77° and 70° for the decrosslinked and crosslinked PFMA brushes, respectively.

The PFMA-*r*-PPFPMA and PFMA-*r*-PHEMA brushes are more hydrophobic and more hydrophilic than the PFMA brush and showed the WCA values of 90° and 65°, respectively (**Table 2.2**, entries 2 and 3). After the crosslinking with DIMI, the WCA value decreased to 85° and 54°, respectively (**Table 2.2**, entries 2 and 3). The change in the cosine of WCA tended to increase in the order of the most hydrophobic PFMA-*r*-PPFPMA brush (cos(85°) – cos(90°) = 0.087), pure PFMA brush (cos(70°) – cos(77°) = 0.117), and the most hydrophilic PFMA-*r*-PHEMA brush (cos(54°) – cos(65°) = 0.165). This result suggests that the change in the surface pressure by the crosslinking became more significant in this order. A hydrophobic brush is not much swollen with water and would not effectively bridge to the liquid-vapor interface even in the non-crosslinked state. Therefore, the inhibition of the bridging effect by the crosslinking would be marginal.[27] In contrast, a hydrophilic brush is swollen with water and would effectively bridge to the liquid-vapor interface without the crosslinking. The crosslinking would significantly inhibit the bridging effect and give a smaller WCA. The decrosslinking of the crosslinked PFMA-*r*-PPFPMA and PFMA-*r*-PHEMA brushes was also achieved at 110 °C. These results demonstrate that the DA and rDA reactions are applicable for PFMA-based brushes with different comonomers (different hydrophobicity).

In addition, the apparent solid-vapor surface tension (γ_S) was determined for the uncrosslinked and crosslinked brushes by measuring the contact angles using water and

diiodomethane (CH_2I_2) droplets and by using equations (3)–(5). The results are summarized in **Table 2.2**. The γ_S value increased by the crosslinking from 44.4 mJ/m^2 to 50.0 mJ/m^2 for PFMA, from 32.7 mJ/m^2 to 38.2 mJ/m^2 for PFMA-*r*-PPFPMA, and from 46.8 mJ/m^2 to 53.6 mJ/m^2 for PFMA-*r*-PHEMA. Thus, the surface wettability was able to be modulated via the crosslinking and decrosslinking of the brushes and the use of hydrophilic and hydrophobic comonomers.

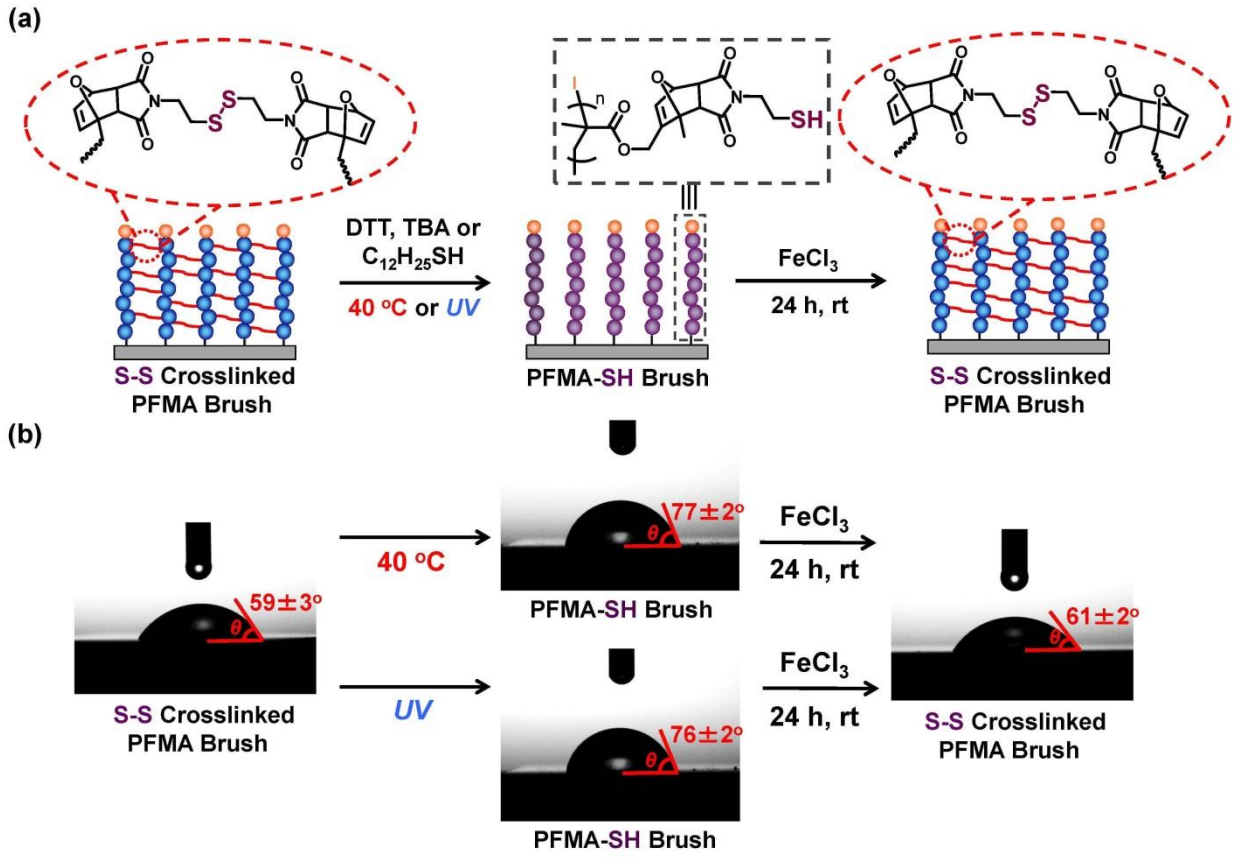

Figure 2.4. (a) S-S crosslinked PFMA brush, decrosslinked PFMA-SH brush generated via thermal- or photo-stimuli, and S-S recrosslinked brush generated via oxidative SH coupling. (b) WCA analysis of S-S crosslinked PFMA brush, decrosslinked PFMA-SH brush, and S-S recrosslinked brush.

2.3.4. Photo- and Redox-Responsive Polymer Brushes. Instead of DIMI, DSMI was used as a functional crosslinker with a disulfide (S-S) bond. The PFMA brush was crosslinked with DSMI via the DA reaction at 70 °C to give a disulfide-bond crosslinked PFMA (S-S crosslinked PFMA) brush (**Figure 2.4a**). The WCA of the S-S crosslinked PFMA brush was 59° (**Figure 2.4b**), which is smaller than that of the DIMI-crosslinked PFMA brush, because the diethyl disulfide group in DSMI is more hydrophilic than the diphenylmethane group in DIMI.

The S-S bond of the S-S crosslinked PFMA brush was able to reversibly be cleaved and regenerated through reduction-oxidation reactions. For the reduction (S-S dissociation), we used a thermal or photo stimulus under a mild condition (40 °C or UV light). The wafer with the S-S crosslinked PFMA brush was heated in a DMF solution of dithiothreitol (DTT, 5wt%) or tributylamine (TBA, 5wt%) as a reducing agent at 40 °C for 10 h (**Figure 2.4b**) or was irradiated in a DMF solution containing a photo-initiator (Irgacure D-2959) and either DTT or TBA under a UV light (365 nm, 900 mW/cm^2) for 30 min (**Figure 2.4b**). The S-S bond was converted to thiols, generating a decrosslinked thiol-functionalized PFMA (PFMA-SH) brush (**Figure 2.4a**). The WCA of the S-S crosslinked PFMA brush was 59°, as mentioned above, and those of the decrosslinked PFMA-SH brushes increased to 76°–77°. The increase in the WCA indicates higher surface pressures and the successful decrosslinking of the brushes via the thermal and photo-irradiation treatments. The use of DTT and TBA gave the same results (the same WCA). The S-S bond was slowly cleaved in the presence of TBA even without the heating at 40 °C or the UV irradiation.[55] At room temperature, the WCA increased from 59° to 63° for 30 min and to 67° for 10 h. The heating and the UV irradiation were effective to accelerate the S-S bond cleavage reaction. Instead of DTT and TBA, 1-dodecanethiol ($C_{12}H_{25}SH$, 25wt%) was also successfully used to decrosslink the S-S crosslinked PFMA brush. The obtained PFMA-SH brushes were able to be crosslinked again via an oxidative coupling of thiols using iron(III) chloride in a mild condition (room temperature for 24 h).

After the re-crosslinking, the WCA was recovered to 61°, which is close to that (59°) of the original S-S crosslinked PFMA brush. This result demonstrates the stimuli-responsive crosslinking and decrosslinking of the S-S crosslinked PFMA brush.

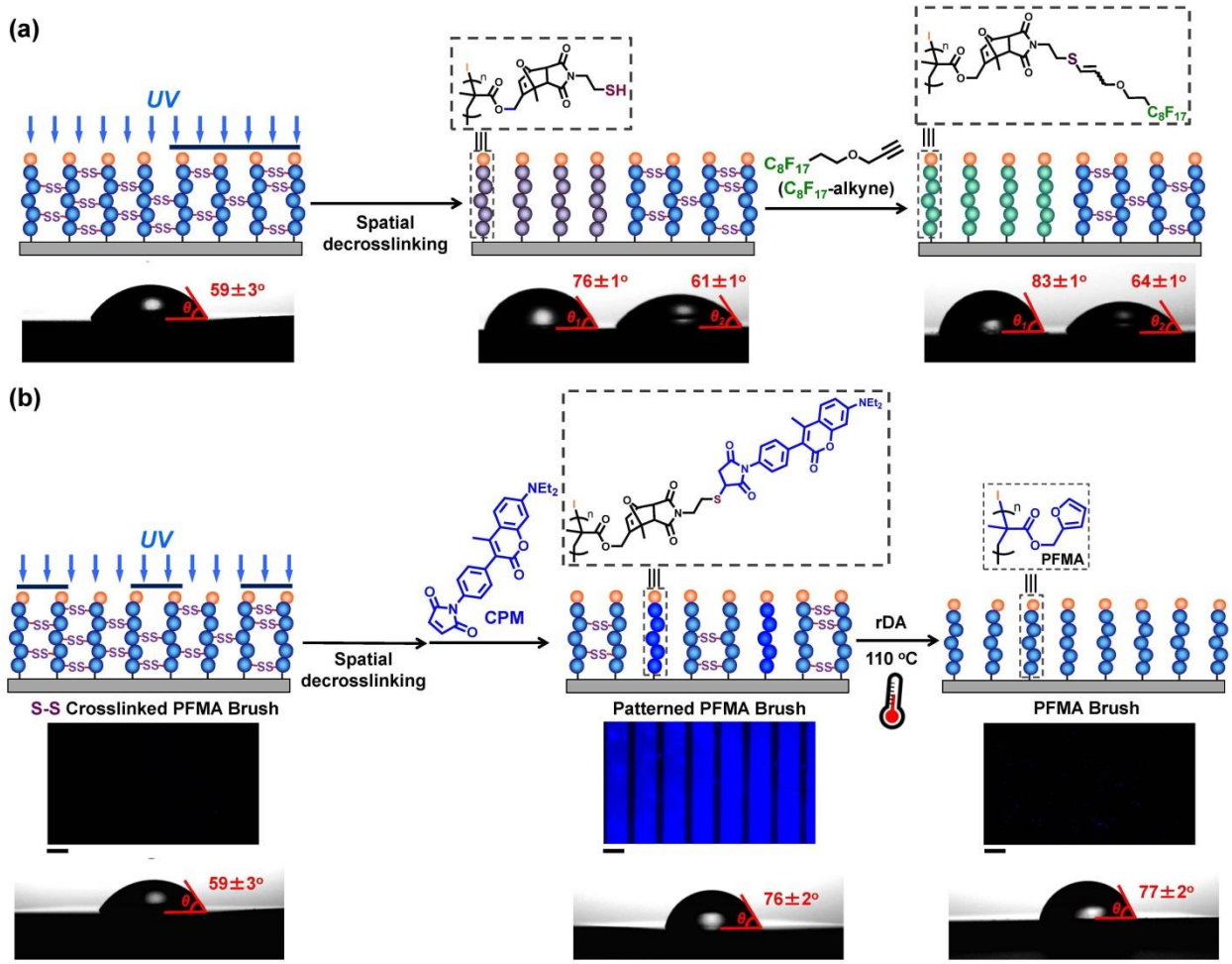

Figure 2.5. (a) Synthesis and WCA analysis of binary patterned PFMA brushes. (b) A sequence of drawing, labeling (CPM fluorophore labeling), and erasure of the brush pattern on a single surface, fluorescence microscope images, and WCA analysis. The scale bar indicates 50 μm in the fluorescence microscope images.

2.3.5. Spatial Control of Functional Polymer Brushes. Spatially controlled (patterned) polymer brushes have attracted attention towards various applications to, e.g., bio-microarrays,

optoelectronic interfaces, and microfluidic systems.[56–62] Exploiting the photo-responsive S-S cleavage demonstrated above, we spatially decrosslink the S-S crosslinked PFMA brush and created a binary patterned brush with crosslinked and decrosslinked areas. A uniform S-S crosslinked PFMA brush was prepared first, subsequently a half of the surface was covered with a clean silicon wafer, and the surface was irradiated by UV light (**Figure 2.5a**). The unmasked area was converted to a decrosslinked PFMA-SH brush, generating a binary patterned brush with two different WCAs of 76° for the decrosslinked PFMA-SH brush and 61° for the unreacted S-S crosslinked PFMA brush (**Figure 2.5a**). The PFMA-SH brush further reacted with 3-((2-perfluorooctyl)ethoxy)propyne (C_8F_{17}-alkyne, **Chapter 2.6**) through a thiol-yne addition. The perfluorinated moiety was successfully attached on the PFMA-SH brushes, increasing the WCA to 83° (**Figure 2.5a**). Thus, the binary patterned surface with tailored hydrophobicity and hydrophilicity was successfully obtained. Meanwhile, the S-S bond slowly dissociated during the WCA analysis due to the light irradiation for imaging, resulting in the slight increase in the WCA from 59° to 64° for the S-S crosslinked PFMA brush area (**Figure 2.5a**).

The spatial decrosslinking also offered a striped patterned PFMA brush. The use of a striped photomask (with masked 25 μm and unmasked 50 μm pitches (**Figure S2.1**)) led to a patterned brush with the S-S crosslinked PFMA and decrosslinked PFMA-SH domains after the UV irradiation (**Figure 2.5b**). The PFMA-SH domain was subsequently labelled with a fluorophore-containing maleimide, 7-diethylamino-3-(4-maleimidophenyl)-4-methylcoumarin (CPM), though thiol–maleimide Michael addition (**Figure 2.5b**). The fluorescence microscopy image shows a clear striped pattern, demonstrating the successful decrosslinking of the S-S crosslinked PFMA brush and subsequent functionalization of the brush in a patterned manner. The obtained patterned brush was heated in a DMF solution of FMA (as a trap of the maleimides) at 110 °C and underwent the rDA reaction (**Figure 2.5b**).

Both the fluorophore (CPM) and the crosslinker (DSMI), which were linked to the PFMA brush, were released from the PFMA brush via the rDA reaction, recovering the original uniform uncrosslinked PFMA brush. (The WCA (77°) of the recovered brush (**Figure 2.5b**) was identical to that (77°) of the original PFMA brush (**Table 2.2**, entry 1).) (In **Figure 2.5b**, the similarity of the WCA (76°) of the patterned PFMA brush to that of the recovered PFMA brush (77°) would be coincidence.) Therefore, combining the DA reaction, the photo-patterning, the SH functionalization, and the rDA reaction, we were able to draw, label, and erase the brush pattern on a single surface, which is a unique feature of the present approach.

2.4. Conclusion

The concentrated PFMA brushes were crosslinked in the presence of the bismaleimide crosslinkers at 70 °C via the DA reaction and decrosslinked at 110 °C via the rDA reaction, offering the temperature-responsive reversible PFMA brush gels. The wettability of the PFMA brush was tuned by the crosslinking and decrosslinking and the use of hydrophobic and hydrophilic comonomers in the PFMA brush. The use of the DSMI crosslinker further provided the S-S bond at the crosslinking point. The S-S bond was cleaved and regenerated by the reductive and oxidative stimuli, respectively, offering another decrosslinking/crosslinking pathway. Using the photo-induced reduction, binary and striped patterned brushes with the crosslinked and decrosslinked domains were obtained. The combination of the DA/rDA reaction with the reversible S-S bond cleavage offered multi-responsive brush gels, e.g., enabling a sequence of drawing, labeling, and erasure of the brush gel pattern on a single surface. The reversible crosslinking, multi-responsiveness, access to patterned structures, and metal-free synthetic procedure are attractive features of the present approach. The applications on the modulation of surface wettability, surface patterning, rewritable surface, and spatial fluorescence labeling demonstrated in the present work may be exploited for

adsorptive/desorptive interfaces, rewritable interfaces, and molecular recognition and sensing interfaces, for example.

2.5. Experimental Section

2.5.1. Preparation of Alkyl Iodide Initiator-Immobilized Silicon Wafer. A silicon wafer (8 mm × 8 mm) was cleaned with acetone (with sonication for 30 min), chloroform (with sonication for 30 min), and isopropanol (with sonication for 30 min). After drying under nitrogen flow, the wafer was placed in an ozone cleaner and radiated for 30 min. The wafer was immersed in a mixture of 6-(2-iodo-2-isobutyryloxy)-hexyltriethoxysilane (IHE, **Figure 2.1**), ethanol, and aqueous ammonia solution (1/89/10 (w/w/w)) at room temperature in a dark condition for one day. The wafer was washed with ethanol, sonicated in ethanol for 30 min, and dried under nitrogen flow to give an IHE-immobilized silicon wafer.

2.5.2. Surface-initiated Polymerization for Chapter 2. The IHE-immobilized silicon wafer was immersed in a mixture of FMA (1.2 g , 7.2 mmol, 8000 mM), 2-iodo-2-methylpropionitrile (CP−I, **Figure 2.1**, 1.4 mg, 7.2 μmol, 8 mM), and tetra-*n*-octylammonium iodide (ONI, **Figure 2.1**, 34 mg, 0.058 mmol, 64 mM) in a Schlenk flask and heated at 60 °C under argon atmosphere with magnetic stirring for 6 h.

2.5.3. General Procedure of Surface-initiated Polymerization. The wafer was inclined to the wall of the Schlenk flask, and the stir bar was located underneath the wafer. After the polymerization, the solution was cooled to room temperature. A portion of the solution was diluted with tetrahydrofuran (THF) and analyzed with gel permeation chromatography (GPC) to determine the molecular weight of the free polymer (non-immobilized polymer formed from CP−I (non-immobilized alkyl iodide initiator)). It should be noted that the GPC was calibrated

with standard poly(methyl methacrylate)s (PMMAs) and that the molecular weights determined with GPC were not absolute values but PMMA-calibrated values. Another portion of the solution was diluted with dimethyl sulfoxide-d_6 (DMSO-d_6) and analyzed with proton nuclear magnetic resonance (^{1}H NMR) to determine the monomer conversion. The wafer was washed with acetone and dried under nitrogen flow. The polymer brush was scratched for the measurement of the height gap between the scratched and unscratched areas by using an atomic force microscope (AFM). The brush thickness presented in all tables was subtracted by the thickness of the IHE initiator layer (2 nm). The number-average molecular weight (M_n), polymer dispersity ($Đ = M_w/M_n$, where M_w is the weight-average molecular weight) of the free polymer, and the dry thickness (h) of the polymer brush are summarized in **Table 2.1**. For determining the thickness of the swollen polymer brush, we placed the wafer with the polymer brush in toluene for 30 min. The wet wafer (the swollen polymer brush covered with the solvent layer) was analyzed with AFM shortly before drying.

2.5.4. General Crosslinking Procedure of PFMA Brushes. The wafer with the PFMA brush was immersed in a mixture of a crosslinker (1wt% for DIMI or 0.5wt% for DSMI) and DMF (1.5 g (99wt%) for DIMI and 1.0 g (99.5wt%) for DSMI) in a Schlenk flask and heated at 70 °C under argon atmosphere with magnetic stirring for 14 h. The wafer was cleaned by ultra-sonication in acetone for 30 min and dried under nitrogen flow.

2.5.5. General Thermal Decrosslinking Procedure of Crosslinked PFMA Brushes. The wafer with the crosslinked PFMA brush was immersed in a mixture of a crosslinker trap (FMA (5wt%) or 2-furyl methyl ketone (5wt%)) and DMF (1.5 g (95wt%) for FMA and 2.0 g (95wt%) for 2-furyl methyl ketone) in a Schlenk flask and heated at 110 °C with magnetic stirring for 14 h. The wafer was cleaned by ultra-sonication in acetone for 30 min and dried under nitrogen flow.

2.5.6. Calculation of Graft Density and Surface Occupancy.[23,24] As mentioned, the M_n values determined with GPC were not absolute values but PMMA-calibrated values. Therefore, in the present work, we estimated the degree of polymerization (DP) of the polymer from the $[monomer]_0/[CP{-}I]_0$ ratio multiplied by the monomer conversion during the polymerization ($DP = ([monomer]_0/[CP{-}I]_0) \times$(monomer conversion)). This estimate is not strictly accurate but would be viewed as a good approximation.

The graft density (σ) of the polymer brush was calculated using the estimated DP value and the dry thickness (h) of the polymer brush according to *equation* (1):

$$\sigma = \frac{h\rho N_A}{\mathrm{DP} \times (\text{molecular weight of monomer})} \quad (1)$$

where ρ is the polymer density, N_A is the Avogadro's number, and DP × (molecular weight of monomer) is the estimated molecular weight of the polymer. The polymer density of PFMA is 1.26 g/mL (in bulk).[63] The polymer density of poly(2-hydroxyethyl methacrylate) (PHEMA) is 1.15 g/mL (in bulk).[64]

The surface occupancy (σ*) of the polymer brush was calculated using the estimated DP value and the *h* value according to *equation* (2):

$$\sigma^* = \frac{h}{0.25\ \text{nm} \times \text{DP}} \times 100\ (\%) \qquad (2)$$

where the length of a repeating unit in the polymer was assumed to be 0.25 nm.

2.5.7. Calculation of Surface Free Energy.[65,66] The surface energy (solid-vapor surface tension) (γ_S) of the polymer brush was obtained by measuring the water and diiodomethane contact angles and by using Owens-Wendt (extended Fowkes') *equations (3)–(5)*:

$$(1 + \cos\theta)\gamma_L = 2\sqrt{\gamma_S^d \gamma_L^d} + 2\sqrt{\gamma_S^p \gamma_L^p} \qquad (3)$$

$$\gamma_L = \gamma_L^d + \gamma_L^p \qquad (4)$$

$$\gamma_S = \gamma_S^d + \gamma_S^p \qquad (5)$$

where θ is the contact angle, γ_L is the liquid-vapor surface tension, γ_L^d and γ_L^p are the liquid-vapor surface tensions of the dispersive and polar components, respectively, and γ_S^d and γ_S^p are the solid-vapor surface tensions of the dispersive and polar components, respectively. The surface tension values of the liquids used for calculation were γ_L^d(water) = 21.8 mJ/m^2, γ_L^p(water) = 51.0 mJ/m^2, γ_L^d(diiodomethane) = 48.5 mJ/m^2, and γ_L^p(diiodomethane) = 2.3 mJ/m^2. Equation (3) is valid when there is no surface pressure. In the presence of surface pressure, the obtained γ_S value will be an apparent value.

2.6. Appendix

2.6.1. Materials and Instrument

2.6.1.1. Materials. Furfuryl methacrylate (FMA) (97%, Sigma-Aldrich, USA), 2-hydroxyethyl methacrylate (HEMA) (>95%, Tokyo Chemical Industry (TCI), Japan), 2,2,3,3,3-pentafluoropropyl methacrylate (PFPMA) (98%, TCI), 2-iodo-2-methylpropionitrile (CP−I) (>95%, TCI), tetra-*n*-octylammonium iodide (ONI) (>98%, TCI), 4,4'-bismaleimidodiphenylmethane (DIMI) (>96%, TCI), bis(2-maleimidoethyl) disulfide (DSMI) (>98%, TCI), 2-furyl methyl ketone (FMK) (>99% Sigma-Aldrich), DL-dithiothreitol (DTT) (>97%, Sigma-Aldrich), 1-dodecanethiol ($C_{12}H_{25}SH$) (>95%, TCI), tributylamine (TBA) (>98%, TCI), 2-hydroxy-4'-(2-hydroxyethoxy)-2-methylpropiophenone (Irgacure D-2959) (98%, Sigma-Aldrich), iron(III) chloride ($FeCl_3$) (>97%, Sigma-Aldrich), 7-diethylamino-3-(4-maleimidophenyl)-4-methylcoumarin (CPM) (>95%, Sigma-Aldrich), propargyl bromide (>97%, TCI), 1*H*,1*H*,2*H*,2*H*-heptadecafluoro-1-decanol (>98%, TCI), sodium hydroxide (99%, VWR Chemicals, USA), *α,α,α*-trifluorotoluene (99%, Sigma-Aldrich), isopropanol (>99.5%, TCI), ammonia solution (28% in water, TCI), acetone (≥99.5%, Fisher Scientific, USA), chloroform (>99.2%, VWR Chemicals), ethanol (≥99.5%, absolute, Fisher Scientific), tetrahydrofuran (THF) (>99.5%, Kanto Chemical, Japan), dichloromethane (99.8%, Fisher Scientific), hexane (>99%, International Scientific, Singapore), diethyl ether (>99.7%, International Scientific), *N*,*N*-dimethylformamide (DMF) (for reaction, anhydrous, >99.8%, Sigma-Aldrich), DMF (for GPC analysis, >99.5%, Kanto Chemical), and toluene (99.8%, Tedia, USA) were used as received. A silicon wafer (produced by Czochralski process, thickness: 525 ± 25 μm) was purchased from Matsuzaki Seisakusho (Japan). 6-(2-Iodo-2-isobutyryloxy)hexyltriethoxysilane (IHE) (>95%) was provided through the courtesy of Godo Shigen Co., Ltd. (Japan). The glass photomasks (Hunan Omnisun Information Material, China)

are polished on both sides with a patterned low-reflective chrome film on one side. **Figure S2.1** shows the photomask used in this work.

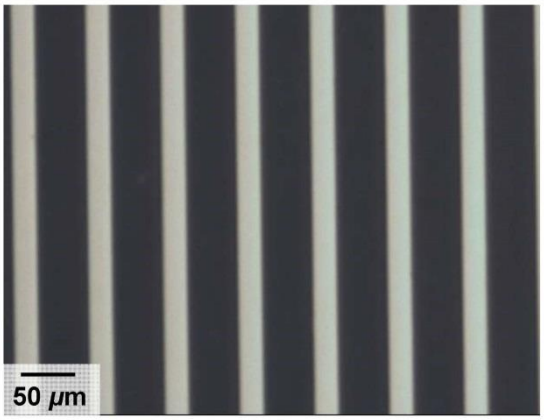

Figure S2.1. Optical microscope image of the photomask used in this work. The dark area is unmasked and the bright area is masked.

2.6.1.2. GPC. The GPC analysis with THF as an eluent was performed on a Shimadzu (Kyoto, Japan) LC-2030C Plus liquid chromatograph equipped with a Shodex (Tokyo, Japan) LF-804 mixed gel column (300 × 8.0 mm; bead size = 6 μm; pore size = 3000 Å) and a Shodex KF-804L mixed gel column (300 × 8.0 mm; bead size = 7 μm; pore size = 1500 Å). The GPC analysis using DMF as an eluent was performed on a Shodex (Tokyo, Japan) GPC-101 liquid chromatograph equipped with two Shodex KF-804L mixed gel columns. The flow rate was 1.0 mL/min (THF) or 0.8 mL/min (DMF) (40 °C for both THF and DMF). The DMF eluent contained LiBr (10 mM). Sample detection and quantification were conducted using a Shimadzu refractive index detector (RID-20A) for THF-GPC and a Shodex differential refractometer RI-101 for DMF-GPC. The column system was calibrated with standard poly(methyl methacrylate)s (PMMAs) in the THF and DMF systems.

2.6.1.3. NMR. The ^{1}H NMR spectra were recorded on a Bruker (Germany) BBFO400 spectrometer (400 MHz) or a Bruker AV300 spectrometer (300 MHz) at ambient temperature. ^{19}F NMR spectra were recorded on a Bruker AV300 spectrometer (282 MHz) at ambient temperature. Chloroform-*d* ($CDCl_3$, Cambridge Isotope Laboratories, USA) and dimethyl sulfoxide-d_6 (DMSO-d_6, Cambridge Isotope Laboratories, USA) were used as NMR solvents, and the chemical shift was calibrated using the residual undeuterated solvent as the internal standard for the ^{1}H NMR analysis. α,α,α-Trifluorotoluene was added as a reference standard for the ^{19}F NMR analysis. The monomer conversion was determined with ^{1}H NMR.

2.6.1.4. UV-LED Light. The UV light source was a Hamamatsu Photonics (Japan) UV-LED light (365 (± 10) nm wavelength, model: C11924-101). The light energy (mW/cm^2) was measured with a Coherent (USA) laser power meter (FieldMate).

2.6.1.5. UV-Ozone Cleaner. The cleaning of the silicon wafers was conducted with a digital UV-ozone cleaner (PSD Pro Series, Novascan Technologies, Germany).

2.6.1.6. Contact Angle Measurement. The water-contact angle analysis of the polymer brushes was carried out with a DM-701 contact angle meter (Kyowa Interface Science, Japan).

2.6.1.7. AFM. The brush thickness was determined with an atomic force microscope (AFM) (Probe Station AFM5000II, Hitachi High-Technologies, Japan) using a cantilever PRC-DF40P.

2.6.1.8. XPS. The X-ray photoelectron spectroscopy (XPS) analysis was carried out with a Phoibos 100 spectrometer and a monochromatic Mg X-ray radiation source (SPECS, Germany).

2.6.1.9. Confocal Fluorescence Microscopy. The fluorescence images were taken with Zeiss Observer Z1 (Germany) using the filter set 38 under autoexposure.

2.6.2. DA and rDA Reactions of FMA and PFMA in Solution

2.6.2.1. Model Reaction of FMA and DIMI. A mixture of FMA (0.093 g, 0.56 mmol, 20 eq), DIMI (0.010 g, 0.028 mmol, 1 eq), and DMSO-d_6 (1.0 g) was heated in a Schlenk flask at 70 °C under argon atmosphere for 8 h (**Figure S2.2**).

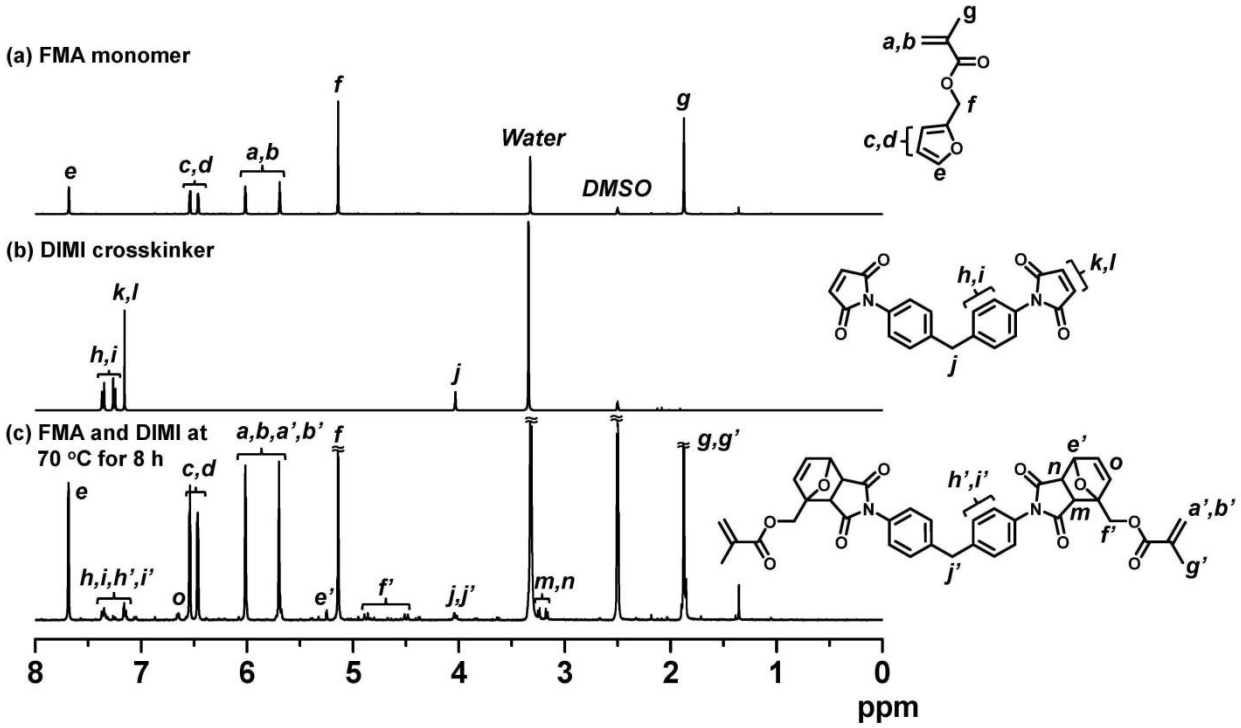

Figure S2.2. ^{1}H NMR spectra of (a) FMA monomer, (b) DIMI crosslinker, and (c) the reaction mixture of FMA (0.093 g, 0.56 mmol, 20 eq) and DIMI (0.010 g, 0.028 mmol, 1 eq) in DMSO-d_6 (1.0 g) at 70 °C for 8 h.

2.6.2.2. Crosslinking of PFMA with DIMI. PFMA was synthesized by heating a mixture of FMA (1.2 g, 7.2 mmol), CP-I (1.4 mg, 7.2 μmol), and BNI (34 mg, 0.058 mmol) in a Schlenk flask at 60 °C under argon atmosphere with magnetic stirring. After 6 h, the mixture was cooled to room temperature and diluted with THF (3 mL). The polymer was reprecipitated in hexane/ethanol mixture (60 mL, v/v = 4/1), collected by filtration, and dried in vacuo to give a

PFMA (monomer conversion = 13%) (M_n = 24000 and $Đ$ = 1.35 (PMMA-calibrated GPC values)). For the crosslinking, a mixture of the PFMA (0.17 g, monomer unit = 2.8 M, 210 eq), DIMI (1.7 mg, 0.013 M, 1 eq), and DMF (0.17 g) was heated in a Schlenk flask at 70 °C under argon atmosphere for 14 h.

2.6.2.3. Decrosslinking of Crosslinked PFMA. A mixture of the crosslinked PFMA swollen in DMF (50wt%), FMA (2.5wt%), and additional DMF (47.5wt%) was heated in a Schlenk flask at 110 °C for 24 h. After cooling to room temperature, a part of the reaction mixture was diluted with THF for GPC analysis.

2.6.3. Synthesis and Crosslinking/Decrosslinking of Polymer Brushes

2.6.3.1. Preparation of PFMA-*r*-PPFPMA Brush. The IHE-immobilized silicon wafer was heated in a mixture of FMA (0.60 g, 3.6 mmol, 4000 mM), PFPMA (0.79 g, 3.6 mmol, 4000 mM), CP−I (1.4 mg, 0.0073 mmol, 8 mM), and ONI (34 mg, 0.058 mmol, 64 mM) in a Schlenk flask at 60 °C under argon atmosphere with magnetic stirring for 8 h (**Table 2.1**, entry 2). (The wafer was inclined to the wall of the Schlenk flask, and the stir bar was located underneath the wafer for all experiments with magnetic stirring in this section (**Chapter 2.6.3**).) After the polymerization, the wafer was rinsed with acetone, sonicated in acetone for 30 min, and dried under nitrogen flow. The thickness of the polymer brush in the dry state was determined by AFM.

2.6.3.2. Preparation of PFMA-*r*-PHEMA Brush. The IHE-immobilized silicon wafer was heated in a mixture of FMA (0.60 g, 3.6 mmol, 4000 mM), HEMA (0.47 g, 3.6 mmol, 4000 mM), CP−I (1.4 mg, 0.0073 mmol, 8 mM), and ONI (34 mg, 0.058 mmol, 64 mM) in a Schlenk flask at 60 °C under argon atmosphere with magnetic stirring for 24 h (**Table 2.1**, entry 3). After the polymerization, the wafer was rinsed with acetone, sonicated in acetone for

30 min, and dried under nitrogen flow. The thickness of the PFMA-*r*-PHEMA brush in the dry state was determined by AFM.

2.6.3.3. General Thermal Decrosslinking of S-S Crosslinked PFMA Brush. The wafer with the S-S crosslinked PFMA brush was immersed in a mixture of a reducing agent (DTT (0.11 g), TBA (0.11 g), or $C_{12}H_{25}SH$ (0.67 g)) and DMF (2.0 g) in a Schlenk flask and heated at 40 °C under argon atmosphere with magnetic stirring for 10 h. The wafer was cleaned by ultra-sonication in acetone for 30 min and dried under nitrogen flow.

2.6.3.4. General Photo-induced Decrosslinking of S-S Crosslinked PFMA Brush. The wafer with the S-S crosslinked polymer brush was immersed in a mixture of Irgacure D-2959 (0.06 g), a reducing agent (DTT (0.06 g), TBA (0.06 g) or $C_{12}H_{25}SH$ (0.60 g)), and DMF (1.14 g for DTT and TBA or 0.60 g for $C_{12}H_{25}SH$) in a Schlenk flask and irradiated (365 nm, irradiation power = 900 mW/cm^2) under argon atmosphere with magnetic stirring for 30 min. The wafer was cleaned by ultra-sonication in acetone for 30 min and dried under nitrogen flow.

2.6.3.5. Recrosslinking of PFMA-SH Brush. The wafer with the PFMA-SH brush was immersed in a mixture of $FeCl_3$ (0.020 g), dichloromethane (0.25 g), and DMF (0.75 g) in a Schlenk flask and stirred at room temperature for 24 h. The wafer was cleaned by ultra-sonication in acetone for 30 min and dried under nitrogen flow.

2.6.3.6. Synthesis of Binary PFMA-SH Brush. A half of the wafer with the S-S crosslinked PFMA brush was covered with a clean silicon wafer and fixed with a Teflon tape. This wafer was immersed in a mixture of Irgacure D-2959 (0.06 g), TBA (0.06 g), and DMF (1.14 g) in a Schlenk flask and irradiated (365 nm, irradiation power = 900 mW/cm^2) under argon atmosphere with magnetic stirring for 30 min. The wafer was cleaned by ultra-sonication in acetone for 30 min and dried under nitrogen flow. In another way, two drops of a mixture composed of Irgacure D-2959 (0.06 g), TBA (0.06 g), and anhydrous DMF (1.14 g) was put

onto the wafer with the S-S crosslinked PFMA brush. A coverslip was placed on the droplet to form an ultrathin solution layer, and a clean silicon wafer was placed atop of the coverslip, which was irradiated (365 nm, irradiation power = 900 mW/cm^2) for 30 min. The wafer was cleaned by ultra-sonication in acetone for 30 min and dried under nitrogen flow.

2.6.3.7. Reaction of Binary PFMA-SH Brush with C_8F_{17}-alkyne. The wafer with the binary brush with the S-S crosslinked PFMA domain and the PFMA-SH domain was immersed in a mixture of C_8F_{17}-alkyne (0.5 mg, 1 eq), TBA (1 mg, 5 eq), and DMF (1.0 mL) in the dark at room temperature for 1 min. The wafer was cleaned by ultra-sonication in acetone for 15 min and dried under nitrogen flow. The synthesis of C_8F_{17}-alkyne is described below (**Chapter 2.6.4**).

2.6.3.8. Synthesis of Striped-Patterned Brushes and Fluorescent Labeling. Two drops of a mixture composed of Irgacure D-2959 (0.06 g), TBA (0.06 g), and anhydrous DMF (1.14 g) was put onto the wafer with the S-S crosslinked PFMA brush. A coverslip was placed on the droplet to form an ultrathin solution layer, and the striped-patterned photomask (**Figure S2.1**) was placed atop of the coverslip, which was irradiated (365 nm, irradiation power = 900 mW/cm^2) for 30 min. The wafer was cleaned by ultra-sonication in acetone for 30 min and dried under nitrogen flow. The wafer with the patterned brush with the S-S crosslinked PFMA domains and the PFMA-SH domains was immersed in a mixture of CPM (0.5 mg, 1 eq), TBA (1 mg, 4 eq), and DMF (1.0 mL) in the dark at room temperature for 1 min. The wafer was rinsed with THF and dried under nitrogen flow.

2.6.4. Synthesis of 3-((2-perfluorooctyl)ethoxy)propyne (C_8F_{17}-alkyne)

The synthesis of C_8F_{17}-alkyne was referred to the literature *with* a *slight modification*.[17] *1H,1H,2H,2H*-Heptadecafluoro-1-decanol (5.0 g, 10.8 mmol) and sodium hydroxide (1.0 g, 25 mmol) were placed in a round-bottom flask with anhydrous THF (40 mL), and the mixture was

stirred for 10 min at 0 °C. A solution of propargyl bromide (1.92 g, 16.2 mmol) in THF (10 mL) was added dropwise to the reaction mixture. The reaction mixture was gradually warmed to room temperature and stirred for 24 h. To the reaction mixture, diethyl ether (20 mL) was added, and the solution was poured into deionized water (20 mL). The separated aqueous layer was extracted with diethyl ether (3 × 20 mL). The combined organic layers were merged and washed with 10wt% HCl aqueous solution, saturated $NaHCO_3$ aqueous solution, and brine. After drying over $MgSO_4$ and evaporating, the crude was purified by a silica gel column chromatography (eluent: hexane/diethyl ether = 10/1). After drying under vacuum, C_8F_{17}-alkyne was obtained as a colorless oil. Yield: 44% (2.41 g, 4.80 mmol); ^{1}H NMR (300 MHz, 298 K, $CDCl_3$) (**Figure S2.3**) δ 4.18 (*d*, *J* = 2.32 Hz, 2H, –CC$\underline{H_2}$O–), 3.82 (t, *J* = 6.81 Hz, 2H, –OC$\underline{H_2}$CH_2C$_8$F$_{17}$), 2.46 (*t*, 2.07, 1H, $\underline{H}$C≡C–), 2.44 (*m*, 2H, –OCH$_2$C$\underline{H_2}$C$_8$F$_{17}$); ^{19}F NMR (282 MHz, 298 K, $CDCl_3$) (**Figure S2.4**) δ -81.7, -114.3, -122.6, -122.8, -123.6, -124.5, -127.0 ppm.

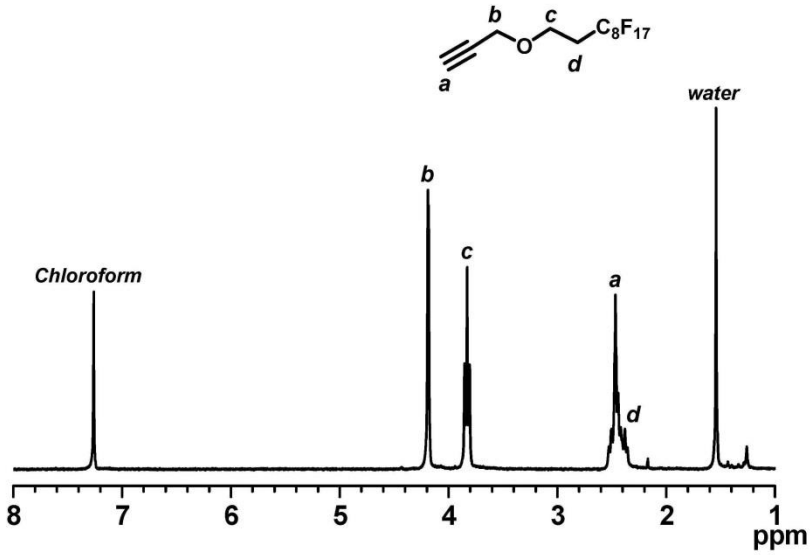

Figure S2.3. ^{1}H NMR spectrum (300 MHz, 298 K, $CDCl_3$) of 3-((2-perfluorooctyl)ethoxy)propyne (C_8F_{17}-alkyne).

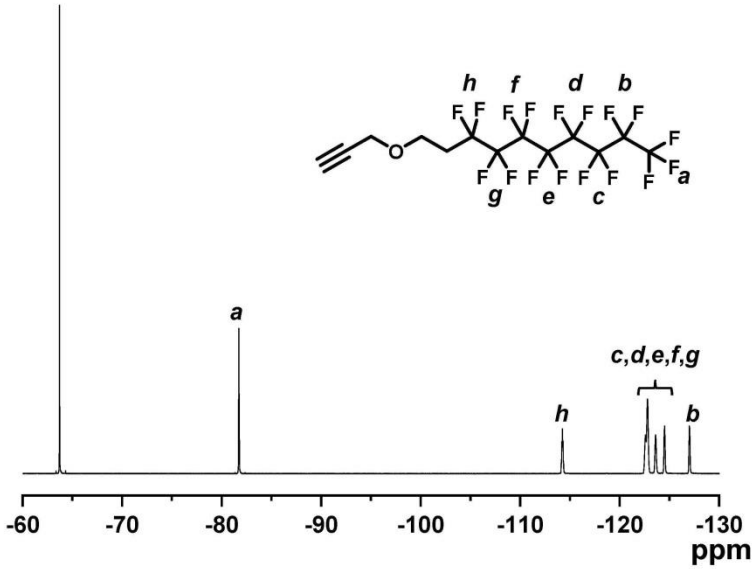

Figure S2.4. ^{19}F NMR spectrum (282 MHz, 298 K, $CDCl_3$) of 3-((2-perfluorooctyl)ethoxy)propyne (C_8F_{17}-alkyne). *α,α,α*-Trifluorotoluene was uses as a reference standard with a calibration signal at -63.72 ppm.

2.6.5. XPS spectra

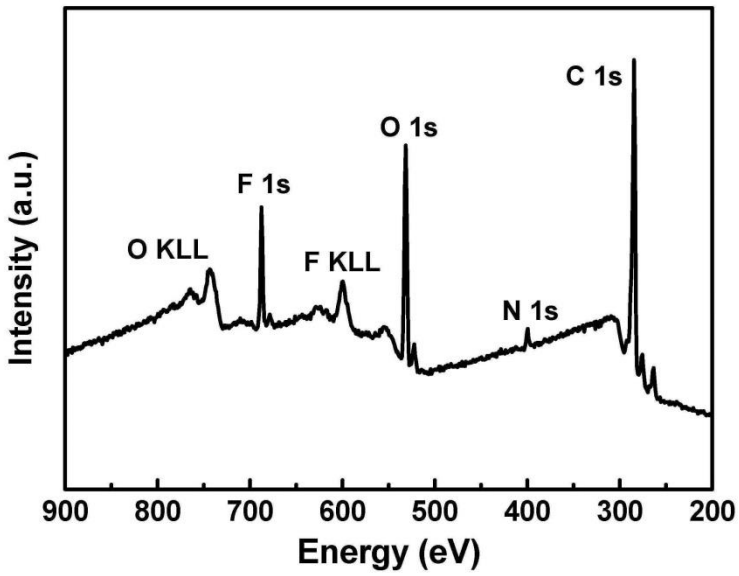

Figure S2.5. XPS survey spectrum of the crosslinked PFMA-*r*-PFPMA copolymer brushes with DIMI. The synthesis and characterization of PFMA-*r*-PFPMA are given in **Table 2.1** (entry 2).

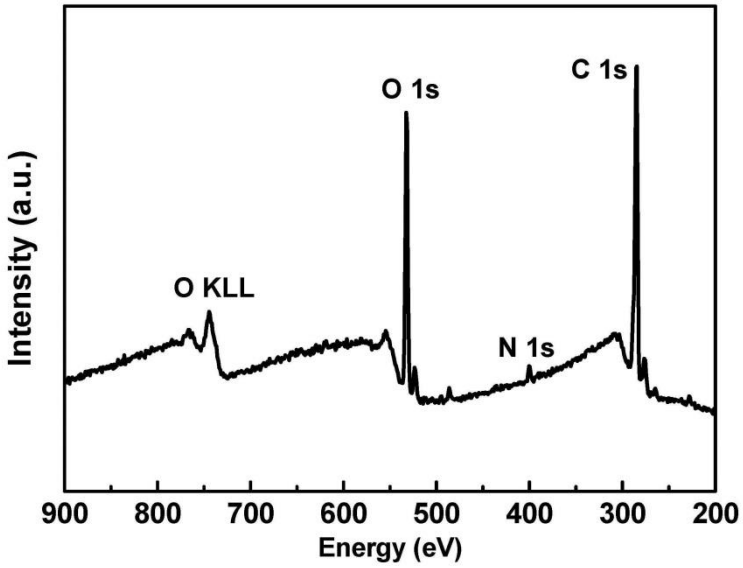

Figure S2.6. XPS survey spectrum of the crosslinked PFMA-*r*-PHEMA copolymer brushes with DIMI. The synthesis and characterization of PFMA-*r*-PHEMA are given in **Table 2.1** (entry 3).

Reference(s)

(1) Mendes, P. M. *Chem. Soc. Rev.* **2008**, *37*, 2512−2529.

(2) Yang, H. et al. *Acc. Chem. Res.* **2014**, *47*, 2106−2115.

(3) Su, B. et al. *J. Am. Chem. Soc.* **2016**, *138*, 1727−1748.

(4) Gupta, R. K. et al. *J. Mater. Chem. A* **2017**, *5*, 16025−16058.

(5) Keating, J. J., IV. et al. *ACS Appl. Mater. Interfaces* **2016**, *8*, 28383−28399.

(6) Zoppe, J. O. et al. *Chem. Rev.* **2017**, *117*, 1105−1318.

(7) Chen, W.-L. et al. *Macromolecules* **2017**, *50*, 4089−4113.

(8) Wu, J.-G. et al. *ACS Appl. Mater. Interfaces* **2019**, *11*, 21294−21307.

(9) Ma, S. et al. *NPG Asia Mater.* **2019**, *11*, 24.

(10) Stuart, M. A. C. et al. *Nat. Mater.* **2010**, *9*, 101−113.

(11) Chen, T. et al. *Prog. Polym. Sci.* **2010**, *35*, 94−112.

(12) Li, B. et al. *Acc. Chem. Res.* **2015**, *48*, 229−237.

(13) Hirai, T. et al. *Polym. Chem.* **2017**, *8*, 5456−5468.

(14) Badoux, M. et al. *Polym. Chem.* **2019**, *10*, 2925−2951.

(15) Goto, A. et al. *J. Am. Chem. Soc.* **2013**, *135*, 11131−11139.

(16) Ohtsuki, A. et al. *J. Am. Chem. Soc.* **2015**, *137*, 5610−5617.

(17) Wang, C.-G.; Goto, A. *J. Am. Chem. Soc.* **2017**, *139*, 10551−10560.

(18) Liu, X. et al. *Angew. Chem. Int. Ed.* **2019**, *58*, 5598−5603.

(19) Xu, H. et al. *Macromolecules* **2019**, *52*, 2156−2163.

(20) Wang, C.-G. et al. *Macromolecules* **2019**, *52*, 2712−2718.

(21) Mao, W. et al. *Polym. Chem.* **2020**, *11*, 53−60.

(22) Wang, C.-G. et al. *Macromolecules* **2020**, *53*, 51−58.

(23) Wang, C.-G. et al. *Angew. Chem. Int. Ed.* **2018**, *57*, 13504−13508.

(24) Wang, C.-G. et al. *ACS Appl. Mater. Interfaces* **2019**, *11*, 14478−14484.

(25) Tsujii, Y. et al. *Adv. Polym. Sci.* **2006**, *197*, 1−45.

(26) Huang, W. et al. *Angew. Chem. Int. Ed.* **2001**, *40*, 1510−1512.

(27) Dehghani, E. S. et al. *Langmuir* **2016**, *32*, 10317−10327.

(28) Yu, J. et al. *Science* **2018**, *360*, 1434−1438.

(29) Zhang, P. et al. *Adv. Sci.* **2019**, *6*, 1900996.

(30) Wu, J. et al. *Prog. Org. Coat.* **2019**, *134*, 153−161.

(31) Dehghani, E. S. et al. *Eur. Polym. J.* **2018**, *99*, 415−421.

(32) Benetti, E. M. et al. *Adv. Funct. Mater.* **2010**, *20*, 939–944.

(33) Costantini, F. et al. *Chem. Eur. J.* **2010**, *16*, 12406–12411.

(34) Li, A. et al. *Adv. Mater. Interfaces* **2014**, *1*, 1300007.

(35) Ramakrishna, S. N. et al. *Macromolecules* **2015**, *48*, 7106–7116.

(36) Dehghani, E. S. et al. *Macromolecules* **2017**, *50*, 2495–2503.

(37) Dehghani, E. S. et al. *Macromolecules* **2017**, *50*, 2932–2941.

(38) Loveless, D. M. et al. *Angew. Chem. Int. Ed.* **2006**, *45*, 7812−7814.

(39) Mocny, P.; Klok, H.-A. *Macromolecules* **2020**, *53*, 731−740.

(40) Funel, J.-A.; Abele, S. *Angew. Chem. Int. Ed.* **2013**, *52*, 3822−3863.

(41) Gandini, A. *Prog. Polym. Sci.* **2013**, *38*, 1−29.

(42) Liu, Y.-L.; Chuo, T.-W. *Polym. Chem.* **2013**, *4*, 2194−2205.

(43) Tasdelen, M. A. et al. *Prog. Polym. Sci.* **2016**, *52*, 19−78.

(44) Vauthier, M. et al. *Adv. Funct. Mater.* **2019**, *29*, 1806765.

(45) Jiang, Y. et al. *Biomaterials* **2014**, *35*, 4969−4985.

(46) Arumugam, S. et al. *J. Am. Chem. Soc.* **2012**, *134*, 179−182.

(47) Yameen, B. et al. *Chem. Commun.* **2013**, *49*, 8623−8625.

(48) Gevrek, T. et al. *Macromolecules* **2014**, *47*, 7842−7851.

(49) Roling, O. et al. *Org. Biomol. Chem.* **2014**, *12*, 7828−7835.

(50) Roling, O. et al. *Angew. Chem. Int. Ed.* **2015**, *54*, 13126−13129.

(51) Yuksekdag, Y. N. et al. *ACS Macro Lett.* **2017**, *6*, 415−420.

(52) Lange, J. et al. *Polymer* **1998**, *39*, 2537−2542.

(53) Li, A. et al. *Macromolecules* **2011**, *44*, 5344−5351.

(54) Cohen Stuart, M. A. et al. *Langmuir* **2006**, *22*, 1722−1728.

(55) Parker, A. J.; Kharasch, N. *Chem. Rev.* **1959**, *59*, 583−628.

(56) Chen, T. et al. *Chem. Soc. Rev.* **2012**, *41*, 3280−3296.

(57) Jung, K. et al. *Adv. Mater.* **2019**, 1903850.

(58) Wang, S. et al. *Mater. Chem. Front.* **2020**, *4*, 692−714.

(59) Page, Z. A. et al. *ACS Cent. Sci.* **2017**, *3*, 654−661.

(60) Narupai, B. et al. *Angew. Chem. Int. Ed.* **2018**, *57*, 13433−13438.

(61) Chen, C. et al. *Chem. Commun.* **2018**, *54*, 13738−13741.

(62) Chen, C. et al. *Polym. Chem.* **2019**, *10*, 5913−5919.

(63) Ellis, B.; Smith, R. *Polymers: A Property Database*, 2nd ed. Boca Raton: CRC Press, Boca Raton, **2008**, pp. 690.

(64) Yoshikawa, C. et al. *Macromolecules* **2006**, *39*, 2284−2290.

(65) Owens, D. K.; Wendt, R. C. *J. Appl. Polym. Sci.* **1969**, *13*, 1741−1747.

(66) Kozbial, A. et al. *Langmuir* **2014**, *30*, 8598−8606.

Chapter 3 Polymer Coupling via Hetero-Disulfide Exchange and its Applications to Rewritable Polymer Brushes

3.1. Abstract: An iodide-terminated polymer (Polymer-I) is converted to a thiol-terminated polymer (Polymer-SH) using HSCH2CH2SH in a remarkably short time (10 min). Polymer-SH is further converted to a pyridyl disulfide-terminated polymer (Polymer-SS-Py). The hetero-coupling of Polymer-SH and Polymer-SS-Py is successfully achieved to quantitatively generate a polymer disulfide (Polymer-SS-Polymer). Exploiting this efficient hetero-coupling technique, Polymer-SH is attached (grafted) on an Py-SS-immobilized surface to generate a polymer brush via a disulfide (-SS-) linkage (writing process). The -SS- linkage is cleaved by the treatment with dithiothreitol (DTT) to detach the polymer from the surface (erasing process). Subsequently, another Polymer-SH is attached on the surface to generate another polymer brush (rewriting process). Thus, a writable, erasable, and rewritable polymer brush surface is achieved. Hydrophilic, hydrophobic, and super-hydrophobic polymers (Polymer-SH) are attached on the surface, tailoring the surface wettability in the writing-erasing-rewriting cycles. Polymer-SH is also attached on a chain-end Py-SS-functionalized polymer brush surface, generating a rewritable block copolymer brush surface. A patterned block copolymer brush surface is also obtained using photo-irradiation and a photo-mask in the erasing process. The metal-free synthetic procedure, accessibility to patterned brushes, and switchable surface properties via the writing-erasing-rewriting process are attractive features of the present approach.

KEYWORDS: *rewritable surface, polymer brush, hetero-disulfide exchange, surface patterning, functional surface*

3.2. Introduction

Chain-end functionalized polymers are of great interest for their use as building blocks to create architecturally designed polymers.[1,2] Rosen, B. M. et al. reported a novel nucleophilic thio-bromo ‘‘Click’’ reaction to obtain dendritic macromolecules via a divergent iterative two-step growth approach.[3,4] Thiol (SH)-terminated polymers are useful building blocks that can connect with other polymers and small molecules for creating block copolymers,[5-9] branched polymers,[10-14] and bio-conjugates.[15,16] SH-terminated polymers have also been anchored on gold and functional surfaces via sulfur-gold interaction and SH-ene click reactions, for example, generating polymer brushes on surfaces.[11,14,17-20] Such polymer brushes have extensively been used in bio-sensing and bio-diagnostic applications, for example.[21-24]

Living (reversible-deactivation) radical polymerization (LRP) is an efficient method for synthesizing polymers with narrow molecular weight distributions.[25-34] LRP is based on the reversible activation of a dormant species (Polymer-X) to the propagating radical (Polymer$^{\bullet}$). The resulting polymer (Polymer-X) possesses a capping agent (X) at the chain end. Post-transformation of X to SH affords SH-terminated polymers (Polymer-SH). Our research group developed an organocatalyzed LRP, termed reversible complexation mediated polymerization (RCMP),[35-40] using a polymer-iodide (Polymer-I) as a dormant species and iodide anion (I^-) as a catalyst **(Scheme 3.1a)**. Polymer-I and I^- are supposed to form a halogen-bonding complex (Polymer-I$\cdots I^-$), which subsequently reversibly generates Polymer$^{\bullet}$ and $I_2^{\bullet-}$. I^- is used in the form of salts such as tetra-*n*-butylammonium iodide ($Bu_4N^+I^-$ (BNI) **(Figure 3.1)**).[35] The advantages of RCMP are no use of special capping agents or metals and the amenability to a range of functional monomers. The post-transformation of I to SH can generate Polymer-SH.[41]

Scheme 3.1. (a) Reversible Activation in Reversible Complexation-Mediated Polymerization (RCMP); (b) Disulfide Exchange Reaction between Sulfhydryl Moieties and Pyridyl Disulfide.

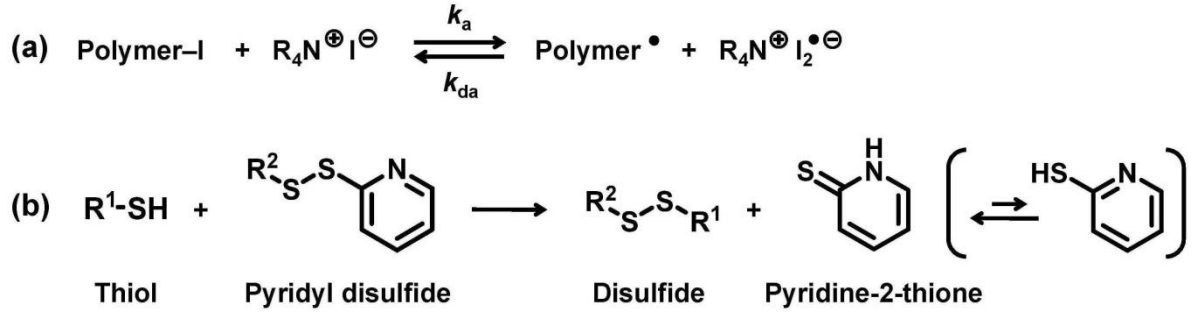

Symmetric disulfides (R^1-SS-R^1) are widely synthesized via homo-coupling of thiols (R^1-SH) or their derivatives in the presence of oxidants such as hydrogen peroxide and iodine (I_2). The synthesis of asymmetric disulfides (R^1-SS-R^2) is more challenging, but several efficient methods are available.[42] A useful method to obtain R^1-SS-R^2 is hetero-coupling of R^1-SH and a pyridyl disulfide (R^2-SS-Py) via a thiol-disulfide exchange (**Scheme 3.1b**).[43,44] The S-Py moiety is a good leaving group, and the generated pyridine-2-thione is non-reactive and incapable of participating in further disulfide exchanges.[43,44] Thus, the asymmetric R^1-SS-R^2 is selectively generated. As well as small molecules and biomolecules, synthetic polymers have been utilized for the homo-coupling[3,6,45–47] and the hetero-coupling.[4,48,49]

Surface functionalization is of great importance, because it can efficiently tailor surface properties such as physicochemical, optical, and mechanical properties.[50-56] Reversible surface functionalization techniques, which fabricate and remove functional groups in reversible manners, have attracted attention for creating rewritable (write-erase-rewrite) surfaces. Various small molecules and bio-(macro)molecules were reversibly anchored to surfaces via reversible thiol−quinone methide click reaction,[57] disulfide exchange,[58-64] and Diels–Alder[65,66] reactions, generating rewritable surfaces.[67] Photo-chemical reactions were also utilized to obtain

patterned rewritable surfaces for biomedical and biosensor applications.[57,58] Synthetic polymers were also reversibly anchored to surfaces via reversible Diels–Alder reactions,[68,69] generating rewritable polymer brushes on surfaces. Barner-Kowollik et al. attached poly(isobornyl acrylate), polystyrene, and poly(ethylene glycol) on silicon surface via reversible Diels–Alder reaction and obtained polymer brushes with different hydrophobicity and hydrophilicity for tailoring the surfaces properties.[68] Costanzo et al. attached perfluorinated polymers on glass slides and capillary surfaces via reversible Diels–Alder reaction to create thermo-responsive tailorable surface.[69] However, in the field of synthetic polymer, a polymer possessing an SH group at the chain end (Polymer-SH) has not been utilized for creating rewritable polymer brushes via disulfide exchange.

Scheme 3.2. Schematic Illustration of Rewritable Polymer Brushes using different thiol-functionalized polymers.

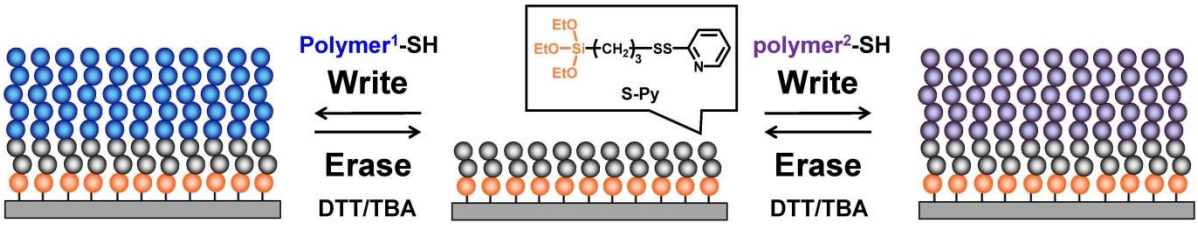

In the present paper, we studied the polymer coupling via hetero-disulfide exchange and utilized this coupling reaction to create re-writable polymer brush surfaces using synthetic Polymer-SH **(Scheme 3.2)**. We studied polyacrylates (Polymer = polyacrylate). We synthesized Polymer-I via RCMP. Taking advantage of the weak carbon-iodide bond, we attained a remarkably fast chain-end transformation (10 min) of Polymer-I to generate

Polymer-SH. Polymer-SH was further converted to Polymer-SS-Py. We successfully attained the homo-coupling of Polymer-SH and the hetero-coupling of Polymer-SH and Polymer-SS-Py, while polymer-polymer reactions are often difficult even if the reactions are efficient for small molecules. We utilized this hetero-coupling reaction to attach Polymer-SH on an Py-SS-immobilized silicon surface (**Scheme 3.2**) and obtained a polymer brush with a disulfide (-SS-) linkage (writing process). The -SS- linkage can be cleaved by the treatment with dithiothreitol (DTT) in a basic condition to detach the polymer from the surface (**Scheme 3.2**) (erasing process). Subsequently, another Polymer-SH was attached on the surface to generate another polymer brush (**Scheme 3.2**) (rewriting process). Thus, the writable, erasable, and rewritable polymer brush surface was achieved. In this present work, we attached hydrophilic, hydrophobic, and super-hydrophobic polymers (Polymer-SH), tailoring the surface wettability in the writing-erasing-rewriting cycles. We further utilized the "polymer-polymer" hetero-coupling to attach Polymer-SH on a chain-end Py-SS-functionalized polymer brush surface to obtain a rewritable block copolymer brush surface. An advantage of the present approach is that only a mild condition (room temperature) is required for the writing, erasing, and rewriting processes. In the erasing (disulfide cleavage) process, instead of using a basic condition, photo-irradiation can also be utilized, which enabled the preparation of a patterned block copolymer brush surface using a photo-mask. The metal-free synthetic procedure, mild reaction condition (room temperature), accessibility to patterned brushes (using photo-irradiation), and switchable surface properties via the writing-erasing-rewriting process are attractive features of the present approach. Such rewritable polymer brush and block copolymer brush surfaces may potentially be used in rewritable microarray technologies and sensing interfaces. **Figure 3.1** shows the structures of monomers, alkyl iodide initiating dormant species, polymerization catalysts, and sulfur-containing compounds used in the present work.

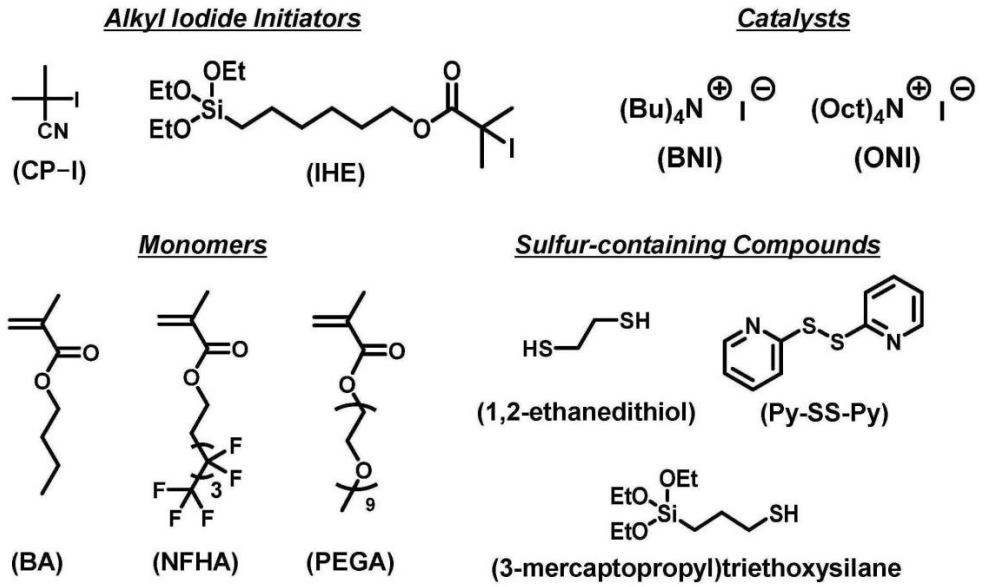

Figure 3.1. Structures of alkyl iodides, catalysts, monomers, and sulfur-containing compounds used in this work.

3.3. Results and Discussion

3.3.1. Preparation of PBA-I. We carried out the RCMP of butyl acrylate (BA (**Figure 3.1**)) (50 equiv) using 2-iodo-2-methylpropionitrile (CP-I (**Figure 3.1**)) (1 equiv) as an alkyl iodide initiating dormant species and BNI (4 equiv) as a catalyst at 110 °C for 5 h and obtained a poly(butyl acrylate)-iodide (PBA-I) possessing a CP group at the initiating chain end and an iodide at the growing chain end (monomer conversion = 40%). The polymer had M_n = 3700 and $Đ$ (= M_w/M_n) = 1.16 after the purification by reprecipitation in a methanol/water (1/1 (v/v)) mixture, where M_n and M_w are the number- and weight-average molecular weights, respectively, and $Đ$ is the dispersity. The M_n and M_w values described in the present paper are not absolute values but were obtained with poly(methyl methacrylate)-calibrated gel permeation chromatography (GPC). Thus, the M_n and M_w values and their related discussion described in the present paper are viewed as estimates.

3.3.2. Chain-end Transformation of PBA-I to PBA-SH. In our previous paper, we reported the transformation of PBA-I to a thiol-terminated PBA-SH; PBA-I was reacted with cysteamine ($NH_2CH_2CH_2SH$) bearing a primary amine (NH_2) and an SH group **(Scheme 3.3)**.[41,70] The substitution of I with the NH_2 group generated Polymer-SH with the intact SH group (Form **1** in **Scheme 3.3**). Form **1** further underwent intramolecular amidation to generate another form of Polymer-SH with a cyclic chain end (Form **2** in **Scheme 3.3**). Because the chain-end of Form **2** is sterically more hindered than that of Form **1**, the SH group in Form **2** can be less reactive than that of Form **1** for further reactions. Thus, it is desirable to selectively obtain Form **1**.

Scheme 3.3. Chain-end Transformation of Polymer-X to Two Forms.

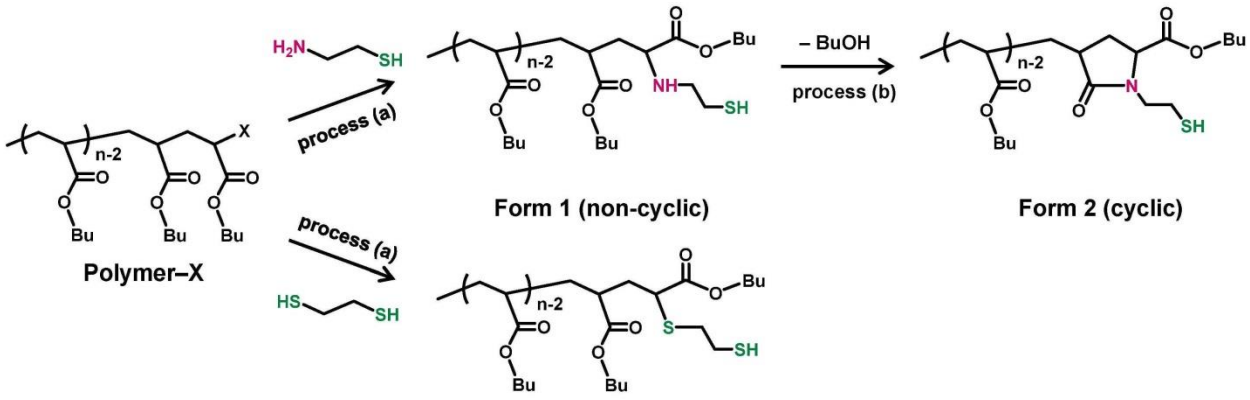

Anastasaki and Hawker et al. developed an elegant method to obtain Polymer-S-R, using a thiol (R-SH) in a basic condition.[71] Polymer-Br, which was obtained via atom transfer radical polymerization (ATRP),[26,27] was reacted with R-SH. The SH group underwent the substitution with Br in the basic condition to generate Polymer-S-R. The basic condition induced the substitution using the SH group.

In the present work, we exploited their method for the chain-end transformation of Polymer-I. We used 1,2-ethanedithiol ($HSCH_2CH_2SH$) in a basic condition. One of the two SH groups would undergo the substitution with I in the basic condition, and the other SH group would remain intact to generate Polymer-SH (**Scheme 3.3**). Because of the absence of the reactive amine, no cyclization would take place, selectively generating Polymer-SH with a non-cyclic chain end (Form **1**).

While Polymer-Br required a relatively long reaction time (~12 h) for the quantitative chain-end transformation to Polymer-S-R, the use of Polymer-I facilitated the chain-end transformation to Polymer-S-R (R = CH_2CH_2SH) and significantly shortened the reaction time (10 min in the present work) as an additional benefit, because of the weaker carbon-iodide bond than the carbon-bromide bond.

A mixture of the above-obtained PBA-I (1 equiv, 20 wt%), $HSCH_2CH_2SH$ (20 equiv), diisopropylamine ($^iPr_2NH$) (4 equiv) (a mild base), and *N*,*N*-dimethylformamide (DMF) (80 wt%) (a solvent) was stirred in the dark at room temperature for 10 min. The base ($^iPr_2NH$) was required to deprotonate (activate) SH to form a reactive S^- for undergoing the substitution reaction and to neutralize the HI generated in the reaction. While triethylamine (TEA) was used in the Polymer-Br system, TEA was a too strong base for the Polymer-I system. Polymer-I and TEA can form a Polymer-I···NR_3 complex via halogen bonding.[72] The complex can subsequently generate Polymer$^\bullet$, which abstracts a hydrogen from SH to yield Polymer-H as a side product. $^iPr_2NH$ is a weaker base and has a larger steric hindrance than TEA so that $^iPr_2NH$ may significantly suppress the formation of the complex and hence Polymer-H (side product). The steric hindrance of $^iPr_2NH$ may also prevent the nucleophilic substitution of the iodide on the polymer chain end by the amine ($^iPr_2NH$).

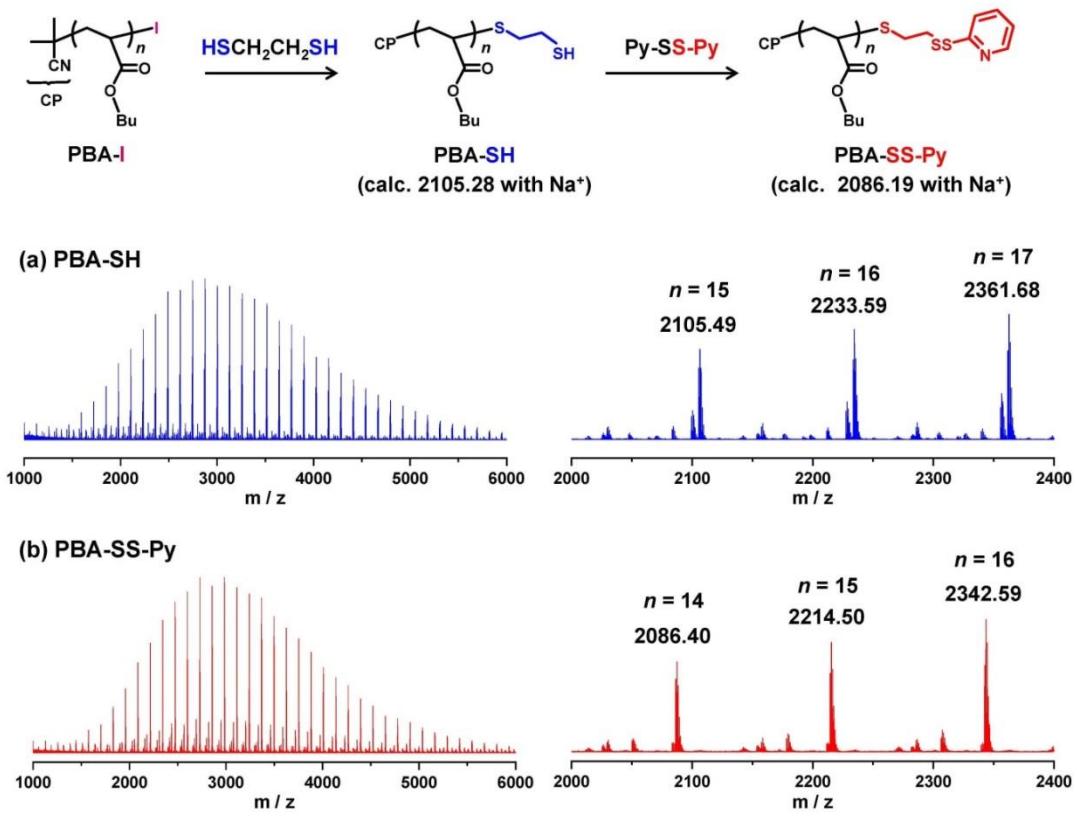

Figure 3.2. MALDI-TOF-MS spectra of (a) PBA-SCH_2CH_2SH (PBA-SH) and (b) PBA-SCH_2CH_2-SS-Py (PBA-SS-Py).

After the reaction, the mixture was diluted with DMF and the polymer was purified by reprecipitation in a methanol/water (1/1 v/v) mixture five times to remove trace amounts of $HSCH_2CH_2SH$ and other low-molecular-weight species, yielding a PBA-SH with M_n = 4000 and $Đ$ = 1.22. **Figure 3.2a** shows the matrix-assisted laser desorption/ionization time-of-flight mass spectrometry (MALDI-TOF-MS) analysis of the obtained polymer. We used trans-2-[3-(4-tert-butylphenyl)-2-methyl-2-propenylidene]malononitrile (DCTB) as a matrix and CF_3COONa as an additive salt. The polymer contains ^{12}C and ^{13}C atoms. For simplicity, the theoretical (calculated) molar masses and the experimental molar masses given in the MALDI-

TOF-MS spectra in the figures are those without ^{13}C atoms (i.e., with only ^{12}C atoms); unless otherwise specified, these molar masses are compared below.

In **Figure 3.2a**, we observe an almost single series of repeated peaks (2105.49 (n = 15), 2233.59 (n = 16), and 2361.68 (n = 17)) with a mass interval of 128.1, which corresponds to the BA monomer unit. The n value is the degree of polymerization of the polymer. The experimental mass of 2105.49 well matches the theoretical mass of 2105.28 for the desired PBA-SH. This result suggests a nearly quantitative chain-end transformation of PBA-I to PBA-SH. Minor series of repeating peaks were also observed. A particular series was observed at 2099.44. This species disappeared upon the subsequent transformation of PBA-SH to PBA-SS-Py, as describe below, suggesting that this species was not generated during the reaction but generated during the MALDI-TOF-MS analysis from the desired PBA-SH. The exact structure of this species is unknown. Thus, we successfully attained the nearly quantitative chain-end transformation of PBA-I to PBA-SH in a very short time (10 min).

3.3.3. Chain-end Transformation of PBA-SH to PBA-SS-Py. A mixture of PBA-SH (1 equiv, 20 wt%), 2,2'-dipyridyl disulfide (Py-SS-Py) (5 equiv), and DMF (80 wt%) was stirred at room temperature for 4 h to obtain PBA-SS-Py (**Figure 3.2**). DMF was used to increase the rate of the thiol-disulfide interchange (S_N2 reaction).[73] After the reaction, the mixture was diluted with DMF and the polymer was purified by the reprecipitation in a mixture of methanol/H_2O (1/1 (v/v)). The polymer was further purified using a preparative GPC to remove trace amounts of small molecules, yielding a PBA-SS-Py with M_n = 4300 and $Đ$ = 1.21. The MALDI-TOF-MS spectrum of the product (**Figure 3.2b**) showed only a single series of repeated peaks for PBA-SS-Py (experimental mass = 2086.40 and theoretical mass = 2086.19 (n = 14)), suggesting a nearly quantitative transformation of PBA-SH to PBA-SS-Py. This result demonstrates the successful synthesis of PBA-SS-Py.

3.3.4. Homo-coupling of PBA-SH. We studied the homo-coupling of PBA-SH via an aerobic oxidation using iodine (I_2) as an oxidant to generate PBA-SS-PBA with a disulfide (-SS-) linkage **(Figure 3.3)**. A mixture of PBA-SH (M_n = 4000 and $Đ$ = 1.22) (1 equiv, 20 wt%), I_2 (2 equiv), and DMF (80 wt%) was stirred in the air at room temperature for 16 h. **Figure 3.3a** shows the GPC chromatograms before (black dashed line) and after (red solid line) the reaction. The original PBA-SH (black dashed line) was virtually perfectly shifted to a higher molecular species (red solid line). The M_n value after the reaction was 7800, which is close to a doubled M_n value of the original PBA-SH (M_n = 4000). The result suggests a nearly quantitative formation of the desired PBA-SS-PBA. The MALDI-TOF-MS spectrum (**Figure 3.3b**) also confirmed that the main product was the desired PBA-SS-PBA; the experimentally observed mass (5082.77) matched the theoretical mass (5082.14 (n + m = 37)) of PBA-SS-PBA, where the n and m values are the degrees of polymerization of the two coupled polymers. The result demonstrates the successful homo-coupling of PBA-SH.

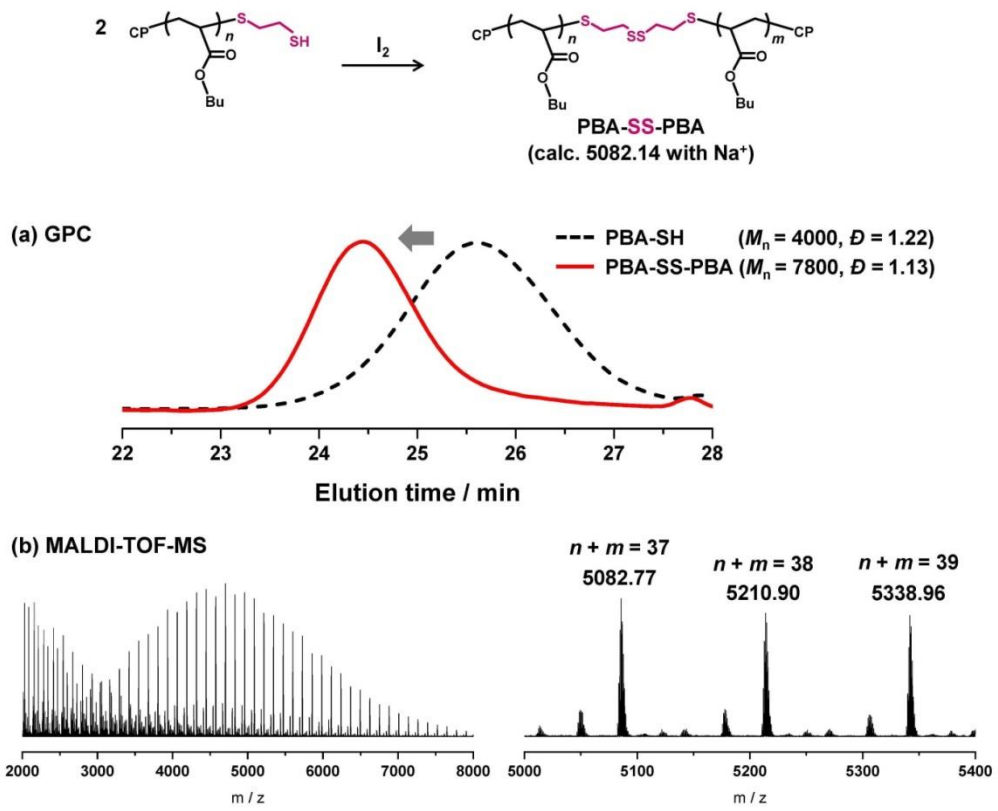

Figure 3.3. (a) GPC traces of PBA-SH (black dashed line) and the polymer product after the homo-coupling of PBA-SH (1 equiv, 20 wt%) using iodine (2 equiv) in DMF (80 wt%) for 16 h (red solid line). (b) MALDI-TOF-MS spectrum of the polymer product after the 16 h reaction.

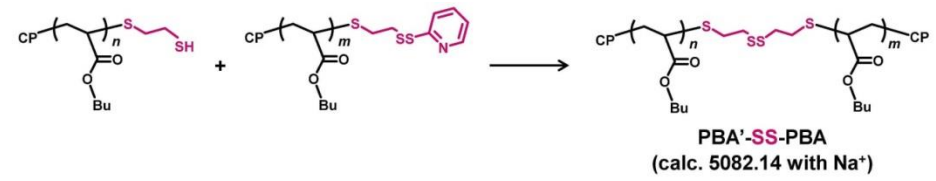
PBA'-SS-PBA
(calc. 5082.14 with Na+)

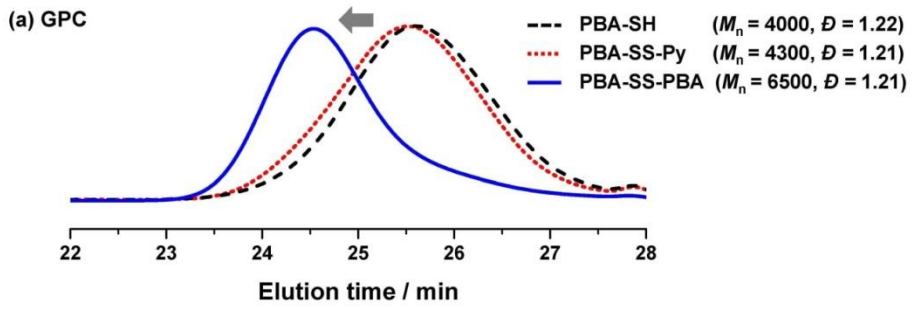
(a) GPC
PBA-SH (Mn = 4000, Đ = 1.22)
PBA-SS-Py (Mn = 4300, Đ = 1.21)
PBA-SS-PBA (Mn = 6500, Đ = 1.21)
Elution time / min

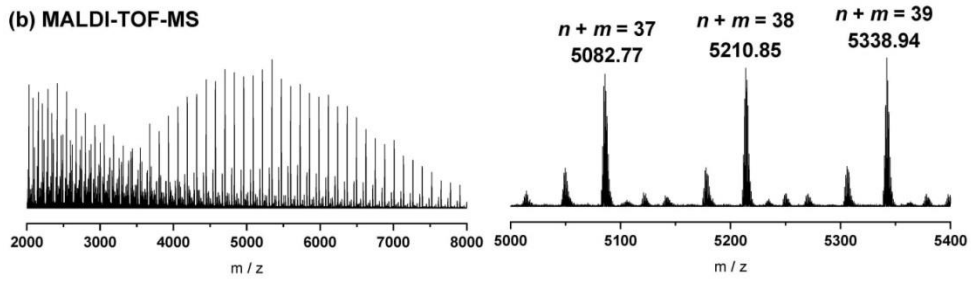
(b) MALDI-TOF-MS
n + m = 37
5082.77
n + m = 38
5210.85
n + m = 39
5338.94
m / z
m / z

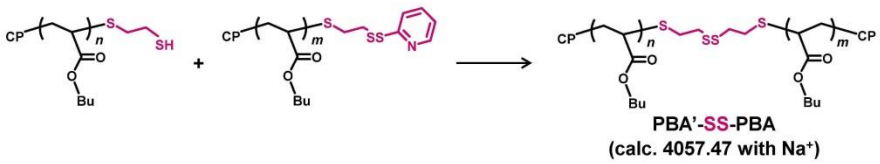
PBA'-SS-PBA
(calc. 4057.47 with Na+)

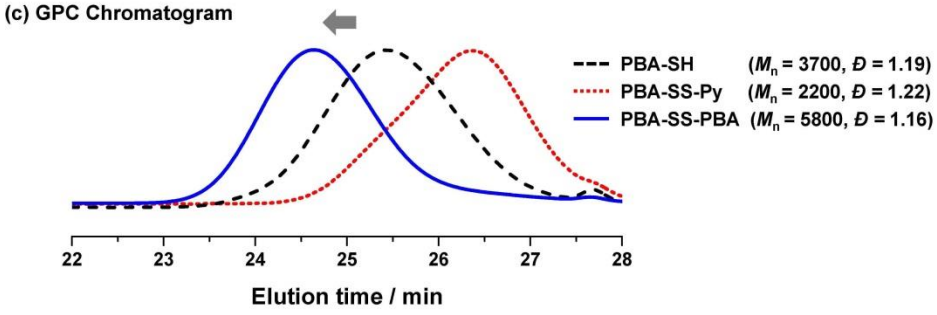
(c) GPC Chromatogram
PBA-SH (Mn = 3700, Đ = 1.19)
PBA-SS-Py (Mn = 2200, Đ = 1.22)
PBA-SS-PBA (Mn = 5800, Đ = 1.16)
Elution time / min

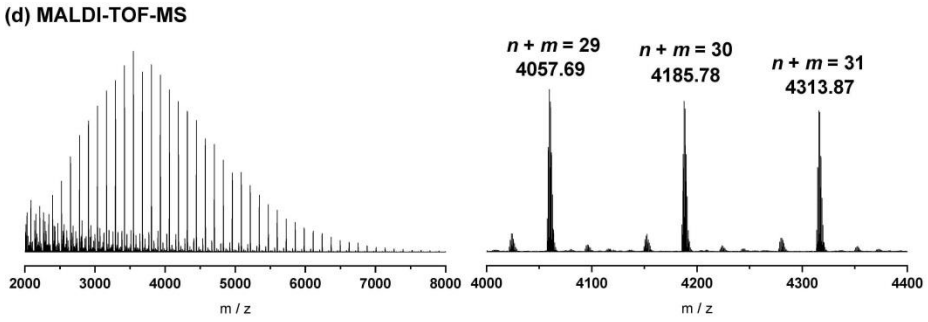
(d) MALDI-TOF-MS
n + m = 29
4057.69
n + m = 30
4185.78
n + m = 31
4313.87
m / z
m / z

Figure 3.4. (a) GPC traces of PBA-SH (M_n = 4000 and $Đ$ = 1.22) (black dashed line), PBA-SS-Py (M_n = 4300 and $Đ$ = 1.21) (red dotted line), and the polymer product after the hetero-coupling of the PBA-SH (1 equiv) and the PBA-SS-Py (nearly 1 equiv) in DMF (solvent) (70 wt%) at room temperature for 16 h (blue solid line). (b) MALDI-TOF-MS spectrum of the polymer product after the 16 h reaction for the sample in (a). (c) GPC traces of PBA-SH (M_n = 3700 and $Đ$ = 1.19) (black dashed line), PBA-SS-Py (M_n = 2200 and $Đ$ = 1.22) (red dotted line), and the polymer product after the hetero-coupling of the PBA-SH (1 equiv) and the PBA-SS-Py (nearly 1 equiv) in DMF (solvent) (70 wt%) at room temperature for 16 h (blue solid line). (d) MALDI-TOF-MS spectrum of the polymer product after the 16 h reaction for the sample in (c).

3.3.5. Hetero-coupling of PBA-SH and PBA-SS-Py. We studied the hetero-coupling of PBA-SH and PBA-SS-Py. A mixture of PBA-SH (M_n = 4000 and $Đ$ = 1.22) (1 equiv), PBA-SS-Py (M_n = 4300 and $Đ$ = 1.21) (nearly 1 equiv), and DMF (solvent) (70 wt%) was stirred at room temperature for 16 h (**Figure 3.4** (**3.4a** and **3.4b**)). **Figure 3.4a** shows the GPC chromatograms of the original PBA-SH (black dashed line), the original PBA-SS-Py (red dotted line), and the product after the reaction (blue solid line). The chromatograms demonstrate that large amounts of PBA-SH and PBA-SS-Py were converted to the higher molecular-weight PBA-SS-PBA via the hetero-coupling. The M_n value after the reaction was 6500, which is somewhat smaller than the expected M_n value for the full conversion to PBA-SS-PBA (approximately 8200), suggesting that some amounts of PBA-SH and PBA-SS-Py remained unreacted. The MALDI-TOF-MS spectrum (**Figure 3.4b**) confirmed that the main product was the desired PBA-SS-PBA; the experimentally observed mass (5082.77) matched the theoretical mass (5082.14 (n + m = 37)) of PBA-SS-PBA.

For more proof of hetero-coupling, we studied the hetero-coupling of PBA-SH and PBA-SS-Py with different M_n values. A mixture of PBA-SH (M_n = 3700 and $Đ$ = 1.19) (1 equiv), PBA-SS-Py (M_n = 2200 and $Đ$ = 1.22) (nearly 1 equiv), and DMF (solvent) (70 wt%) was stirred at room temperature for 16 h (**Figures 3.4c** and **3.4d**). **Figure 3.4c** shows the GPC chromatograms of the original PBA-SH (black dashed line), the original PBA-SS-Py (red dotted line), and the product after the reaction (blue solid line). Because of the different M_n values, the decay of PBA-SH and PBA-SS-Py were clearly (individually) observed. Both of PBA-SH and PBA-SS-Py were almost perfectly converted to the higher molecular-weight PBA-SS-PBA (**Figure 3.4c**). The M_n value after the reaction was 5800, which is close to the expected M_n value for the full conversion to PBA-SS-PBA (approximately 5800). The MALDI-TOF-MS spectrum (**Figure 3.4d**) confirmed that the main product was the desired PBA-SS-PBA; the experimentally observed mass (4057.69) matched the theoretical mass (4057.47 (n +

m = 29)) of PBA-SS-PBA. These results demonstrate almost quantitative hetero-coupling of PBA-SH and PBA-SS-Py. Compared with the above-described hetero-coupling of PBA-SH (M_n = 4000) and PBA-SS-Py (M_n = 4300), the present hetero-coupling of PBA-SH (M_n = 3700) and PBA-SS-Py (M_n = 2200) was more effective (almost quantitative) probably because of the lower molecular weights of PBA-SH and PBA-SS-Py (the easier contact of the two polymer chain ends).

As a control experiment, we attempted the homo-coupling of PBA-SS-Py (20 wt%) in DMF (80 wt%) at room temperature for 16 h. No shift of the GPC chromatogram (**Figure S3.4a** in **Chapter 3.6**) was observed after 16 h, meaning that the homo-coupling of PBA-SS-Py did not occur. We also attempted the homo-coupling of PBA-SH (M_n = 3700 and $Đ$ = 1.19) (20 wt%) in DMF (80 wt%) at room temperature for 16 h. Only a slight shift of the GPC chromatogram (**Figure S3.4b** in **Chapter 3.6**) was observed after 16 h, and the M_n value increased from 3700 (before the reaction) to only 4000 (after the reaction), meaning that the homo-coupling of PBA-SH hardly occurred in this condition (without I_2). (The homo-coupling of PBA-SH smoothly proceeded only in the presence of I_2 (**Figure 3.3**).) Thus, the GPC chromatogram shift observed in **Figure 3.4a** and **3.4c** (without I_2) resulted mainly from the desired hetero-coupling of PBA-SH and PBA-SS-Py.

Hetero-coupling of PBA-SH and PBzA-SS-Py to Generate Block Copolymer. We studied the hetero-coupling of PBA-SH and PBzA-SS-Py, where PBzA is poly(benzyl acrylate). A mixture of PBA-SH (M_n = 3400 and $Đ$ = 1.22) (1 equiv), PBzA-SS-Py (M_n = 3600 and $Đ$ = 1.16) (nearly 1 equiv), and DMF (solvent) (70 wt%) was stirred at room temperature for 16 h **(Figure 3.5)**. **Figure 3.5a** shows the GPC chromatograms using a refractive index (RI) detector for the original PBA-SH (green solid line), the original PBzA-SS-Py (red solid line), and the product after the reaction (blue solid line), demonstrating that large fractions of PBA-SH and PBzA-SS-Py were converted to a higher molecular-weight species, i.e., PBA-SS-

PBzA. The GPC chromatograms were also obtained using an ultraviolet (UV) detector at 280 nm to observe the decay of PBzA-SS-Py separately from the decay of PBA-SH. The PBzA-SS-Py contains aromatic rings and hence is visible at 280 nm, while PBA-SH does not contain aromatic rings and is invisible at 280 nm. **Figure 3.5b** shows the UV-detected GPC chromatograms of PBzA-SS-Py (red solid line) and the product after the 16 h reaction (blue solid line), clearly demonstrating that the generated higher molecular-weight species contained the PBzA segment. Upon the peak resolution of the chromatogram after the 16 h reaction, we estimated the remaining PBzA-SS-Py to be at most 22%. These results suggest the successful hetero-coupling of PBA-SH and PBzA-SS-Py to generate a PBA-SS-PBzA block copolymer with a relatively high efficiency (>78%). For the peak resolution, using the known chromatogram of PBzA-SS-Py (red solid line), we subtracted the chromatogram of the remaining PBzA-SS-Py (red dashed line) from that of the product polymer (blue solid line) to give that of the generated PBA-SS-PBzA block copolymer (green dashed line).

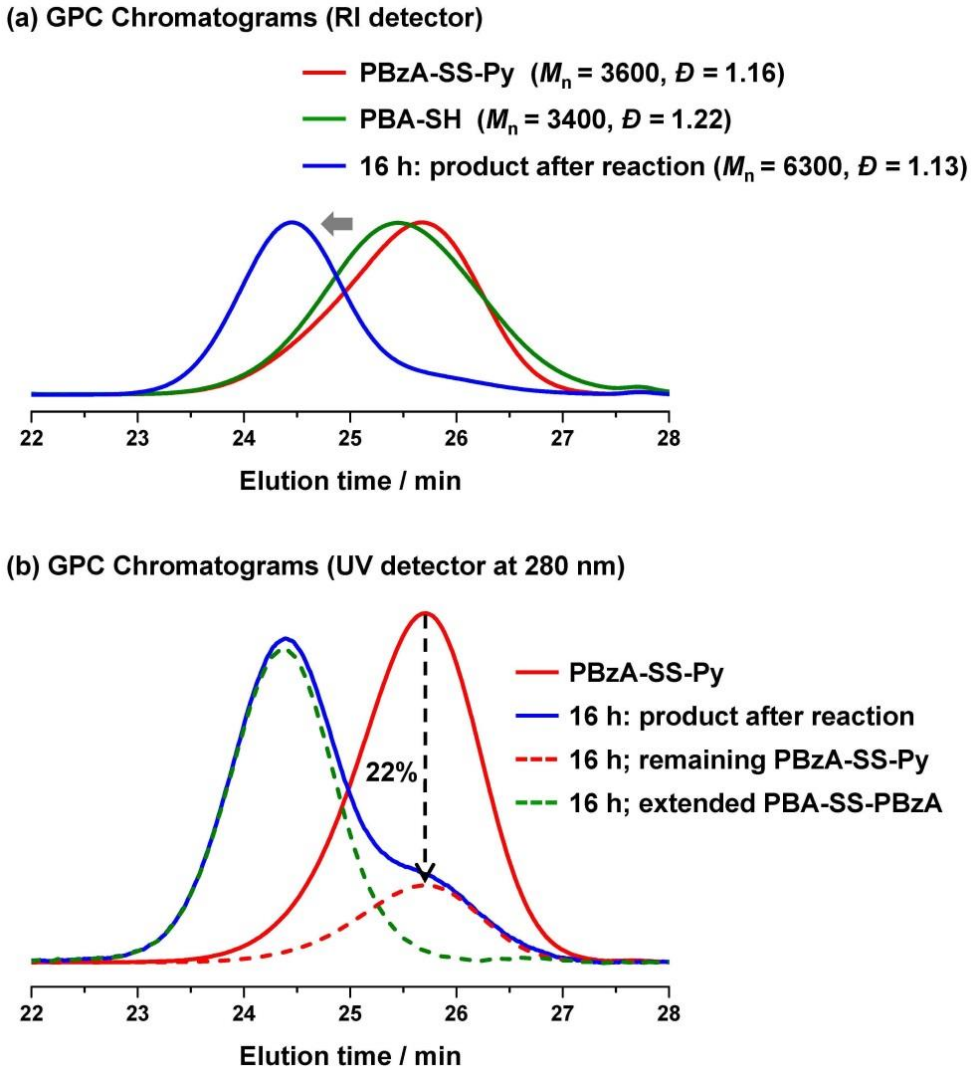

Figure 3.5. (a) GPC traces of PBA-SH (M_n = 3400 and $Đ$ = 1.22) (green solid line), PBzA-SS-Py (M_n = 3600 and $Đ$ = 1.16) (red solid line), and the polymer product after the hetero-coupling of the PBA-SH (1 equiv) and the PBzA-SS-Py (nearly 1 equiv) in DMF (solvent) (70 wt%) at room temperature for 16 h (blue solid line). The detector was a refractive index (RI) detector. (b) GPC traces of PBzA-SS-Py (red solid line) and the polymer product after 16 h (blue solid line). The detector was an ultra violet (UV) detector. Upon the peak resolution of the blue solid line, the red and green dashed lines show the remaining and extended polymers, respectively.

3.3.6. Rewritable Polymer Brush Surface. We exploited the mentioned hetero-coupling reaction to create a rewritable polymer brush surface that enables the sequence of writing, erasing, and rewriting. We prepared three SH-terminated polymers **(Figure 3.6)**, i.e., super-hydrophobic poly(1*H*,1*H*,2*H*,2*H*-nonafluorohexyl acrylate) (PNFHA-SH) (M_n = 5800 and $Đ$ = 1.04), hydrophobic PBA-SH (M_n = 4200 and $Đ$ = 1.20), and hydrophilic poly(poly(ethylene glycol) methyl ether acrylate) (PPEGA-SH) (M_n = 7700 and $Đ$ = 1.13) (**Chapter 3.6**). **Figure 3.6** illustrates the sequence of writing, erasing, and rewriting. We first immobilized (3-mercaptopropyl)triethoxysilane ($(EtO)_3SiCH_2CH_2CH_2SH$ (**Figure 3.1**)) on a silicon wafer via the anchoring $(EtO)_3Si$ group and obtained an SH-functionalized wafer with a water contact angle (WCA) of 75° (**Figure 3.6**). The SH group was subsequently reacted with Py-SS-Py, generating the pyridyl disulfide (Py-SS)-functionalized wafer with a WCA of 76° (**Figure 3.6**). Polymer chains were then tethered to the surfaces via a so-called "grafting-to" approach whereby pre-synthesized polymers with functionalized chain-ends are bound to the solid surfaces. The mentioned pre-synthesized PNFHA-SH was grafted on the wafer via the hetero-coupling of the surface SS-Py group with PNFHA-SH, giving a PNFHA brush on the surface with a WCA of 100° (writing process) (**Figure 3.6**). The PNFHA was grafted to the surface via an -SS- linkage. We subsequently cleaved the -SS- linkage using a reducing agent, i.e., DTT in a basic condition (in the presence of tributylamine (TBA)), regenerating the original SH-immobilized surface with a WCA of 75° (erasing process) (**Figure 3.6**). This surface was again treated with Py-SS-Py and followed by the hetero-coupling with another polymer PBA-SH, giving a PBA brush on the surface with a WCA of 81° (re-writing process) (**Figure 3.6**). The erasing and re-writing cycle was repeatable and reproducible, generating a PNFHA brush with a WCA of 105° again in the third cycle and a PPEGA brush with a WCA of 64° in the fourth cycle (**Figure 3.6**). Thus, we successfully created the re-writable brush surface and tailored the surface wettability ranging from super-hydrophobic to hydrophobic and to

hydrophilic surface nature. The keys to this cycle are the highly efficient hetero-coupling and DTT-mediated disulfide cleavage that enabled the reversible fabrication of Polymer-SH.

The contact angles of the PNFHA brushes in the first (100°) and third (105°) cycles were relatively similar, suggesting that the graft density remained relatively similar in the repeated cycles for the same polymer. The graft-density would depend on the kind and molecular weight of the polymer and would be smaller with an increase in the steric hindrance and molecular weight of the polymer because of the grafting-to approach.

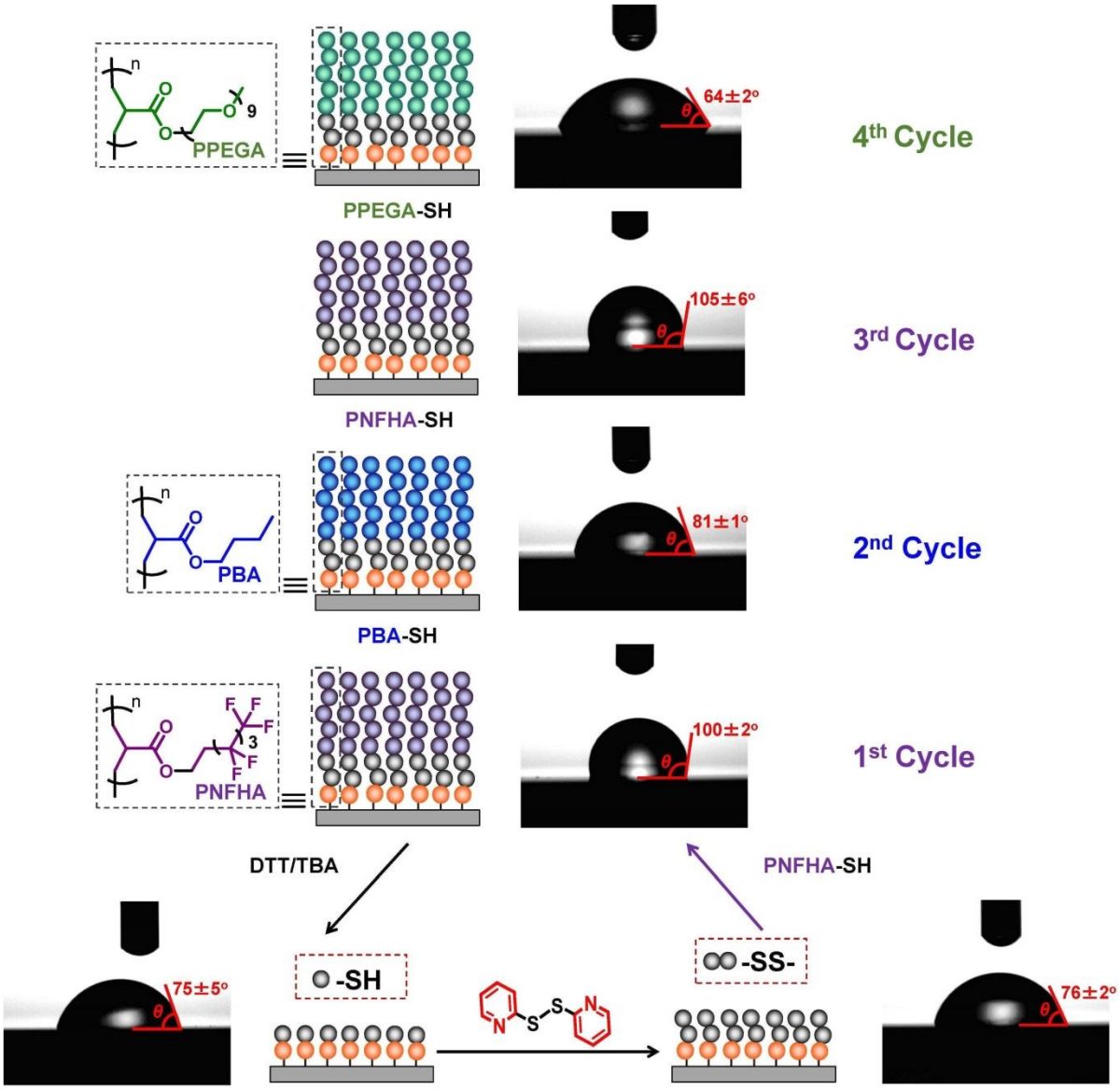

Figure 3.6. Conversion of SH-functionalized surface to Py-SS-functionalized surface, grafting of Polymer-SH to Py-SS-functionalized surface for generating polymer brush, and removal of Polymer-SH from polymer brush for generating SH-functionalized surface in a recycled manner.

To probe the writing and erasing processes, we carried out the X-ray photoelectron spectroscopy (XPS) analysis of the original (Py-SS-immobilized) surface (**Figure 3.7a**), the PNFHA-grafted surface (after the writing process) (**Figure 3.7b**), and the PNFHA-cleaved surface (after the erasing process via the treatment with DTT and TBA) (**Figure 3.7c**) in the first cycle. After the grafting of PNFHA (writing process), the fluorine 1s electron signal (688 eV) originated from the fluorinated pendant groups of PNFHA was clearly observed. After the cleavage of PNFHA via the treatment with DTT and TBA (erasing process), the fluorine signal virtually completely disappeared. The XPS analysis confirmed successful grafting of PNFHA (writing process) and virtually quantitative cleavage of PNFHA (erasing process).

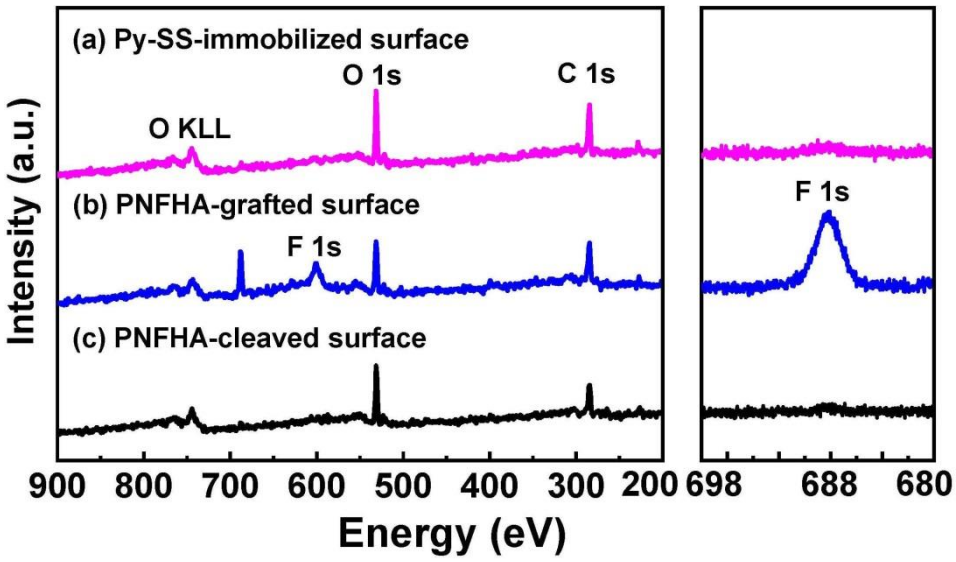

Figure 3.7. XPS survey and high-resolution F 1_S spectra of (a) Py-SS-immobilized surface, (b) PNFHA-grafted surface (after the writing process), and (c) PNFHA-cleaved surface (after the erasing process via the treatment with DTT and TBA).

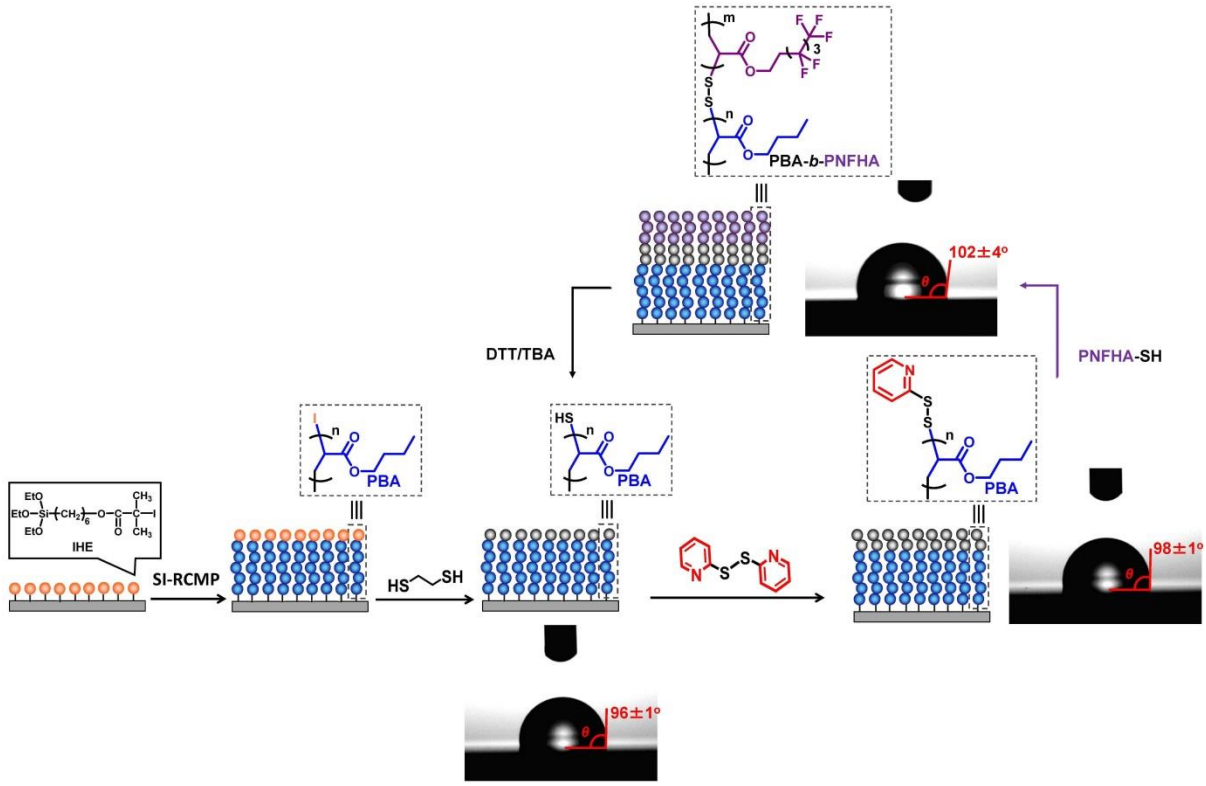

Figure 3.8. Preparation of PBA-I brush via surface-initiated RCMP, chain-end conversion of PBA-I brush to PBA-SH brush, chain-end conversion of PBA-SH brush to PBA-SS-Py brush, grafting of PNFHA-SH to PBA-SS-Py brush for generating block copolymer brush, and removal of PNFHA-SH from the block copolymer brush for generating PBA-SH brush.

3.3.7. Block Copolymer Brush Surface. We further extended the scope of the surface. We exploited the polymer-polymer hetero-coupling to create a rewritable block copolymer brush surface. **Figure 3.8** illustrates the concept and preparation of the rewritable block copolymer surface.

Surface-initiated LRP, which is a "grafting-from" approach, is a useful method to synthesize concentrated polymer brushes covalently tethered to solid surfaces with high grafting densities.[50-55] Such high graft densities render the polymer chains to extend

perpendicular to the surface, and the chain-ends tend to be located at the outermost surface of the polymer brush. We immobilized 6-(2-Iodo-2-isobutyryloxy)hexyltriethoxysilane (IHE (**Figure 3.8**)) on a silicon wafer and obtained the alkyl iodide-immobilized surface.[74-76] The subsequent surface-initiated RCMP of BA from the alkyl iodide initiating dormant species generated a concentrated PBA brush with the iodide chain end. The thickness of the brush was 12 nm and the surface occupancy (σ*) was 13%, which is located in the concentrated regime (σ* >10%) (**Table S3.2** in **Chapter 3.6**). The chain-end iodide was then transformed to SH using $HSCH_2CH_2SH$, generating an SH-terminated PBA brush surface with a WCA of 96° (**Figure 3.8**).

The SH-terminated PBA brush surface was used as a writable and erasable surface (**Figure 3.8**). We treated the brush with Py-SS-Py, generating the Py-SS-terminated PBA brush surface with a WCA of 98°. As mentioned, because of the high graft density, the chain-end Py-SS group tends to be located at the outermost surface and is allowed to react with an external polymer molecule. Via the polymer-polymer hetero-coupling, the pre-synthesized super-hydrophobic PNFHA-SH (M_n = 5800 and $Đ$ = 1.04) was grafted to the PBA brush, generating a PBA-*b*-PNFHA block copolymer brush with a slightly increased WCA of 102° because of the super-hydrophobicity of the PNFHA segment (writing process). The grafted PNFHA segment was then removed via the DTT/TBA-assisted disulfide cleavage, and the surface was restored to the original PBA-SH brush surface with a WCA of 96° (erasing process), displaying the writable and erasable block copolymer surface.

3.3.8. Patterning. We also erased the grafted PNFHA segment from the block copolymer brush in a patterned manner **(Figure 3.9a)** using photo-irradiation. On the PBA-*b*-PNFHA block copolymer brush, a mixture of DTT (5 wt%) and a photo-initiator Irgacure D-2959 (1 wt%) in acetone was dropped. A cover glass was placed to form a thin solution layer, on which

a photomask with a stripe pattern was placed. Subsequently, UV light (wavelength = 365 (± 10) nn) was irradiated for 5 min. The reaction was conducted in a non-basic condition (without TBA), and hence the disulfide cleavage (via an S_N2 process) did not occur in the non-irradiated areas. In the irradiated areas, the disulfide cleavage occurred via a radical process initiated by the photo-decomposition of Irgacure D-2959,[59,60] enabling a patterned erasing of the PNFHA segment. To prove the formation of the pattern, after the UV irradiation, the wafer was immersed in a mixture of a fluorescent molecule 7-diethylamino-3-(4-maleimidophenyl)-4-methylcoumarin (CPM) (**Figure 3.9a**) (1 equiv, 0.03wt%) and TBA (4 equiv) in DMF for 1 min. In the erased areas (bearing SH groups), CPM (bearing a maleimide group) can attach via a thiol-ene Michael-addition. The fluorescence microscope image (**Figure 3.9b**) clearly showed a stripe pattern, demonstrating the successful erasing in a patterned manner. (CPM was used to demonstrate the successful erasing in the present work. A CPM-functionalized patterned surface was also previously prepared in a different synthetic approach for a different demonstration purpose.[75])

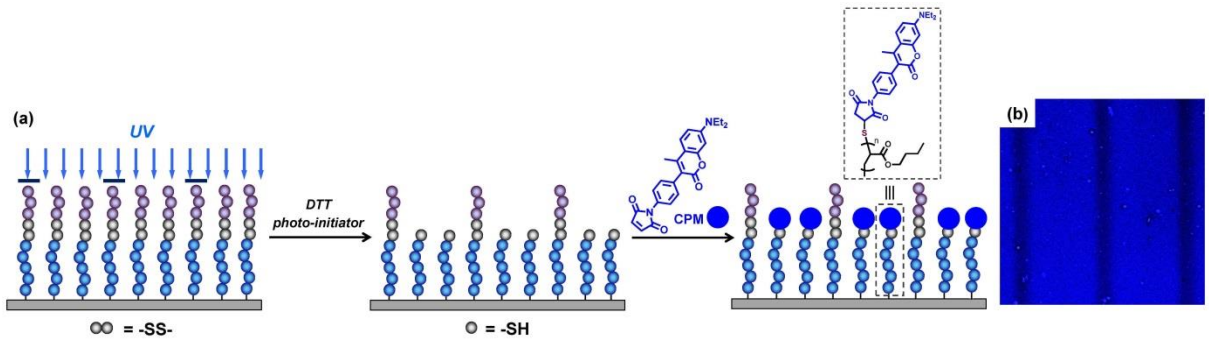

Figure 3.9. (a) Patterned removal (erasing) of PNFHA segment from block copolymer brush using photo-irradiation and a photomask and subsequent attachment of CPM to the erased area. (b) Fluorescence microscope image after the attachment of CPM.

3.4. Conclusion

Polymer-I was converted to Polymer-SH using $HSCH_2CH_2SH$ in a short time (10 min). Polymer-SH was further converted to Polymer-SS-Py. The hetero-coupling of Polymer-SH and Polymer-SS-Py successfully generated Polymer-SS-Polymer (polymer disulfide). Taking advantage of this efficient hetero-coupling reaction, we created rewritable polymer brush and block copolymer brush surfaces. The surface wettability was tailored by attaching hydrophilic, hydrophobic, and super-hydrophobic polymers in the writing-erasing-rewriting cycles. The patterned brush surface was also obtained via a photo-irradiation using a photo-mask in the erasing process. Such rewritable polymer brush and block copolymer brush surfaces may potentially be used in rewritable microarray technologies and sensing interfaces. The metal-free procedure is an attractive feature of the present synthetic technique.

3.5. Experimental Section

3.5.1. Preparation of Polymer-SH. A mixture of Polymer-I (**Chapter 3.6**) (1 equiv, 20 wt%), $HSCH_2CH_2SH$ (20 equiv), $^{i}Pr_2NH$ (4 equiv), and solvent (DMF for Polymer = PBA, PBzA and PPEGA or acetone for Polymer = PNFHA, 80 wt%) in a 50 mL flask was stirred in the dark in the air at room temperature for 10 min for PBA and 2 h for PBzA, PPEGA and PNFHA. After the prescribed time, the mixture was diluted with DMF and the polymer was purified by the reprecipitation in a non-solvent (methanol/H_2O (1/1 (v/v)) for PBA, methanol for PBzA, hexane/diethyl ether (1/1 (v/v)) for PPEGA, and chloroform/methanol (1/3 (v/v)) for PNFHA).

3.5.2. Preparation of Polymer-SS-Py. A mixture of Polymer-SH (1 equiv, 20 wt%), Py-SS-Py (5 equiv), and DMF (80 wt%) in a 50 mL flask was stirred in the air at room temperature for 4 h. After 4 h, the mixture was diluted with DMF and the polymer was purified by the

reprecipitation in a non-solvent (methanol/H_2O (1/1 (v/v)) for PBA, and methanol for PBzA). The polymer was further purified using a preparative GPC to remove trace amounts of small molecules.

3.5.3. Hetero-coupling of PBA-SH and PBA-SS-Py. A mixture of PBA-SH (1 equiv), PBA-SS-Py (nearly 1 equiv), and DMF (70 wt%) in a 4 mL vial was stirred in the air at room temperature for 16 h. The reaction mixture was analyzed with GPC (**Figures 3.4a** and **3.4c**). After 16 h, the mixture was diluted with DMF and the polymer was purified by the reprecipitation in a mixture of methanol/H_2O (1/1 (v/v)) for MALDI-TOF-MS analysis (**Figures 3.4b** and **3.4d**).

3.5.4. Hetero-coupling of PBA-SH and PBzA-SS-Py. A mixture of PBA-SH (1 equiv), PBzA-SS-Py (nearly 1 equiv), and DMF (70 wt%) in a 4 mL vial was stirred in the air at room temperature for 16 h. The reaction mixture was analyzed with GPC (**Figure 3.5**).

3.5.5. Hetero-Coupling of Polymer-SH on Py-SS-immobilized Silicon Wafer. The Py-SS- immobilized silicon wafer (**Chapter 3.6**) was immersed in a mixture of Polymer-SH (10 wt%) and solvent (DMF for PBA-SH and PPEGA-SH and acetone for PNFHA, 90 wt%) in an 8 mL vial in the air at room temperature for 24 h. The wafer was washed with tetrahydrofuran (THF), sonicated in THF for 30 min, and dried under a nitrogen flow.

3.5.6. Removal of Polymer Chain from Silicon Wafer. The silicon wafer fabricated with the polymer brush was immersed in a mixture of DTT (5 wt%), TBA (5 wt%), and solvent (DMF for PBA-SH and PPEGA-SH and acetone for PNFHA, 90 wt%) in an 8 mL vial in the air at room temperature for 14 h. The wafer was washed with THF, sonicated in THF for 30 min, and dried under a nitrogen flow.

3.6. Appendix

3.6.1. Materials and Instrument

3.6.1.1. Materials. Butyl acrylate (BA) (>99%, Tokyo Chemical Industry (TCI), Japan), poly(ethylene glycol) methyl ether acrylate (PEGA) (M_n = 480, Sigma-Aldrich, USA), 1*H*,1*H*,2*H*,2*H*-nonafluorohexyl acrylate (NFHA) (>98%, TCI), benzyl acrylate (BzA) (>97%, TCI), 2-iodo-2-methylpropionitrile (CP-I) (>95%, TCI), (3-mercaptopropyl)triethoxysilane (>96%, TCI), tetra-*n*-octylammonium iodide (ONI) (>98%, TCI), tetrabutylammonium iodide (BNI) (>98%, TCI), 1,2-ethanedithiol ($HSCH_2CH_2SH$) (>99%, TCI), 2,2'-dipyridyl disulfide (Py-SS-Py) (>98%, TCI), diisopropylamine ($^iPr_2NH$) (>99%, Alfa Aesar, USA), tributylamine (TBA) (>98%, TCI), *D*,*L*-dithiothreitol (DTT) (>97%, Sigma-Aldrich), 2-hydroxy-4'-(2-hydroxyethoxy)-2-methylpropiophenone (Irgacure D-2959) (98%, Sigma-Aldrich), lithium bromide (>99.0%, TCI), isopropanol (≥99.7%, Xilong Scientific, China), ammonia solution (28% in water, TCI), acetone (≥99.8%, VWR Chemicals, USA), chloroform (>99.0%, VWR Chemicals), ethanol (≥99.8%, absolute, Fisher Scientific), tetrahydrofuran (THF) (≥99.7%, VWR Chemicals), hexane (>99%, International Scientific, Singapore), diethyl ether (>99.7%, International Scientific), *N*,*N*-dimethyl formamide (DMF) (>99.5%, Kanto Chemical, Japan), methanol (≥99.8%, VWR Chemicals), trans-2-[3-(4-t-butylphenyl)-2-methyl-2-propenylidene]malononitrile (DCTB) (≥99.0%, Sigma-Aldrich), and sodium trifluoroacetate (NaTFA) (>98%, TCI) were used as received. A silicon wafer (produced by Czochralski process, thickness: 525 ± 25 μm) was purchased from Matsuzaki Seisakusho (Japan). 6-(2-Iodo-2-isobutyryloxy)hexyltriethoxysilane (IHE) (>95%) was provided through the courtesy of Godo Shigen Co., Ltd. (Japan). The glass photomasks (Hunan Omnisun Information Material, China) are polished on both sides with a patterned low-reflective chrome film on one side. **Figure S3.1** shows the photomask used in this work.

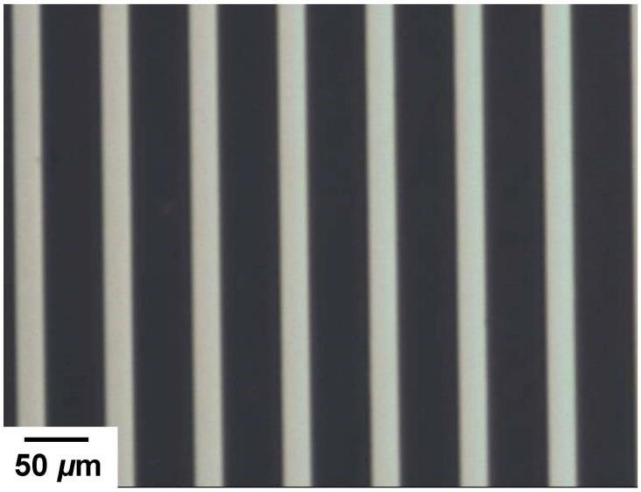

Figure S3.1. Optical microscope image of the photomask used in this work. The dark area is unmasked and the bright area is masked.

3.6.1.2. UV-Ozone Cleaner. The cleaning of the silicon wafers was conducted with a digital UV-ozone cleaner (PSD Pro Series, Novascan Technologies, Germany).

3.6.1.3. UV-LED Light. The UV light source was a Hamamatsu Photonics (Japan) UV-LED light (wavelength = 365 (± 10) nm, energy = 900 mW/cm^2, model: C11924-101). The light energy (mW/cm^2) was measured using a Coherent (USA) laser power meter (FieldMate).

3.6.1.4. Preparative GPC. Polymers were purified with a preparative GPC (LC-9204, Japan Analytical Industry, Tokyo) equipped with JAIGEL 1H and 2H polystyrene gel columns (600×40 mm; bead size = 16 μm; pore size = 20-30 (1H) and 40-50 (2H) Å). Chloroform was used as eluent at a flow rate of 14 mL/min (room temperature).

3.6.1.5. Analytical GPC. The gel permeation chromatograph (GPC) analysis using THF as an eluent was performed on a Shimadzu (Kyoto, Japan) LC-2030C Plus liquid chromatograph equipped with a Shodex (Tokyo, Japan) LF-804 column (300 × 8.0 mm; bead size = 6 μm; pore size = 3000 Å) and a Shodex KF-804L mixed gel column (300 × 8.0 mm;

bead size = 7 μm; pore size = 1500 Å). The GPC analysis using DMF as an eluent was performed on a Shodex (Tokyo, Japan) GPC-101 liquid chromatograph equipped with two Shodex KF-804L mixed gel columns (300 × 8.0 mm; bead size = 7 μm). The flow rate was 0.7 mL/min (THF) or 0.34 mL/min (DMF) (40 °C for both THF and DMF). The DMF eluent contained LiBr (10 mM). Sample detection and quantification were conducted using a Shimadzu refractive index detector (RID-20A) for THF-GPC and a Shodex differential refractometer RI-101 for DMF-GPC. The column system was calibrated with standard poly(methyl methacrylate)s (PMMAs) in the THF and DMF systems. For poly(benzyl acrylate) (PBzA), sample detection and quantification were also conducted using a Shimadzu UV detector (wavelength = 280 nm) for THF-GPC (**Figure 3.5b**).

3.6.1.6. MALDI-TOF-MS. The matrix assisted laser desorption/ionization time-of-flight mass spectrometry (MALDI-TOF-MS) spectra were recorded on a JMS-S3000 SpiralTOF (JEOL Ltd., Japan) at an accelerating potential of 20 kV in the positive spiral mode. We prepared polymer solution (PBA: 10 g/L in THF), matrix solution (DCTB: 60 g/L, in THF), and cationization agent solution (NaTFA: 10 g/L in THF). The polymer solution, the DCTB solution, and the cationization agent solution were mixed in a ratio of (v/v/v = 1/2/1 for PBA-I and PBA-SS-Py and v/v/v = 1/1/0.05 for PBA-SH). Then, 5 μL of the mixed solution was deposited on the target plate spot and dried in the air at room temperature.

3.6.1.7. NMR. The ^{1}H NMR spectra were recorded on a Bruker (Germany) BBFO400 spectrometer (400 MHz) or a Bruker AV500 spectrometer (500 MHz) at ambient temperature. Chloroform-*d* ($CDCl_3$, Cambridge Isotope Laboratories, USA) and acetone-*d* (acetone-d_6, Cambridge Isotope Laboratories, USA) were used as NMR solvents, and the chemical shift was calibrated using the residual undeuterated solvent as the internal standard. The monomer conversion was determined with ^{1}H NMR.

3.6.1.8. Contact Angle Measurement. The water-contact angle (WCA) analysis of the polymer brushes was carried out with a DM-701 contact angle meter (Kyowa Interface Science, Japan).

3.6.1.9. AFM. The brush thickness was determined using an atomic force microscope (AFM) (Probe Station AFM5000II, Hitachi High-Technologies, Japan) using a cantilever PRC-DF40P.

3.6.1.10. Confocal Fluorescence Microscopy. The fluorescence images were taken with Zeiss LSM710 (Germany) using the filter set 38 under autoexposure.

3.6.2. General Synthesis of Polymer-I (PBA-I, PPEGA-I and PNFHA-I)

A mixture of monomer (BA, PEGA, or NFHA 15 g), initiating alkyl iodide dormant species (CP-I), and catalyst (BNI for BA and PEGA and ONI for NFHA) in a 200 mL flask and heated at 110 °C under argon atmosphere with magnetic stirring. After the polymerization, the mixture was cooled to room temperature and diluted with THF. The solution was dropped into a mixture of non-solvent (methanol/H_2O (700 mL, v/v = 1/1) for PBA, hexane/diethyl ether (700 mL, v/v = 1/1) for PPEGA, or chloroform/methanol (700 mL, v/v = 1/3) for PNFHA), and the polymer was purified. **Table S3.1** summarizes the result. The obtained polymers were converted to Polymer-SH and used for rewritable surfaces.

Similarly, we obtained PBA-I polymers that were converted to PBA-SH and PBA-SS-Py and used for coupling reactions in solution.

Table S3.1. Synthesis of Polymer-I.

Entry	Monomer	Catalyst	$[Monomer]_0/[CP-I]_0/[Catalyst]_0$ (mM)[a]	Time (h)	Conv (%)[b]	M_n[c] ($M_{n,theo}$[d])	$Đ$[c]
1	BA	BNI	8000/160/640	5	49	4000 (3300)	1.18
2	NFHA	ONI	8000/266/80	14	45	5200 (4500)	1.05
3	PEGA	BNI	8000/160/640	7.5	31	7700 (7500)	1.13

[a]Polymerizations were performed at 110 °C. [b]Monomer conversion determined using ^{1}H NMR. [c]PMMA-calibrated GPC values of the purified polymer using THF (entries 1 and 2) and DMF (entry 3) as GPC eluents. [d]Theoretical M_n values calculated from ($[Monomer]_0/[CP-I]_0$)×(monomer conversion)×(molecular weight of monomer).

3.6.3. Homo-coupling of Polymers in Solution

3.6.3.1. Aerobic Oxidization of PBA-SH Using Iodine. A mixture of PBA-SH (1 equiv, 0.11 g, 20 wt%), iodine (2 equiv), and DMF (80 wt%) in a 4 mL vial was stirred in the air at room temperature for 16 h. The reaction mixture was analyzed with GPC (**Figure 3.3a**). After 16 h, the mixture was diluted with DMF and the polymer was purified by reprecipitation in a mixture of methanol/H_2O (v/v = 1/1) for MALDI-TOF-MS analysis (**Figure 3.3b**).

3.6.3.2. Homo Coupling Reaction of PBA-SS-Py. A mixture of PBA-SS-Py (0.15 g, 20 wt%) and DMF (80 wt%) in a 4 mL vial was stirred in the air at room temperature for 16 h. The reaction mixture was analyzed with GPC (**Figure S3.4a**).

3.6.3.3. Homo Coupling Reaction of PBA-SH Without Using Iodine in the Air. A mixture of PBA-SH (0.11 g, 20 wt%) and DMF (80 wt%) in a 4 mL vial was stirred in the air at room temperature for 16 h. The reaction mixture was analyzed with GPC (**Figure S3.4b**).

3.6.3.4. Homo Coupling Reaction of PBA-SH Without Using Iodine and Without Air. A mixture of PBA-SH (0.22 g, 20 wt%) and DMF (80 wt%) in a 4 mL vial was stirred without air at room temperature for 16 h. The reaction mixture was analyzed with GPC (**Figure S3.5**).

3.6.4. Preparation of SH- and Py-SS-immobilized Silicon Wafer

3.6.4.1. Preparation of SH-immobilized Silicon Wafer. A silicon wafer (8 mm × 8 mm) was cleaned with acetone (with sonication for 30 min), chloroform (with sonication for 30 min), and isopropanol (with sonication for 30 min). After drying under a nitrogen flow, the wafer was placed in the ozone cleaner and irradiated for 30 min. The wafer was immersed in a mixture of (3-mercaptopropyl)triethoxysilane, ethanol, and aqueous ammonia solution (1/89/10 (w/w/w)) at room temperature in a dark condition for one day. The wafer was washed with ethanol, sonicated in ethanol for 30 min, and dried under a nitrogen flow to give an SH-immobilized silicon wafer.

3.6.4.2. Preparation of Py-SS-immobilized Silicon Wafer. The SH-immobilized silicon wafer was immersed in a mixture of Py-SS-Py (5 wt%) and DMF in an 8 mL vial for 24 h at room temperature. The wafer was washed with THF, sonicated in THF for 30 min, and dried under a nitrogen flow to give a Py-SS-immobilized silicon wafer.

3.6.5. Studies of Block Copolymer Brush

3.6.5.1. Preparation of Alkyl Iodide Initiator-immobilized Silicon Wafer. A silicon wafer (8 mm × 8 mm) was cleaned with acetone (with sonication for 30 min), chloroform (with sonication for 30 min), and isopropanol (with sonication for 30 min). After drying under a nitrogen flow, the wafer was placed in the ozone cleaner and irradiated for 30 min. The wafer was immersed in a mixture of IHE, ethanol, and aqueous ammonia solution (1/89/10 (w/w/w)) at room temperature in a dark condition for one day. The wafer was washed with ethanol, sonicated in ethanol for 30 min, and dried under a nitrogen flow to give an IHE-immobilized silicon wafer.

3.6.5.2. Preparation of PBA-I Brush. The IHE-immobilized silicon wafer was heated in a mixture of BA (1.2 g, 9.36 mmol, 1000 equiv), CP−I (1.8 mg, 0.009 mmol, 1 equiv), and BNI (28 mg, 0.075 mmol, 8 equiv) in a Schlenk flask at 110 °C under argon atmosphere for 24 h **(Table S3.2)**. After the polymerization, the solution was cooled to room temperature. A portion of the solution was diluted with THF and analyzed with GPC to determine the molecular weight of the free polymer (non-immobilized polymer formed from CP−I (non-immobilized alkyl iodide initiator)). Another portion of the solution was diluted with $CDCl_3$ and analyzed with ^1H NMR to determine the monomer conversion. The wafer was rinsed with THF, sonicated in THF for 30 min, and dried under a nitrogen flow to give a PBA-I brush. The polymer brush was scratched, and the height gap between the scratched and unscratched areas was measured using AFM. The dry brush thickness (*h*) presented in **Table S3.2** is the brush thickness after the subtraction of the thickness of the IHE initiator layer (2 nm).

3.6.5.3. Calculation of Surface Occupancy. It should be noted that we used PMMA-calibrated GPC to determine the M_n value (**Table S3.2**) and that this M_n value is not an absolute value. We used this M_n value (= 48000) and the molecular weight of BA (= 128.17) and estimated the degree of polymerization (DP) of the polymer to be 370. As a rough estimate, we used this DP value. The surface occupancy (σ^*) of the polymer brush was calculated using the estimated DP value and the *h* value according to *equation* (1):

$$\sigma^* = \frac{h}{0.25\ \text{nm} \times \text{DP}} \times 100\ (\%) \qquad (1)$$

where the length of a repeating unit in the polymer was assumed to be 0.25 nm. (The C_{sp^3}–C_{sp^3} bond distance is 1.53 Å and the bond angle is 109.5°. The alternate C–C–C distance (length of

the monomer unit) is thus calculated to be 0.25 nm.) The surface occupancy (σ*) was thus calculated to be 0.13.

Table S3.2. Synthesis of PBA-I Brush.[a]

Entry	Conv (%)[b]	M_n[c] ($M_{n,theo}$[d])	$Đ$[c]	h (nm)	σ^*
1	35	48000 (45000)	1.40	12	0.13

[a]Polymerization was performed using a mixture of BA (1000 equiv), CP−I (1 equiv), and BNI (8 equiv) heated at 110 °C for 24 h; [b]Monomer conversion determined with ^{1}H NMR; [c]PMMA-calibrated THF-GPC values of the free polymers; [d]Theoretical M_n value calculated according to ([Monomer]$_0$/[CP−I]$_0$)×(monomer conversion)×(molecular weight of monomer).

3.6.5.4. Preparation of PBA-SH Brush. The silicon wafer with the PBA-I brush was immersed in a mixture of $HSCH_2CH_2SH$ (1 equiv, 5 wt%), $^iPr_2NH$ (0.2 equiv), and DMF in an 8 mL vial in the dark in the air at room temperature for 10 min. The wafer was washed with THF, sonicated in THF for 30 min, and dried under a nitrogen flow to give a PBA-SH brush.

3.6.5.5. Preparation of PBA-SS-Py Brush. The silicon wafer with the PBA-SH brush was immersed in a mixture of Py-SS-Py (5 wt%) and DMF in an 8 mL vial for 24 h at room temperature. The wafer was washed with THF, sonicated in THF for 30 min, and dried under a nitrogen flow to give a PBA-SS-Py brush.

3.6.5.6. Preparation of PBA-*b*-PNFHA Brush. The silicon wafer with the Py-SS-PBA brush was immersed in a mixture of PNFHA-SH (10 wt%) and acetone in an 8 mL vial for 24 h at room temperature. The wafer was washed with THF, sonicated in THF for 30 min, and dried under nitrogen flow to give a PBA-*b*-PNFHA brush.

3.6.5.7. Preparation of Patterned Brush and Fluorescent Labeling. One drop of a mixture composed of Irgacure D-2959 (1 wt%), DTT (5 wt%), and acetone was put onto the

wafer with the PBA-*b*-PNFHA brush. A coverslip was placed on the droplet to form an ultrathin solution layer. A striped-patterned (**Figure S3.1**) photomask was placed atop of the coverslip, which was irradiated (wavelength = 365 (± 10) nm and irradiation power = 900 mW/cm^2) for 5 min. The wafer was cleaned by ultra-sonication in THF for 30 min and dried under a nitrogen flow to give a patterned brush. The wafer with the patterned brush was immersed in a mixture of CPM (0.5 mg, 1 equiv), TBA (1 mg, 4 equiv), and DMF (2.0 mL) in the dark at room temperature for 1 min. The wafer was rinsed with THF and dried under nitrogen flow.

3.6.6. MALDI-TOF-MS Spectrum of PBA-I and ^{1}H NMR Spectra of PBA-I, PBA-SH, and PBA-SS-Py

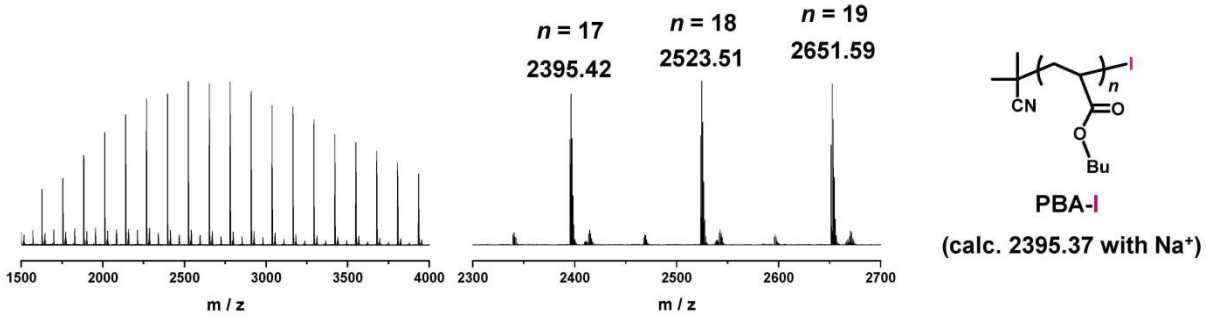

Figure S3.2. MALDI-TOF-MS spectrum of PBA-I.

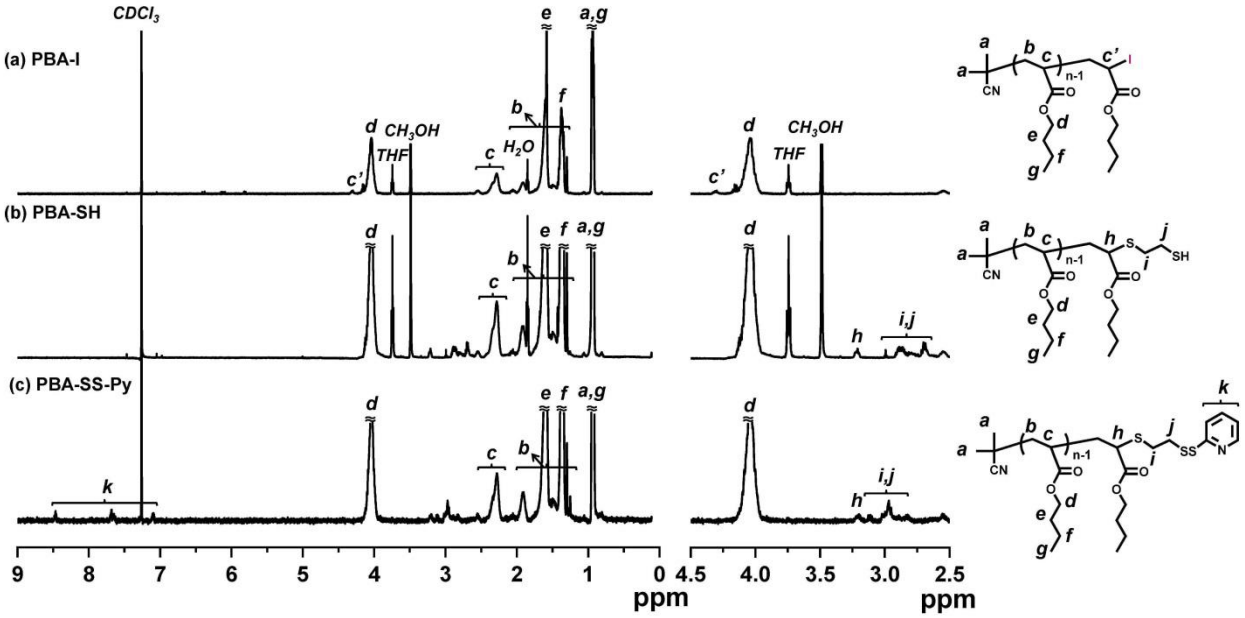

Figure S3.3. ^{1}H NMR spectra of (a) PBA-I, (b) PBA-SH, and (c) PBA-SS-Py.

3.6.7. GPC Spectrum of Homo-coupling of PBA-SH and PBA-SS-Py

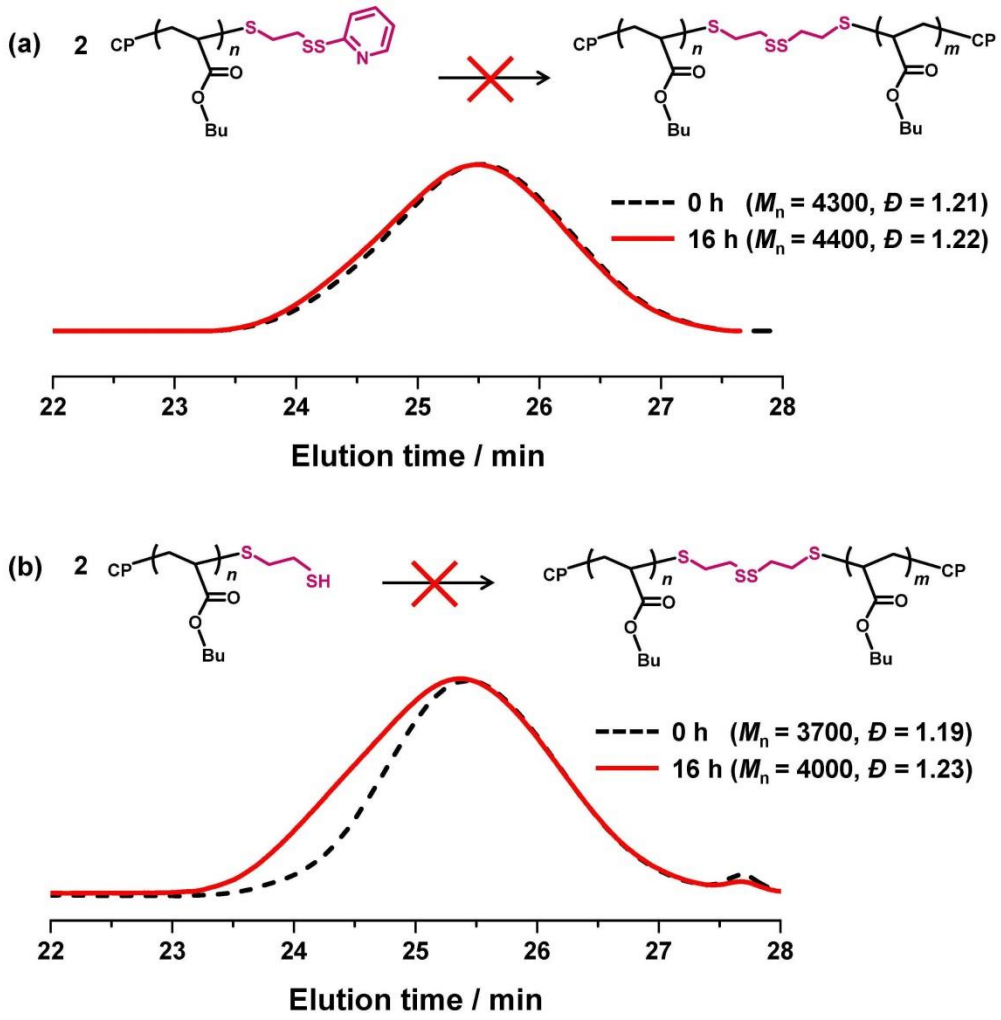

Figure S3.4. (a) GPC traces of PBA-SS-Py (black dashed line) and the polymer product after the homo-coupling of PBA-SS-Py (20 wt%) in DMF (80 wt%) at room temperature for 16 h (red solid line). (b) GPC traces of PBA-SH (black dashed line) and the polymer product after the homo-coupling of PBA-SH (20 wt%) in DMF (80 wt%) at room temperature for 16 h without I_2 (red solid line).

For the homo-coupling of PBA-SH (M_n = 3700 and $Đ$ = 1.19) (20 wt%) in DMF (80 wt%) without I_2 in the air at room temperature for 16 h (**Figure S3.4b**), a slight shift of the GPC chromatogram was observed after 16 h.

As a control experiment, we carried out the same homo-coupling of PBA-SH without I_2 but without air (without oxygen). A slight shift of the GPC chromatogram **(Figure S3.5)** was observed after 16 h, suggesting that the slight shift of the GPC chromatogram (**Figure S3.4b**) was not a resultant of the air oxidation of thiol.

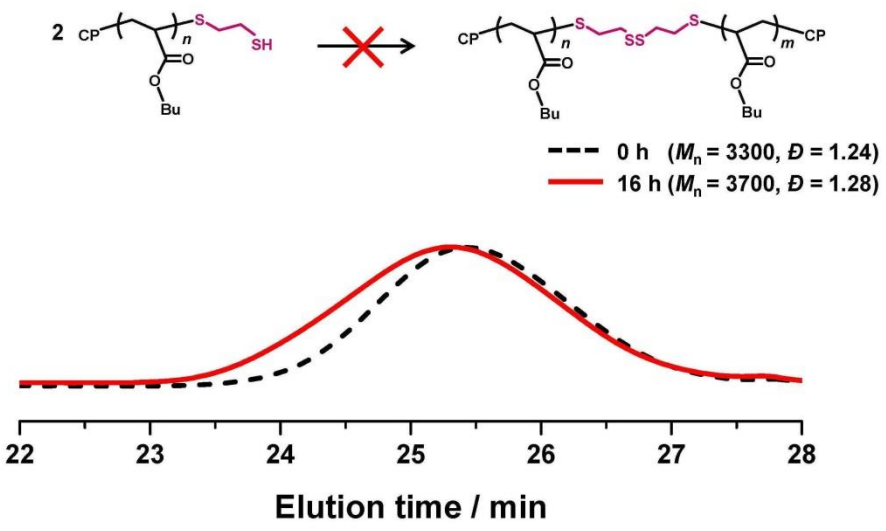

Figure S3.5. GPC traces of PBA-SH (black dashed line) and the polymer product after the homo-coupling of PBA-SH (20 wt%) in DMF (80 wt%) at room temperature for 16 h without I_2 and without air (red solid line), using PBA-SH with M_n = 3300 and $Đ$ = 1.24.

3.6.8. Synthesis of PBzA-SS-Py

A mixture of BzA (15 g, 50 equiv), initiating alkyl iodide dormant species (CP-I) (1 equiv), and catalyst (BNI) (4 equiv) in a 200 mL flask was heated at 110 °C for 1 h under argon atmosphere with magnetic stirring. The monomer conversion was 29%. After the polymerization, the mixture was cooled to room temperature and diluted with THF. The solution was dropped into methanol. The obtained PBzA-I was converted to PBzA-SH and further converted to PBzA-SS-Py (M_n = 3600 and $Đ$ = 1.16 after purification).

Reference(s)

(1) Tasdelen, M. A. et al. *Prog. Polym. Sci.* **2011,** *36*, 455−567.

(2) Wang, K. et al. *Mater. Chem. Front.* **2020**, *4*, 1803−1915.

(3) Rosen, B. M. et al. *J. Polym. Sci., Part A: Polym. Chem.* **2009**, 47, 3931–3939.

(4) Rosen, B. M. et al. *J. Polym. Sci., Part A: Polym. Chem.* **2009**, *47*, 3940–3948.

(5) Tsarevsky, N. V.; Matyjaszewski, K. *Macromolecules* **2002,** *35*, 9009−9014.

(6) Klaikherd, A. et al. *J. Am. Chem. Soc.* **2009,** *131*, 4830−4838.

(7) Sprafke, J. K. et al. *J. Polym. Sci. A Polym. Chem.* **2015**, *53*, 319−326.

(8) Akiyama, T. et al. *J. Polym. Sci. A Polym. Chem.* **2017**, *55*, 3545−3553.

(9) Xu, H. et al. *Polym. Chem.* **2019**, *10*, 5052−5069.

(10) Nair, D. P. et al. *Chem. Mater.* **2013**, *26*, 724−744.

(11) Lowe, A. B. *Polymer* **2014**, *55*, 5517−5549.

(12) Kaur, G. et al. *Mater. Today Chem.* **2018**, *8*, 56−84.

(13) Xu, Z.; Bratlie, K. M. *ACS Biomater. Sci. Eng.* **2018**, *4*, 2276−2291.

(14) Wang, X. et al. *Macromol. Rapid Commun.* **2020**, *41*, 1900540.

(15) McKinlay, C. J. et al. *J. Am. Chem. Soc.* **2016**, *138*, 3510−3517.

(16) Fan, W. et al. *Biomaterials* **2016**, *103*, 101−115.

(17) Escorihuela, J. et al. *Adv. Mater. Interfaces* **2015,** *2*, 1500135.

(18) Cozzens, Y. et al. *Macromolecules* **2019**, *52*, 2900−2910.

(19) Moraes, J. et al. *Small* **2015**, *11*, 482−488.

(20) Yun, H. et al. *ACS Nano* **2020**, *14*, 9644−9651.

(21) Pei, D. et al. *Colloids Surf. B Biointerfaces* **2015**, *126*, 367−373.

(22) Watanabe, A. et al. *J. Polym. Sci. A Polym. Chem.* **2018**, *56*, 1259−1268.

(23) Wiarachai, O. et al. *Langmuir* **2016**, *32*, 1184−1194.

(24) Pan, C. et al. *J. Mater. Chem. B* **2018**, *6*, 556−567.

(25) Nicolas, J. et al. *Prog. Polym. Sci.* **2013,** *38*, 63−235.

(26) Matyjaszewski, K.; Tsarevsky, N. V. *J. Am. Chem. Soc.* **2014,** *136*, 6513−33.

(27) Matyjaszewski, K. *Adv. Mater.* **2018,** *30*, 1706441.

(28) Ouchi, M.; Sawamoto, M. *Macromolecules* **2017**, *50*, 2603−2614.

(29) Keddie, D. J. et al. *Macromolecules* **2012,** *45*, 5321−5342.

(30) Perrier, S. *Macromolecules* **2017**, *50*, 7433−7447.

(31) David, G. et al. *Chem. Rev.* **2006**, *106*, 3936−3962.

(32) Yamago, S. *Chem. Rev.* **2009**, *109*, 5051−5068.

(33) Debuigne, A. et al. *Prog. Polym. Sci.* **2009**, *34*, 211−239.

(34) Destarac, M. *Polym. Chem.* **2018,** *9*, 4947−4967.

(35) Wang, C.-G. et al. *Polym. Chem.* **2020,** *11*, 5559−5571.

(36) Goto, A. et al. *J. Am. Chem. Soc.* **2013,** *135*, 11131−11139.

(37) Ohtsuki, A. et al. *J. Am. Chem. Soc.* **2015,** *137*, 5610−5617.

(38) Wang, C.-G.; Goto, A. *J. Am. Chem. Soc.* **2017,** *139*, 10551−10560.

(39) Xu, H. et al. *Macromolecules* **2019,** *52*, 2156−2163.

(40) Wang, C.-G. et al. *Macromolecules* **2019**, *52*, 2712−2718.

(41) Chen, C. et al. *Macromolecules* **2016,** *49*, 9425−9440.

(42) Mandal, B.; Basu, B. *RSC Adv.* **2014**, *4*, 13854.

(43) Mukherjee, I. et al. *Biomacromolecules* **2018,** *19*, 2286−2293.

(44) Hermanson, G. T. *The Reactions of Bioconjugation.* In *Bioconjugate Techniques*; Elsevier Academic Press: USA, **2013**, pp. 229−258.

(45) Dao, V. H. et al. *Polym. Chem.* **2017**, *8*, 6834−6843.

(46) Yan, J. et al. *ACS Appl. Polym. Mater.* **2020**, *2*, 1634−1643.

(47) Chang, K. et al. *Eur. Polym. J.* **2019**, *112*, 822−831.

(48) Klaikherd, A. et al. *Macromolecules* **2007**, *40*, 8518−8520.

(49) Altinbasak, I. et al. *Polym. Chem.* **2020**, *11*, 7603−7624.

(50) Zoppe, J. O. et al. *Chem. Rev.* **2017,** *117*, 1105−1318.

(51) Chen, W.-L. et al. *Macromolecules* **2017,** *50*, 4089−4113.

(52) Yan, J. et al. *Prog. Polym. Sci.* **2020,** *100*, 101180.

(53) Mocny, P.; Klok, H.-A. *Prog. Polym. Sci.* **2020,** *100*, 101185.

(54) Tsujii, Y. et al. *Adv. Polym. Sci.* **2006**, *197*, 1−45.

(55) Ma, S. et al. *NPG Asia Mater.* **2019**, *11*, 1−39.

(56) Wang, S. et al. *Mater. Chem. Front.* **2020**, *4*, 692−714.

(57) Arumugam, S.; Popik, V. V. *J. Am. Chem. Soc.* **2012,** *134*, 8408−8411.

(58) Gandavarapu, N. R. et al. *Adv. Mater.* **2014,** *26*, 2521−2526.

(59) Du, X. et al. *Adv. Mater.* **2015,** *27*, 4997−5001.

(60) Li, L. et al. *Angew. Chem. Int. Ed.* **2016,** *55*, 13765−13769.

(61) Smith, E. A. et al. *Langmuir* **2001**, *17*, 2502−2507.

(62) Gevrek, T. N. et al. *ACS Appl. Mater. Interfaces* **2018**, *10*, 14399−14409.

(63) Liu, J. et al. *Adv. Funct. Mater.* **2019**, *30*, 1907605.

(64) Dong, Z. et al. *Adv. Mater. Interfaces* **2020**, *7*, 1902100.

(65) Roling, O. et al. *Angew. Chem. Int. Ed.* **2015,** *54*, 13126−13129.

(66) Vauthier, M. et al. *Adv. Funct. Mater.* **2019**, *29*, 1806765.

(67) Goldmann, A. S. et al. *Adv. Mater.* **2019**, *31*, 1902665.

(68) Blinco, J. P. et al. *Adv. Mater.* **2011**, *23*, 4435−4439.

(69) Dirlam, P. T. et al. *Langmuir* **2010**, *26*, 3942−3948.

(70) Chen, C. et al. *Chem. Commun.* **2018,** *54*, 13738−13741.

(71) Anastasaki, A. et al. *Polym. Chem.* **2017,** *8*, 689−697.

(72) Goto, A. et al. *Macromolecules* **2011**, *44*, 8709−8715.

(73) Singh, R.; Whitesides, G. M. *"Thiol-Disulfide Interchange."* In *The Chemistry of Sulfur-Containing Functional Groups*; J. Wiley and Sons Ltd.: London, **1993**.

(74) Wang, C.-G. et al. *Angew. Chem. Int. Ed.* **2018**, *57*, 13504−13508.

(75) Chen, C. et al. *Polym. Chem.* **2019**, *10*, 5913−5919.

(76) Sim, X. M. et al. *ACS Appl. Mater. Interfaces* **2020**, *12*, 28711−28719.

Chapter 4 Size Recognition of External Molecules on Polymer Brushes using Aggregation Induced Emission

4.1. Abstract: Aggregation-induced emission (AIE)-driven fluorescent polymer brushes, i.e., poly(4-(1,2,2-triphenylvinyl)phenyl methacrylate) (PTPMA) brushes, were prepared in patterned manners with different graft-density domains. The obtained patterned brushes served as a conceptually molecular size analyser; namely, the sizes of external molecules were recognized via the changes in the fluorescence intensities of the polymer brushes. Small-size external molecules were able to enter the polymer brush layers, inducing the fluorescent side groups in the brush chains to aggregate and enhancing the fluorescence intensity via AIE. On the other hand, large-size external molecules were unable to enter the polymer brush layer, resulting in no significant change in the fluorescence intensity. The size exclusion (molecular weight) threshold of external molecules depends on the grafting density. As a demonstration, the present work distinguished external molecules with molecular weights of 300 and 1000 via the change in the fluorescence intensity of the brushes with different graft densities. The present patterning technique can tune the grafting density in a wide range and hence may offer patterned brushes with a wide range of analysable molecular sizes.

KEYWORDS: *polymer brush, size recognition, aggregation-induced emission, grafting density, 3D-pattern, polymerization, surface patterning, functional surface*

4.2. Introduction

Fabrication of polymer brushes on solid surfaces offers a useful method to imbue the surface with desired properties such as biological, mechanical, optical, stimuli-responsive, and so on.[1–13] The conformation of the brush polymers in a good solvent (in a swollen state) depends on the grafting density (surface occupancy (σ^*)) (**Figure 4.1**).[14,15] At low graft densities, diluted polymer brushes ($\sigma^* \leq 1-2\%$, typically) will take on a "mushroom" conformation analogous to that of ungrafted (free) polymer chains. As the grafting density increases, brush polymer chains begin to overlap with neighbouring chains and are compelled to stretch away from the surface. The stretched brushes may be categorized into "semi-diluted" polymer brushes ($\sigma^* = 1-10\%$, typically) and concentrated polymer brushes ($\sigma^* \geq 10\%$, typically), where the brush polymer chains tend towards chain extension perpendicular to the surface because of the steric repulsion. The grafting density can significantly affect important properties such as adhesion, friction, and antifouling.[16,17]

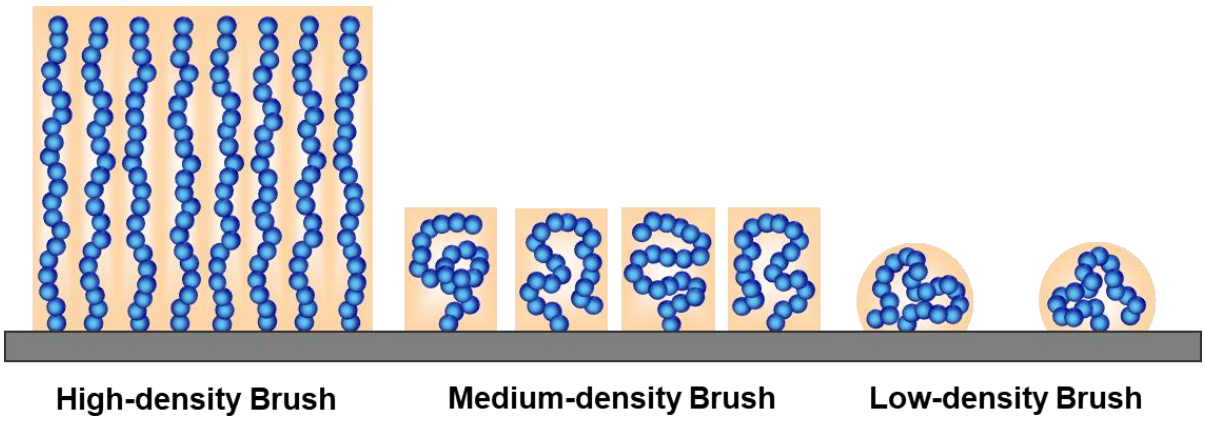

Figure 4.1. Visual representation of high-density, medium-density, and low-density brushes.

Patterned polymer brushes comprising different graft densities have demonstrated significant utility in e.g., bio-microarray technologies, molecular recognition interfaces, and microelectronic devices since different physical properties such as different biocompatibility,

molecular recognition, and electron conductivity are arranged onto a single surface.[18–22] Recent development of lithography techniques such as electron-beam lithography,[23,24] interference laser lithography,[19,25] hypersurface photolithography,[26] scanning-probe lithography,[27–29] and microcontact printing[30,31] has enabled the fabrication of patterns brushes.[32] Patterned brushes with controlled graft densities have also been fabricated using surface-initiated living (reversible-deactivation) radical polymerization from prepatterned initiators.[2,5,8,9,14,15,20,33,34]

Scheme 4.1. Reversible Activation in Reversible Complexation-Mediated Polymerization (RCMP).

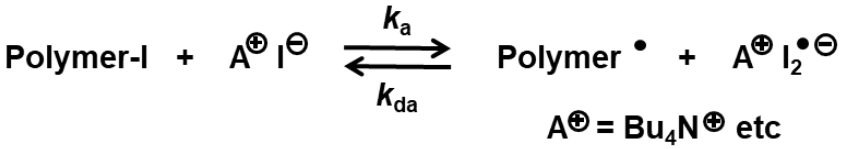

Our research group has developed an organocatalyzed living radical polymerization, termed reversible complexation mediated polymerization (RCMP),[35–40] using a polymer-iodide (Polymer−I) as a dormant species and iodide anion (I^-) as a catalyst (**Scheme 4.1**). The coordination of Polymer−I and I^- yields a halogen-bonding complex (Polymer−I···I^-), which subsequently reversibly generates a propagating radical (Polymer$^•$) and $I_2^{•-}$. I^- is used in the form of salts such as tetra-*n*-butylammonium iodide ($Bu_4N^+I^-$ (BNI)).[35,39] RCMP is a metal-free technique that does not need a special capping agent for the polymerization of a range of functional monomers. We have also prepared polymer brushes on surfaces by immobilizing an initiator, i.e., 6-(2-iodo-2-isobutyryloxy)hexyltriethoxysilane (IHE, **Figure 4.2a**), on surfaces.[41–44] IHE possesses a weak carbon-iodide and was able to undergo rapid degradation (≤ 10 min) upon UV exposure (250−385 nm). We have conducted patterned UV degradation

of the surface-immobilized IHE and RCMP and prepared patterned polymer brushes with controlled graft densities tailored by the UV exposure (IHE-degradation) time.[42]

Luminescent materials are widely used for molecular sensing, information encoding, biological imaging, and so forth.[45–47] Even though many conventional organic luminogens are known for having high quantum efficiencies in dilute solutions, their emission is often impeded by the aggregation-caused quenching (ACQ) effect by which the luminogens undergo partial or complete quenching in the aggregated state.[46] In 2001, Tang et al. pioneered a class of aggregation-induced emission (AIE)-type luminogens (i.e., AIEgens) that exhibited enhanced emission in the aggregated states, which is a phenomenon opposite to ACQ.[48–52] Restriction of the molecular motions in the aggregated state suppresses thermal decay of the exited luminogens, resulting in enhanced photo-emission. AIEgens have also been incorporated in polymers, finding applications in microporous materials and biological applications.[49,53–58] The embedding of AIEgens into polymer brushes has also offered control in optoelectronic properties and sensing applications.[59,60]

In the present work, we synthesized concentrated to semi-diluted polymer brushes via surface-initiated RCMP using an AIE monomer, i.e., 4-(1,2,2-triphenylvinyl)phenyl methacrylate (TPMA (**Figure 4.2a**)) for size recognition of external molecules. We prepared patterned polymer brushes comprising different graft densities to selectively capture external molecules of different sizes and detected the capture of the external molecules in the polymer brushes by the AIE intensities, enabling the size recognition of external molecules. This system is a conceptually new molecular size analyser in oligomeric molecular regions.

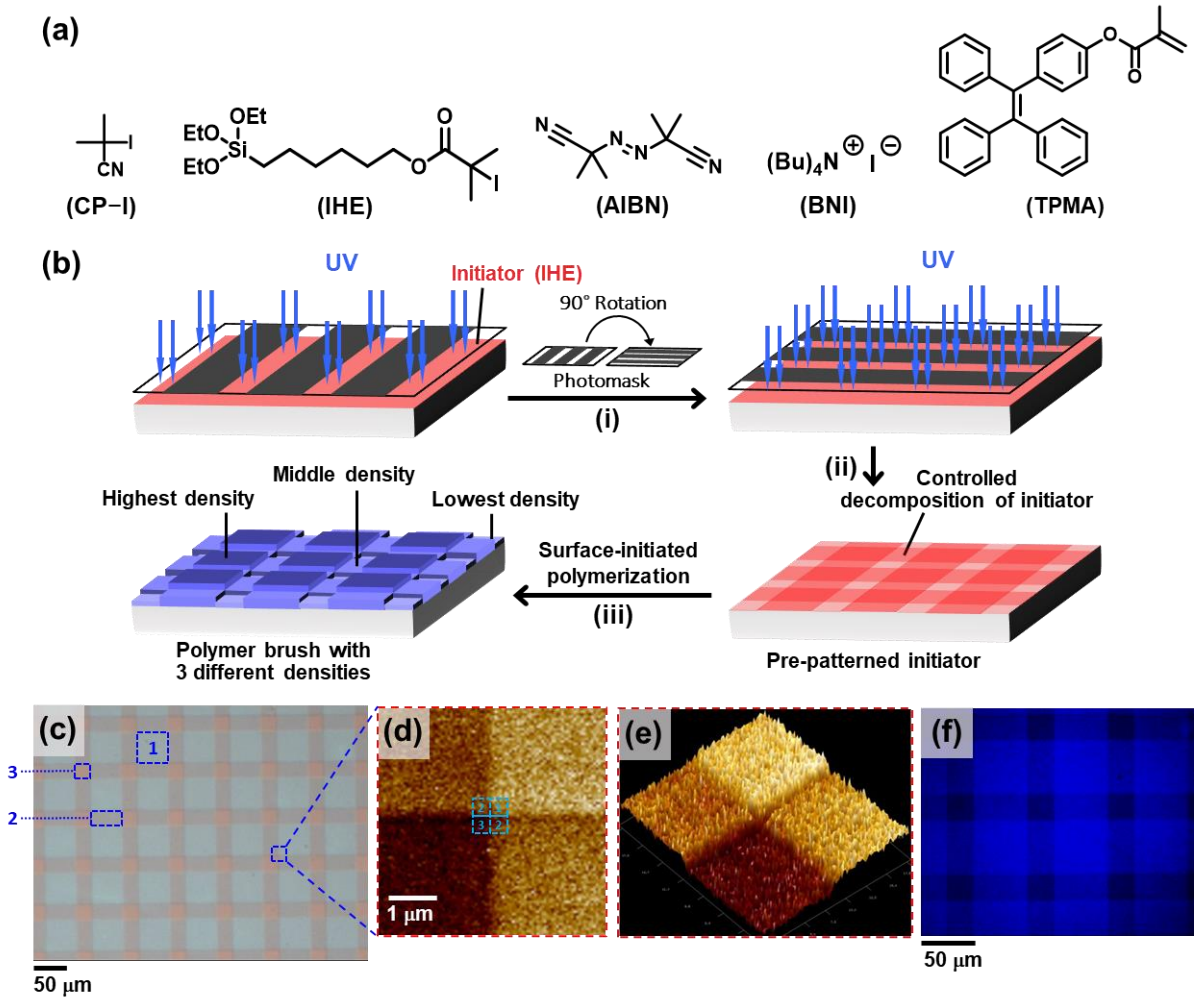

Figure 4.2. (a) Structures of alkyl iodides, azo initiator, catalyst, and monomer used in this study. (b) Visual representation of the fabrication of patterned polymer brushes comprising three different densities. (c) Optical microscopy image, (d) atomic force microscopy (AFM) 2D, (e) AFM 3D, and (f) fluorescence microscopy photos of the polymer brushes outlined in **Table 4.1** (entry 1), respectively.

4.3. Results and Discussion

4.3.1. Patterned Polymer Brushes with Three Different Densities. On a silicon wafer, we uniformly attached a surface-immobilizing initiator IHE (**Figure 4.2a**) bearing an alkyl iodide initiating group and a triethoxysilyl anchoring group. The wafer was exposed to UV light (wavelength = 250–385 nm and intensity = 0.036 W cm^{-2}) for 5 min using a striped

photomask (**Figure S4.1** in **Chapter 4.6**). The wafer was then subjected to another 5 min of UV exposure light following a 90-degree rotation of the same photomask, generating a pattern of IHE comprising three different densities (**Figure 4.2b**). We subsequently carried out surface-initiated RCMP by placing the wafer in a solution (**Figure 4.2a**) of a monomer TPMA (2000 equiv.), a non-immobilized (free) initiator 2-iodo-2-methylpropionitrile (CP−I, 1 equiv.), a catalyst BNI (20 equiv.), a radical initiator 2,2'-azobis(isobutyronitrile) (AIBN, 1 equiv.), and solvent toluene (65 wt% of the whole mixture) at 70 °C for 24 h, yielding a patterned poly(4-(1,2,2-triphenylvinyl)phenyl methacrylate) (PTPMA) brush (**Figure 4.2b**). The molecular weight was modulated by introducing the free initiator (CP−I), and the polymerization rate was enhanced by introducing the radical initiator (AIBN).[15,42]

The optical microscope (**Figure 4.2c**) and atomic force microscope (AFM) (**Figures 4.2d** and **4.2e**) images of the obtained polymer brush show three different brush thicknesses with clear boundaries, demonstrating the successful preparation of a three-dimensionally (3D) patterned polymer brush. The dry thicknesses determined using AFM were 46 nm in region 1, 42 nm in region 2, and 36 nm in region 3. The dry thicknesses determined using AFM range from 45–50 nm in region 1, 40–46 nm in region 2, and 30–41 nm in region 3. The mean thicknesses of (48 ± 3 nm) in region 1, (44 ± 3 nm) in region 2, and (38 ± 3 nm) in region 3 suggest that the error is <5% (= 3 nm/48 nm) in region 1, <6% (= 3 nm/44 nm) in region 2, and <9% (= 3 nm/38 nm) in region 3. The free polymer produced from the free initiator (CP−I) had an M_n value of 210000 and a dispersity ($Đ = M_w/M_n$) value of 1.68 (**Table 4.1** (entry 1)), where M_n and M_w are the number- and weight-average molecular weights, respectively. The relatively large $Đ$ value was ascribed to the relatively high molecular weight targeted and the polymer chains newly formed from the radical initiator (AIBN). Because the M_n value was determined with poly(methyl methacrylate) (PMMA)-calibrated gel permeation chromatography (GPC) and was not an absolute value, we estimated the degree of polymerization (DP) of the polymer

to be 1700 from the multiplication of the $[monomer]_0/[CP{-}I]_0$ ratio by the monomer conversion (**Table 4.1** (entry 1)). In some cases, the degree of polymerization and the molecular weight of free polymers produced from the free initiators show similarities to the corresponding brush polymers, and there are some cases where the degree of polymerization and the molecular weight differs.[61-71] In our system, this correlation is not clear. This estimate is not strictly accurate but should be regarded as an approximation. Utilizing this DP value and considering an equivalent M_n value for the graft and free polymers, the surface occupancy (σ^*) was calculated to be 11% in region 1, 10% in region 2, and 8% in region 3. Thus, a tailored combination of brushes with different graft densities was accessed. The fluorescence microscope image (**Figure 4.2f**) shows that the fluorescence intensity increased with an increase in the brush thickness (surface occupancy) and matched the respective areas of the optical microscope and AFM images.

Table 4.1. Fabrication of Patterned Polymer Brushes with Three Graft Densities.[a]

Entry	$[TPMA]_0/[CP{-}I]_0/[BNI]_0/[AIBN]_0$ (equiv.)[b]	Solvent	Conv (%)[c]	M_n[d] ($M_{n,theo}$[e])	$Đ$[d]	DP[f]	Region	h (nm)	σ^* (%)
1	2000/1/20/1	Toluene 65 wt%	87	210000 (720000)	1.68	1700	1	46	11
							2	42	10
							3	36	8
2	2000/1/20/1	Toluene 65 wt%	88	180000 (730000)	1.61	1800	NA[g]	NA[g]	NA[g]

[a]Polymerizations were performed at 70 °C for 24 h. [b]The target DP at a full (100%) monomer conversion was 2000. [c]Monomer conversion determined with ^{1}H NMR. [d]PMMA-calibrated THF-GPC values of the free polymers. [e]Theoretical M_n values calculated according to $([monomer]_0/[CP{-}I]_0)\times$(monomer conversion)×(molecular weight of monomer)+(molecular weight of CP−I). [f]Estimated DP values according to DP = $([monomer]_0/[CP{-}I]_0)\times$(monomer conversion). [g]Not analyzed.

We fabricated another patterned fluorescent brush (**Figure 4.3**). One-third of a uniformly IHE-immobilized wafer was irradiated with UV light for 5 min, while the rest (two-thirds) of

the wafer was covered with a mask. The mask was then shifted to cover one-third of the wafer, and the rest (two-thirds) of the wafer was exposed to UV light for an additional 5 min, generating a pattern of IHE comprising three different densities (**Figure 4.3a**). After a surface-initiated RCMP of TPMA (**Table 4.1** (entry 2)), we obtained a patterned fluorescent polymer brush. **Figures 4.3b** and **4.3c** show the non-fluorescent and fluorescence images of the obtained polymer brush, respectively, the latter of which clearly displays three different fluorescence intensities. The reproducibility of the synthesis of the patterned brush was confirmed, as shown in **Chapter 4.6** (**Table S4.1** and **Figure S4.3**).

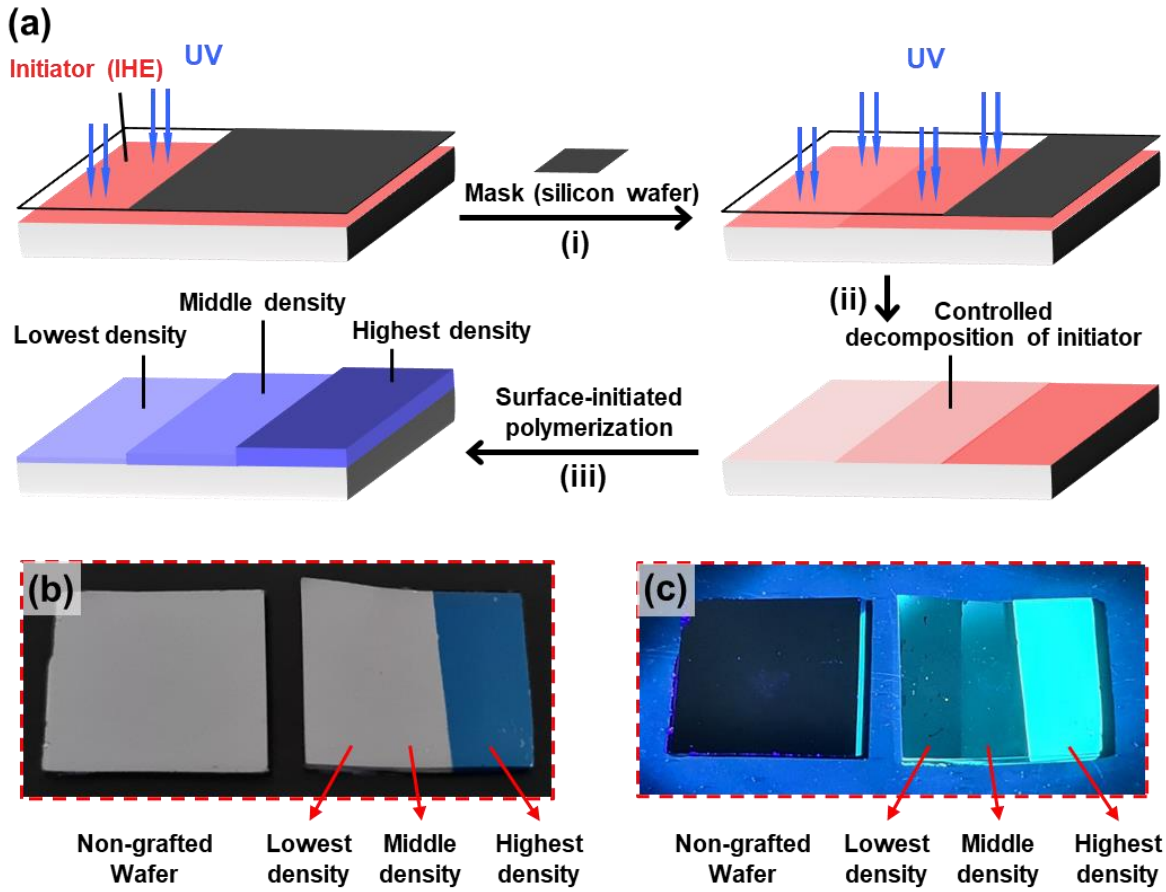

Figure 4.3. (a) Visual representation of the fabrication of patterned polymer brushes comprising three different densities. (b and c) Photographs illustrating the polymer brush outlined in **Table 4.1** (entry 2) (b) not under and (c) under UV irradiation (excited wavelength = 365 (± 10) nm).

4.3.2. Size Recognition of External Molecules on Polymer Brushes. We prepared two-density patterned polymer brushes (**Table S4.2** in **Chapter 4.6**) and used them to study size recognition of external molecules, i.e., poly(ethylene glycol)s (PEGs) with different molecular weights. For the three-density patterned brush (**Figure 4.3c**), the fluorescence intensity (brush thickness) of the lowest grafting density region was too small to suit this study, and hence we prepared two-density patterned brushes with concentrated (σ^* = 15–20%) and semi-diluted (σ^* = 7–11%) regions. For the synthesis of the two-density patterned brushes, we halved the DP

from 1700–1800 (three-density patterns) to 550–770 (two-density patterns) to narrow the molecular weight distribution ($Đ$ = 1.25–1.39) (**Table S4.2** in **Chapter 4.6**).

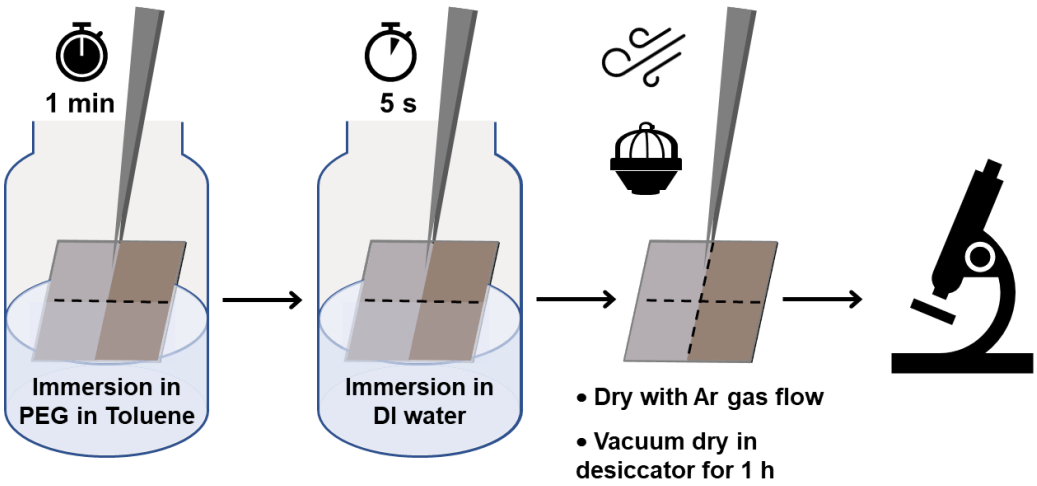

Figure 4.4. Procedure of size recognition experiment on polymer brush.

As shown in **Figure 4.4**, a half area of the two-density patterned brushes was immersed in a mixture of PEG (M_n = 300) (50 wt%) and toluene (50 wt%) for ca. 1 min, while the other half area remained non-immersed. The brushes were subsequently immersed in deionized water for ca. 5 s to remove (rinse) extra outer-surface PEG molecules from the brush surface. Subsequently, the brushes were dried, and their fluorescence intensities were measured with a fluorescence stereomicroscope (**Figures 4.5a**, **4.5b**, and **4.5c**). The same experiment was also conducted using a larger-molecular weight PEG (M_n = 1000) instead of PEG (M_n = 300) (**Figures 4.5d**, **4.5e**, and **4.5f**).

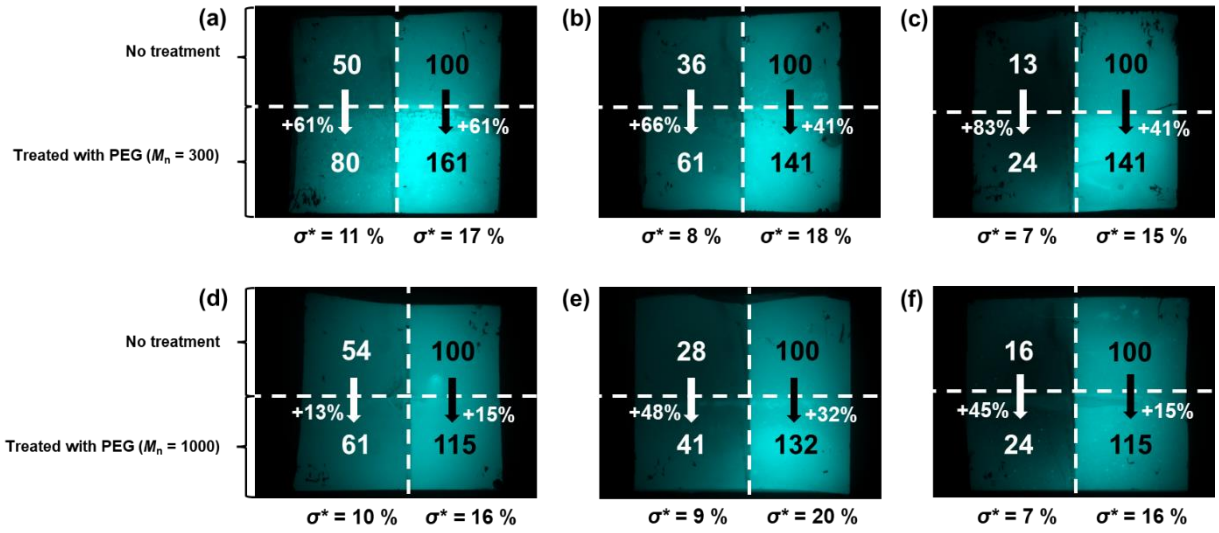

Figure 4.5. (a–c) Fluorescence microscopy photos of the polymer brushes are detailed in **Table S4.2** (entries 1, 3, and 5, respectively) after immersion in the PEG (M_n = 300) solution, immersion in deionized water, and drying. (d–f) Fluorescence microscopy photos of the polymer brushes are detailed in **Table S4.2** (entries 2, 4, and 6, respectively) after immersion in the PEG (M_n = 1000) solution, immersion in deionized water, and drying. The numbers indicate the corrected total cell fluorescence (CTCF) (corrected for the background intensity (**Chapter 4.6**)). The CTCF values are normalized to that (set to 100) of the concentrated brush untreated with PEG (right-top corner in each image).

Table 4.2. Change in Fluorescence Intensity via Treatment with PEG (External Molecule).

Entry	Brush[a]	σ^* (%)	Corrected Total Cell Fluorescence (CTCF)					
			No Treatment[b]	Treated with PEG (M_n = 300)	Change (%)[c]	No Treatment[b]	Treated with PEG (M_n = 1000)	Change (%)[c]
1	Concentrated	16–17	100	161	61 ↑	100	115	15 ↑
	Semi-diluted	10–11	50	80	61 ↑	54	61	13 ↑
2	Concentrated	18–20	100	141	41 ↑	100	132	32 ↑
	Semi-diluted	8–9	36	61	66 ↑	28	41	48 ↑
3	Concentrated	15–16	100	141	41 ↑	100	115	15 ↑
	Semi-diluted	7	13	24	83 ↑	16	24	45 ↑

[a]The synthetic conditions of the polymer brushes are given in **Table S4.2**. [b]The CTCF for the concentrated brush is normalized to 100. [c]The change (%) is calculated as [(florescence intensity with PEG treatment)–(fluorescence intensity with no treatment)]/(fluorescence intensity with no treatment).

The values given in the images in **Figure 4.5** are fluorescence intensities normalized to that (set to 100) of the concentrated brush untreated with PEG (without immersion in the PEG solution) (right-top corner in each image). For the concentrated brushes (σ^* = 15–20%), by treating with PEG (M_n = 300), the fluorescence intensity increased from 100 (untreated) to 141–161 (treated) (**Figures 4.5a**, **4.5b**, and **4.5c**), while by treating with PEG (M_n = 1000), the fluorescence intensity less significantly increased only from 100 (untreated) to 115–132 (treated) (**Figures 4.5d**, **4.5e**, and **4.5f**) (**Table 4.2**). Small external molecules, i.e., PEG (M_n = 300), can readily diffuse into the concentrated brush layer. PEG is hydrophilic (amphiphilic). The (1,2,2-triphenylvinyl)phenyl (TP) side groups in the polymer brush chains are aromatic and hydrophobic (**Figure 4.6a**). Because the TP groups are immiscible with PEG, the TP groups tended to aggregate in the presence of PEG (**Figure 4.6b**), which would drive more intense AIE (higher fluorescence intensity). Concentrated polymer brush chains are highly stretched because of the steric hindrance of the neighbouring brush chains and hence prevent large-size external molecules from diffusing into the brush layer (size exclusion).[15] Therefore, large external molecules, i.e., PEG (M_n = 1000), were difficult to enter the concentrated

polymer brushes (**Figure 4.6c**), resulting in a less significant increase in fluorescence intensity. As the grafting density decreases, brush polymer chains became more flexible and sterically less hindered so that large external (PEG) molecules could diffuse into the brush layer and enhanced the aggregation of the TP groups. Therefore, the sizes of external molecules (two PEGs with different molecular weights) were recognized by significant and less significant changes in the fluorescence intensity, demonstrating a concept of an AIE-based molecular size analyser.

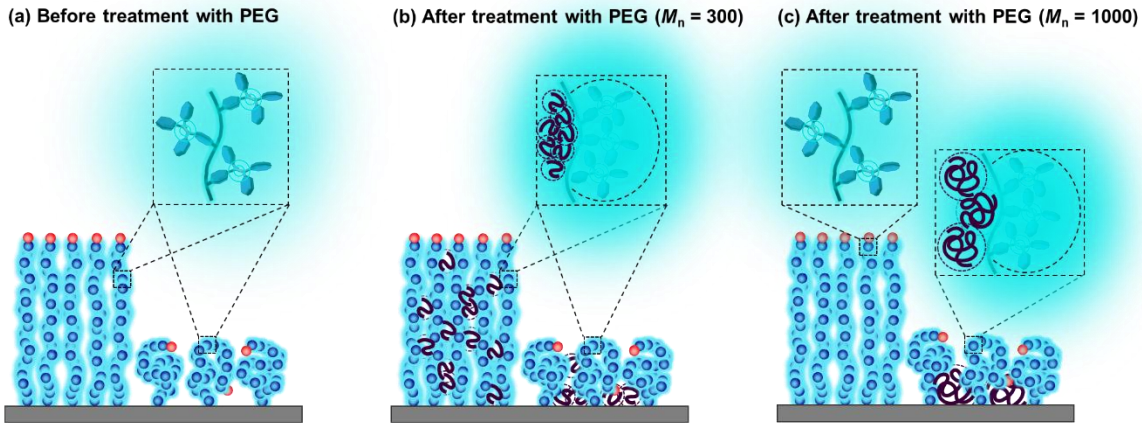

Figure 4.6. Schematic illustration of the size recognition of PEG (M_n = 300 and M_n = 1000).

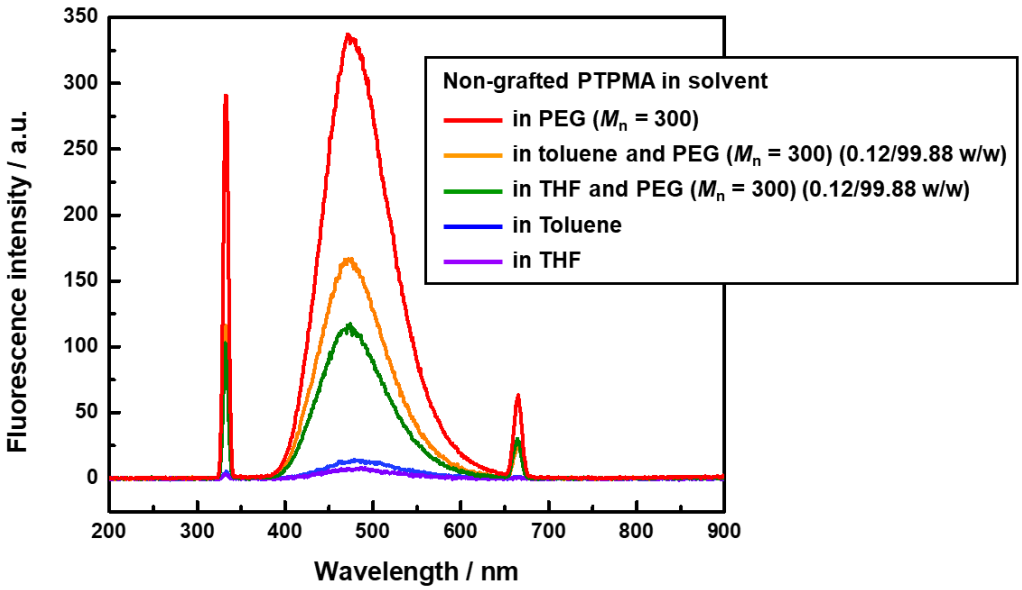

Figure 4.7. Fluorescence spectra of non-grafted PTPMA (M_n = 110,000 and $Đ$ = 1.38) (0.1 mM of the monomer (TPMA) unit) dissolved in solvents. The excitation wavelength was 332 nm.

To confirm that the hydrophilic environment (PEG) drove the aggregation (AIE) of the TP groups, we studied the fluorescence intensities of the non-grafted PPTMA dissolved in several solvents. **Figure 4.7** shows the fluorescence spectra of the non-grafted PTPMA (M_n = 110,000 and $Đ$ = 1.38) (0.1 mM of the monomer (TPMA) unit) dissolved in tetrahydrofuran (THF) (purple line), toluene (blue line), a mixture of THF and PEG (0.12/99.88 w/w) (green line), a mixture of toluene and PEG (0.12/99.88 w/w) (orange line), and PEG (red line), where we used PEG (M_n = 300). THF and toluene are hydrophobic solvents. The fluorescent intensity increased with an increase in the PEG fraction from 8.26 a.u. (pure THF) and 14.4 a.u. (pure toluene) to 117 a.u. (THF/PEG = 0.12/99.88 w/w) and 167 a.u. (toluene/PEG = 0.12/99.88 w/w). The intensity further increased to 337 a.u. in pure PEG. The solutions were transparent in all studied cases, suggesting that the PTPMA chains were macroscopically dissolved even in the presence of PEG but that the TP groups in the PTPMA chains tended to aggregate microscopically in the presence of PEG. The result supports that the PEG molecules entered

the polymer brush layer and drove the TP groups to aggregate and enhance the fluorescence intensity via AIE.

Table 4.2 summarizes the graft densities (σ^* value (surface occupancy)) of the brushes, the fluorescence intensities on the PEG-non-treated brushes, and the fluorescence intensities on the PEG-treated brushes. In the absence of UV light, the σ^* value of the brush ranges from 15–20%. The mean σ^* value (17 ± 2%) suggests that the error in the surface coverages presented in **Table 4.1** is <11% (= 2%/17%). This relatively small value (<11%) falls within the experimental error in σ^* value. The fluorescent intensities were obtained from **Figure 4.5**. For the-non-treated brushes, the fluorescence intensities (normalized to 100 at the right-top corner in each image in **Figure 4.5**) of the concentrated brushes (σ^* = 15–20%) were larger than those (13–54 at the left-top corner in each image in **Figure 4.5**) of the semi-diluted brushes (σ^* = 7–11%) because of the larger brush thickness of the concentrated brushes. The fluorescence intensities increased by the treatment of PEG for all brushes because of the more intense AIE driven by the presence of PEG. **Table 4.2** also lists the change (increase) (%) in the fluorescence intensity by the PEG treatment calculated as change = (increase in fluorescence intensity)/(original fluorescence intensity), i.e., 61% = (161–100)/100 for the concentrated brush treated with PEG (M_n = 300) in **Table 4.2** (entry 1) and **Figure 4.5a**, for example. The fluorescence change (%) tended to increase from 41–61% (concentrated brush) to 61–83% (semi-diluted brush) with PEG (M_n = 300) and from 15–32% (concentrated brush) to 13–48% (semi-diluted brush) with PEG (M_n = 1000) (**Table 4.2**) with a decrease in the grafting density. The result suggests that, as the grafting density decreased, brush polymer chains became more flexible and sterically less hindered so that more external solute (PEG) molecules could diffuse into the brush layer and enhanced the aggregation of the TP groups.

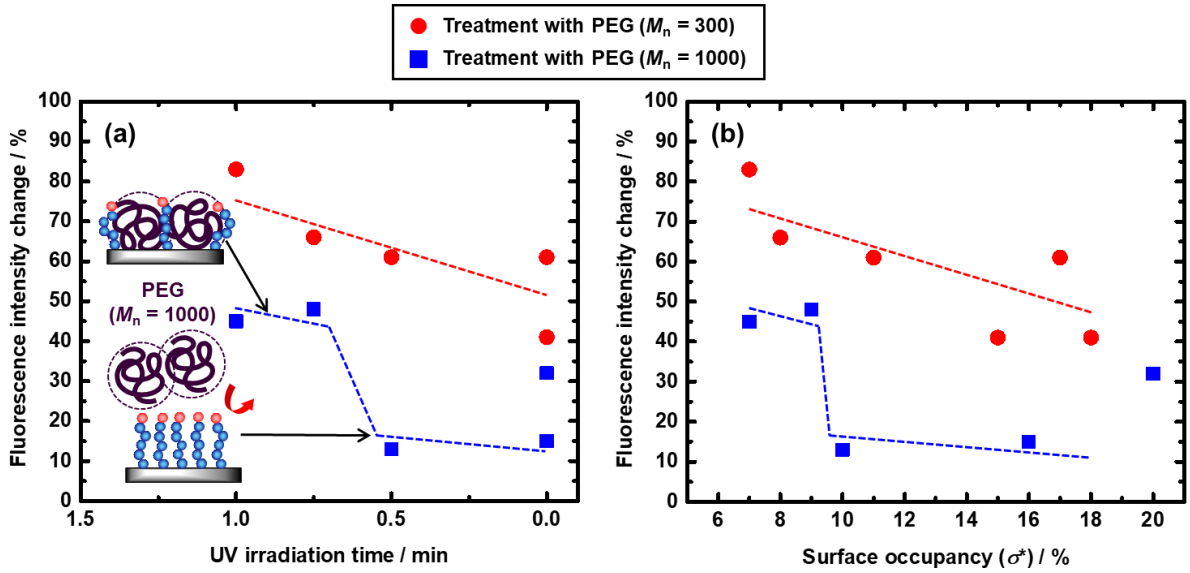

Figure 4.8. Plots of fluorescent intensity change (%) vs (a) UV-irradiation time for the degradation of the surface initiator (IHE) and (b) surface occupancy (σ*) of the generated polymer brushes. The grafting density (surface occupancy (σ*)) is calculated as {(dry thickness of the polymer brush)/[(0.25 nm)×(estimated DP value)]}×100%, where the length of a repeating unit in the polymer was assumed to be 0.25 nm. The dashed lines are guides for the eyes.

Figure 4.8a shows the plots of the fluorescence change (increase) (%) in the fluorescence intensity by the PEG treatment calculated as change = (increase in fluorescence intensity)/(original fluorescence intensity) vs the UV irradiation time in the degradation of the surface initiator (IHE). With no UV irradiation (no degradation of IHE to generate concentrated brushes), the grafting density should be identical, but the experimental σ* values in the six runs (**Table 4.2** and **Figure 4.5**) slightly varied at 15–20%, which is viewed as an experimental error range. **Figure 4.8b** uses the σ* values in the horizontal axis. Red circles show the fluorescence changes by the treatment with PEG (M_n = 300), and blue squares show those by the treatment with PEG (M_n = 1000).

At the high σ^* (≥10%) region, except a data point at σ^* = 20% (blue square), the fluorescence change was virtually negligible (13–15%) with PEG (M_n = 1000), while the fluorescence change was significant (41–61%) with PEG (M_n = 300). This trend was because the small molecule (PEG (M_n = 300)) can diffuse in the brush layer while the large molecule (PEG (M_n = 1000)) is difficult to diffuse in the brush layer due to the steric hindrance in the high-density brushes. At the lower σ^* (<10%) region, using PEG (M_n = 1000), a sharp rise in the fluorescence change was observed, suggesting that the large molecule (PEG (M_n = 1000)) started to diffuse in the brush layer. The results suggest that the size exclusion threshold is at the σ^* value of 9–10% for the molecular weight of 1000. The red line shows no size exclusion. The blue line shows a clear transition suggesting the occurrence of size exclusion.

Therefore, if we test an external molecule using a patterned brush combining a high-density brush at $\sigma^* \geq 10\%$ with a lower-density brush at $\sigma^* < 10\%$, we may find if the molecular weight of the external molecule is below or above 1000 from the fluorescence change. Namely, if a high-density brush at $\sigma^* \geq 10\%$ exhibits virtually no fluorescence change but a lower-density brush at $\sigma^* < 10\%$ exhibits increased fluorescence, we may find that the molecular weight of the external molecule is above 1000, while if both brushes exhibit increased fluorescence, we may find that it is below 1000. The threshold molecular weight depends on the σ^* value (should be larger for a smaller σ^* value). Thus, we used the patterned PTPMA brushes to recognize the sizes of the external hydrophilic (PEG) molecules by the fluorescence intensity change.

4.4. Conclusion

We fabricated patterned fluorescent brushes with tailored three- and two-graft densities in different geometric patterns, i.e., squares or rectangles. The two-density patterned fluorescent brushes were successfully used to recognize the sizes of external molecules (two PEGs with different molecular weights (M_n = 300 and 1000)). The smaller-size PEG molecules (M_n = 300)

were able to enter the polymer brush layers, inducing the fluorescent (TP) groups in the brush chains to aggregate and enhancing the fluorescence intensity via AIE. The larger-size PEG molecules (M_n = 1000), on the other hand, were unable to enter the high-density polymer brushes at $\sigma^* \geq 10\%$, resulting in no significant change in the fluorescence intensity. The size exclusion threshold of external molecules depends on grafting density. At the size exclusion threshold, we were able to distinguish molecules at a particular molecular weight (1000 in the present study) from the change and no change in the fluorescence. Such polymer brushes may potentially serve as a conceptually new AIE-based molecular size analyser. The facile and rapid patterning of the alkyl iodide (IHE) initiator (within 10 min) using UV light (250–385 nm), the broad range of the tuneable graft densities, and the metal-free synthesis of the brushes are appealing aspects of the present method to create patterned AIE-based fluorescence surfaces.

4.5. Experimental Section

4.5.1. Preparation of Alkyl Iodide Initiator-Immobilized Silicon Wafer. Refer to Chapter 2.5.1.

4.5.2. Preparation of Prepatterned Wafer. A photomask was rinsed with acetone and dried using nitrogen gas. The photomask was exposed to radiation in the ozone cleaner for 0.5 h before use. The photomask was placed atop an IHE-immobilized wafer before exposing the wafer to UV light (250−385 nm). The wafer was washed with acetone and dried using nitrogen gas.

4.5.3. Surface-initiated Polymerization. A prepatterned IHE-immobilized silicon wafer was placed in a mixture of monomer (TPMA) (0.5 g), initiating alkyl iodide dormant species

(CP−I), azo initiator (AIBN), catalyst (BNI), and solvent toluene (0.9 g) in a Schlenk flask at 70 ^{o}C with stirring in an inert environment for 24 h.

4.5.4. General Procedure of Surface-initiated Polymerization. Refer to Chapter 2.5.3. Chloroform-*d* was used as the NMR solvent. The dry brush thickness (*h*) presented in **Table 4.1** and **Table S4.2** is the brush thickness after the subtraction of the thickness of the IHE initiator layer (2 nm).

4.6. Appendix

4.6.1. Materials and Instrument

4.5.1.1. Materials. 2-bromo-1,1,2-triphenylethylene (>98%, Tokyo Chemical Industry (TCI), Japan), 4-hydroxyphenylboronic acid (>97%, TCI), tetrakis(triphenylphosphine)palladium(0) ($Pd(PPh_3)_4$) (99%, Sigma-Aldrich, USA), potassium carbonate (K_2CO_3) (for reaction, anhydrous, ≥99%, Sigma-Aldrich), tetrabutylammonium bromide (TBAB) (>98%, TCI), methacrylic acid (MAA) (>99%, TCI), *N,N'*-dicyclohexylcarbodiimide (DCC) (99%, Sigma-Aldrich), 4-dimethylaminopyridine (DMAP) (>99%, TCI), tetrahydrofuran (THF) (for reaction, anhydrous, ≥99.9%, Sigma-Aldrich), sodium carbonate (Na_2CO_3) (for reaction, anhydrous, 99.9%, Quality Reagent Chemical (QRëC), New Zealand), sodium chloride (NaCl) (>99.5%, Goodrich Chemical Enterprise (GCE), Singapore), sodium sulfate (Na_2SO_4) (for reaction, anhydrous, >99%, UNI-CHEM, Serbia), silica gel (spherical, 60μm, for flash chromatography, TCI), 2-iodo-2-methylpropionitrile (CP-I) (>95%, TCI), tetrabutylammonium iodide (BNI) (>98%, TCI), 2,2'-azobis(isobutyronitrile) (AIBN) (98%, Wako Pure Chemical Industries, Japan), polyethylene glycol 1000 (PEG (M_n = 1000)) (TCI), polyethylene glycol 300 (PEG (M_n = 300)) (TCI), acetone (≥99.8%, Fisher Chemical, USA), chloroform (≥99.8%, Fisher Chemical), 2-propanol

(≥99.7%, J.T. Baker, USA), ethanol (≥99.8%, absolute, Fisher Chemical), ammonia solution (28% in water, TCI), dichloromethane (99.8%, Fisher Chemical), toluene (≥99.8%, TEDIA, USA), hexane (>99%, International Scientific, Singapore), ethyl acetate (99.9%, VWR Chemicals, USA), and THF (≥99.8%, Fisher Chemical) were used as received. A silicon wafer (produced by the Czochralski process, thickness: 525 ± 25 μm) was purchased from Matsuzaki Seisakusho (Japan). 6-(2-Iodo-2-isobutyryloxy)hexyltriethoxysilane (IHE) (>95%) was provided through the courtesy of Godo Shigen Co., Ltd. (Japan). The glass photomasks (Hunan Omnisun Information Material, China) are polished on both sides with a patterned low-reflective chrome film on one side. **Figure S4.1** shows the photomask used in this work.

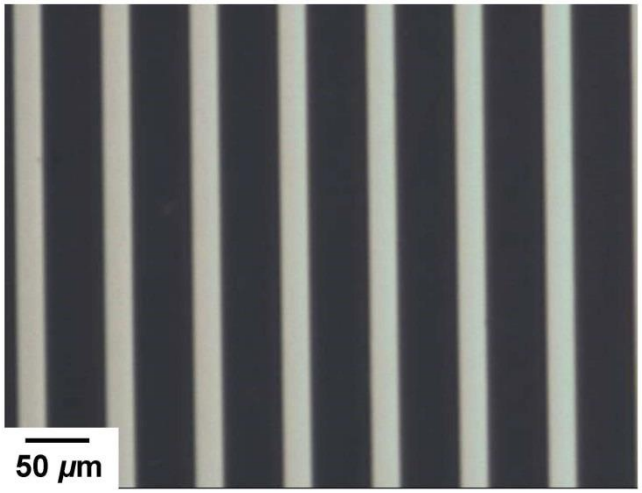

Figure S4.1. Optical microscope image of the photomask used in this work. The dark area is unmasked and the bright area is masked.

4.6.1.2. UV-Ozone Cleaner. Refer to Chapter 2.6.1.5.

4.6.1.3. UV-LED Light (for Patterning (Degradation of Surface Initiator (IHE)). The UV light source was a xenon lamp (MAX-302, Asahi Spectra, Japan, 300 W electric power at

full power) equipped with a mirror module (MAX-UV model, Asahi Spectra, band pass at 250−385 nm).

4.6.1.4. UV-LED Light (for Figure 4.3c and Figure S4.3b). Refer to Chapter 2.6.1.4.

4.6.1.5. Analytical GPC. Refer to Chapter 2.6.1.2.

4.6.1.6. NMR. Refer to Chapter 2.6.1.3.

4.6.1.7. Contact Angle Measurement. Refer to Chapter 2.6.1.6.

4.6.1.8. AFM. Refer to Chapter 2.6.1.7. The AFM images (**Figures 4.2d** and **4.2e**) were obtained with a MultiMode Scanning Probe Microscope (Bruker) in the ScanAsyst^{TM} mode using a cantilever (ScanAsyst-Air, Bruker).

4.6.1.9. Confocal Fluorescence Microscopy. Refer to Chapter 3.6.1.10. For visualization, Zeiss Filter set 49 (DAPI) was used.

4.6.1.10. Stereo Fluorescence Microscope. The fluorescence images were taken with Zeiss Stereo Lumar V12 (Germany) using the Zeiss Filter set 01 (UV) under autoexposure. The images for PTPMA brushes treated with PEG (M_n = 300 and 1000) were processed using ImageJ software to calculate the corrected total cell fluorescence (CTCF) by following the formula, i.e., CTCF = (integrated density) − (area of the selected cell × mean fluorescence of background readings).

4.6.1.11. Ultraviolet-visible Spectroscopy. The UV-Vis absorption spectrum for the non-grafted polymer in a mixture of THF and PEG (M_n = 300) (0.12/99.88 w/w) was recorded on a Shimadzu UV-3600 (Kyoto, Japan) at room temperature with a quartz cell with an optical path length of 1 cm.

4.6.1.12. Fluorescence Spectroscopy. The fluorescence spectra for the non-grafted polymer in several solvents were recorded on a Varian Cary Eclipse optical spectrometer (Agilent, Santa Clara, US). The excitation wavelength was 332 nm.

4.6.2. Synthesis of Aggregation-Induced Emission (AIE) Monomer

Scheme S4.1. Synthesis of 4-(1,2,2-triphenylvinyl)phenyl methacrylate (TPMA).

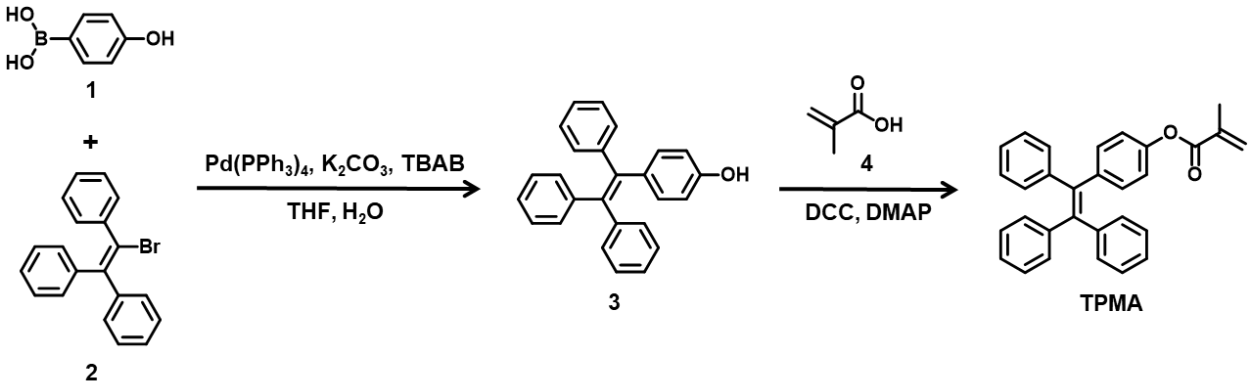

4.6.2.1. Synthesis of 4-(1,2,2-triphenylvinyl)phenol (3) (Scheme S4.1). 4-hydroxyphenylboronic acid (compound **1**) (4.94 g, 35.8 mmol) and 2-bromo-1,1,2-triphenylethylene (compound **2**) (10 g, 29.8 mmol) were dissolved in a mixture of THF (60 mL) and deionized water (30 mL) under nitrogen atmosphere (using standard Schlenk technique). $Pd(PPh_3)_4$ (276 mg, 0.24 mmol), K_2CO_3 (2.06 g, 14.9 mmol), and TBAB (805 mg, 1.67 mmol) were then added, and the mixture was heated at 70 °C for 10 h with magnetic stirring. After cooling to ambient temperature, the mixture was transferred to a separatory funnel and the layers were allowed to separate. The organic layer was separated, and the aqueous layer was further extracted with 3 × 80 mL ethyl acetate. The combined organic layers were washed with brine (aqueous NaCl solution), dried over anhydrous Na_2SO_4, filtered, and concentrated *in vacuo*. The product was purified by column chromatography (silica gel, 10:1

hexane: ethyl acetate, v/v) to give the desired 4-(1,2,2-triphenylvinyl)phenol (compound **3**) as a white solid (6.95 g, 67% yield). ^{1}H NMR ($CDCl_3$, 300 MHz): δ7.15 – 6.97 (m, 15H), 6.89 (d, *J* = 8.6 Hz, 2H), 6.55 (d, *J* = 8.6 Hz, 2H), 4.68 (s, 1H).

4.6.2.2. Synthesis of 4-(1,2,2-triphenylvinyl)phenyl methacrylate (TPMA). MAA (compound **4**) (2.49 g, 28.9 mmol), DMAP (470 mg, 3.85 mmol), and DCC (7.94 g, 38.5 mmol) were dissolved in anhydrous THF (60 mL) under nitrogen atmosphere (using standard Schlenk technique), and the resulting mixture was stirred at room temperature for 0.5 h. 4-(1,2,2-triphenylvinyl)phenol (compound **3**) (6.70 g, 19.2 mmol) was then added dropwise to the reaction mixture, and the system was stirred at room temperature for 48 h. The reaction mixture was then poured into a saturated aqueous Na_2CO_3 solution (50 mL) and stirred for a further 0.5 h. The mixture was transferred to a separatory funnel and the layers were allowed to separate. The organic layer was separated, and the aqueous layer was further extracted with 3 × 70 mL dichloromethane. The combined organic layers were washed with brine (aqueous NaCl solution), dried over anhydrous Na_2SO_4, filtered, and concentrated *in vacuo*. The product was purified by column chromatography (silica gel, 10:1 hexane: ethyl acetate, v/v) to give the desired 4-(1,2,2-triphenylvinyl)phenyl methacrylate (TPMA) as a white solid (6.81 g, 85% yield). ^{1}H NMR ($CDCl_3$, 300 MHz): δ7.06 (ddd, *J* = 8.6, 4.7, 2.5 Hz, 17H), 6.86 (d, *J* = 8.7 Hz, 2H), 6.29 (s, 1H), 5.71 (s, 1H), 2.02 (s, 3H).

4.6.3. ^{1}H NMR Spectra of 4-(1,2,2-triphenylvinyl)phenol (3) and TPMA

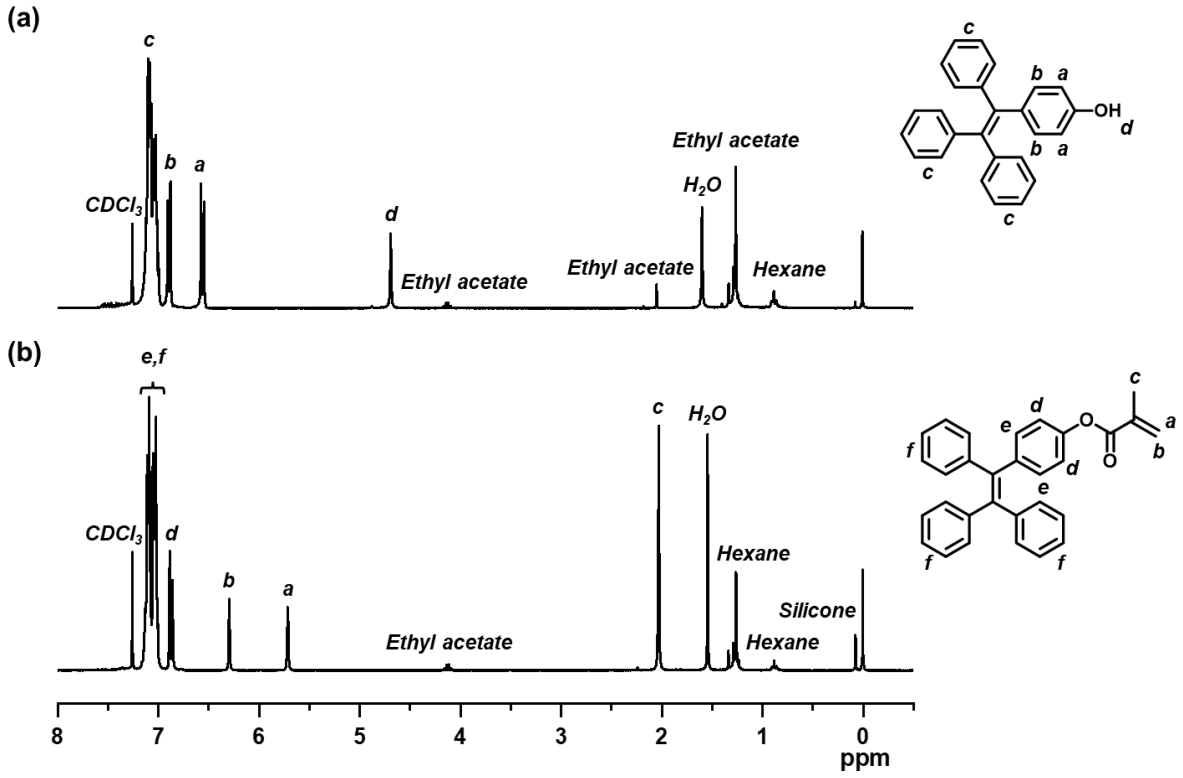

Figure S4.2. ^{1}H NMR spectra of (a) compound **3** and (b) TPMA in $CDCl_3$.

4.6.4. Patterned Polymer Brush with Three Different Densities

4.6.4.1. General Procedure of Surface-initiated Polymerization. Refer to Chapter 4.5.4.

An experiment (**Table S4.1** (**entry 1**) and **Figure S4.3**) was carried out in the same condition as that in **Table 4.1** (**entry 2**) and **Figure 4.3**, confirming the reproducibility of the synthesis of the patterned brush.

Table S4.1. Patterned PTPMA brushes with three graft densities.[a]

entry	exposure time (min)[b]	$[TPMA]_0/[CP-I]_0/[BNI]_0/[AIBN]_0$ (equiv.)[c]	solvent	conv (%)[d]	M_n[e] ($M_{n,theo}$[f])	$Đ$[e]	water contact angle (°)
1	10 | 5 | 0	2000/1/20/1	Toluene 65 wt%	90	210 000 (750 000)	1.58	89, 89, 89

[a]Polymerization was performed at 70 °C for 24 h. [b]UV light (250−385 nm) was used to degrade IHE. [c]The target DP at a full (100%) monomer conversion was 2000. [d]Monomer conversion determined with ^{1}H NMR. [e]PMMA-calibrated THF-GPC values of the free polymer. [f]Theoretical M_n value calculated according to $([monomer]_0/[CP-I]_0)\times$(monomer conversion)×(molecular weight of monomer)+(molecular weight of CP−I).

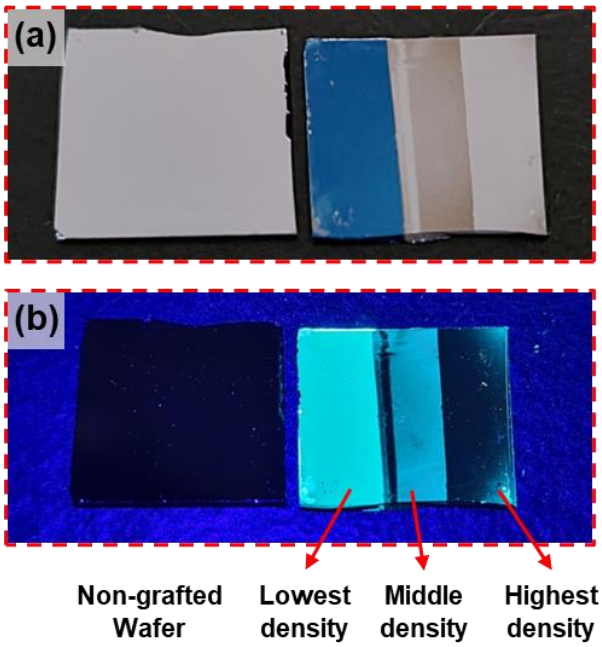

Figure S4.3. Photos of PTPMA brush with 3 densities obtained in **Table S4.1** (**entry 1**) (a) not under and (b) under UV irradiation (excited wavelength = 365 (± 10) nm).

4.6.5. Studies of Patterned PTPMA Brush with 2 Different Densities

4.6.5.1. Preparation of Patterned PTPMA Brush with 2 Different Densities. A half of an IHE-immobilized wafer (with IHE attached uniformly) was irradiated with UV light for

1.00 or 0.75 or 0.50 min, while the rest (half) of the wafer was covered with a mask, generating a pattern of IHE with two different densities.

4.6.5.2. Calculation of Surface Occupancy. Refer to Chapter 3.6.5.3. The degree of polymerization (DP) of the polymer was estimated from the multiplication of the $[monomer]_0/[CP{-}I]_0$ ratio by the monomer conversion.

Table S4.2. Patterned PTPMA brushes with two graft densities.[a]

entry[b]	exposure time (min)[c]	$[TPMA]_0/[CP{-}I]_0/[BNI]_0/[AIBN]_0$ (equiv.)	solvent	conv (%)[d]	M_n[e] ($M_{n,theo}$[f])	$Đ$[e]	DP[g]	h (nm)	σ* (%)	water contact angle (°)
1	0 | 0.5	1000/1/10/0.5	Toluene 65 wt%	65	100 000 (270 000)	1.29	650	28 | 18	17 | 11	89, 89
2				71	120 000 (300 000)	1.38	710	28 | 18	16 | 10	89, 89
3	0 | 0.75	1000/1/10/0.5	Toluene 65 wt%	64	100 000 (270 000)	1.30	640	28 | 13	18 | 8	88, 88
4				55	92 000 (230 000)	1.25	550	28 | 13	20 | 9	88, 88
5	0 | 1	1000/1/10/0.5	Toluene 65 wt%	77	120 000 (320 000)	1.39	770	28 | 13	15 | 7	88, 88
6				70	110 000 (290 000)	1.30	700	28 | 13	16 | 7	88, 89

[a]Polymerizations were performed at 70 °C for 24 h. [b]The target DP at a full (100%) monomer conversion was 1000. [c]UV light (250−385 nm) was used to degrade IHE. [d]Monomer conversion determined with ^{1}H NMR. [e]PMMA-calibrated THF-GPC values of the free polymers. [f] Theoretical M_n values calculated according to $([monomer]_0/[CP{-}I]_0)\times$(monomer conversion)×(molecular weight of monomer)+(molecular weight of CP−I). [g]Estimated DP values according to DP = $([monomer]_0/[CP{-}I]_0)\times$(monomer conversion).

An IHE-immobilized wafer exhibits a water contact angle (WCA) of 85° before UV radiation. The WCA may depend on graft densities, but in this particular case, the WCA is decided by the chemical structure of the brush polymers and is independent of the graft densities.

4.6.6. Synthesis and Purification of Non-Grafted PTPMA

4.6.6.1. Preparation of Non-Grafted PTPMA. A mixture of monomer TPMA (0.5 g, 1000 equiv.), initiating alkyl iodide dormant species (CP−I, 0.23 mg, 1 equiv.), azo initiator (AIBN, 0.10 mg, 0.5 equiv.), catalyst (BNI, 4.4 mg, 10 equiv.), and solvent toluene (0.9 g) in a Schlenk flask was heated at 70 °C with stirring in an inert environment for 24 h. After the polymerization, the mixture was cooled to room temperature and diluted with THF. The polymer was purified by reprecipitation in hexane three times to remove residual traces of monomer and other low-molecular-weight molecules, yielding a PTPMA with M_n = 110,000 and $Đ$ = 1.38. The obtained polymer was used for UV-vis absorption (**Figure S4.4**) and fluorescence (**Figure 4.7**) analyses.

4.6.7. Fluorochrome Absorption-Emission Spectra of Non-Grafted PTPMA

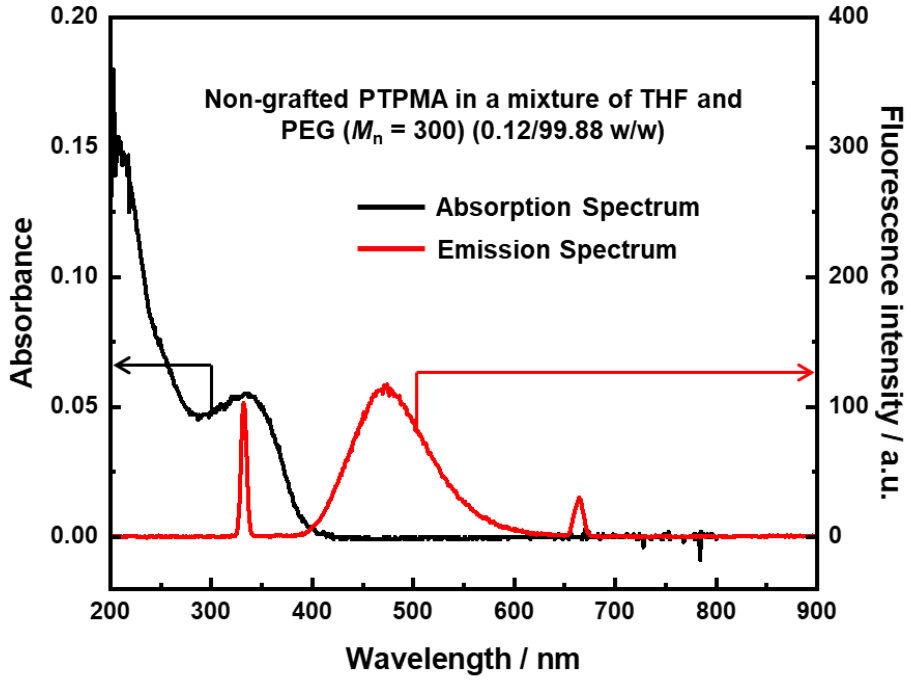

Figure S4.4. Absorption (black line) and emission (red line) spectra of non-grafted PTPMA (0.1 mM of the monomer (TPMA) unit) in a mixture of THF and PEG (M_n = 300) (0.12/99.88 w/w). The excitation wavelength for the fluorescence spectrum was 332 nm.

Figure S4.4 shows the absorption (black line) and emission (red line) spectra of the non-grafted PTPMA (0.1 mM of the monomer (TPMA) unit) in a mixture of THF and PEG (M_n = 300) (0.12/99.88 w/w). The polymer was first dissolved in THF. Subsequently, PEG (M_n = 300) was added. An approximate mirror image relation of the two spectra, a slight overlap at the higher wavelength of the absorption spectrum with the lower wavelength of the emission spectrum, and a relatively small Stokes' shift suggest that the emission of the PT groups was mainly fluorescence.

4.6.8. Experimental Error Range in Plots of Fluorescent Intensity Change vs UV-Irradiation Time for Degradation of Surface Initiator (IHE) and Surface Occupancy (σ*) of Polymer Brushes

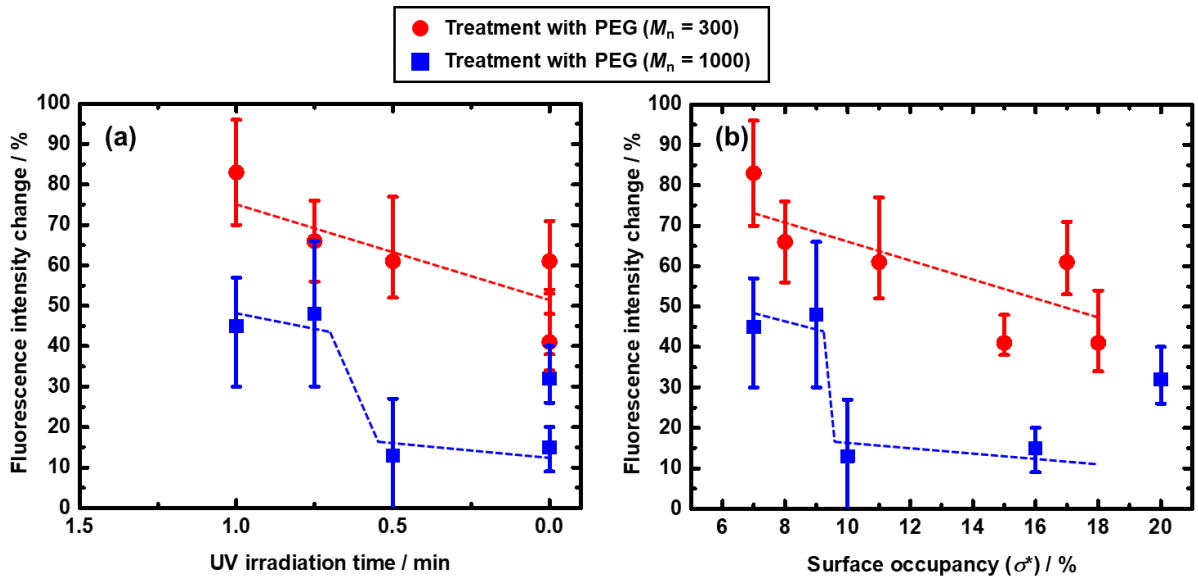

Figure S4.5. Plots of fluorescent intensity change (%) vs (a) UV-irradiation time for the degradation of the surface initiator (IHE) and (b) surface occupancy (σ*) of the generated polymer brushes. The bars represent the experimental error ranges. The dashed lines are guides for the eyes.

Figure S4.5 shows an experimental error range for each data point in **Figure 4.8**. To obtain the fluorescent intensity values in **Figure 4.5**, we measured fluorescent intensity values at 6–19 spots in each of the four divisions in (a)–(f), removed 1–4 highest values and 1–4 lowest values, and took an average of the rest of the values. The range of the rest of the values corresponds to the error bar range in **Figure S4.5**.

4.6.9. Fluorochrome Emission Spectra of Polyethylene Glycol (PEG)

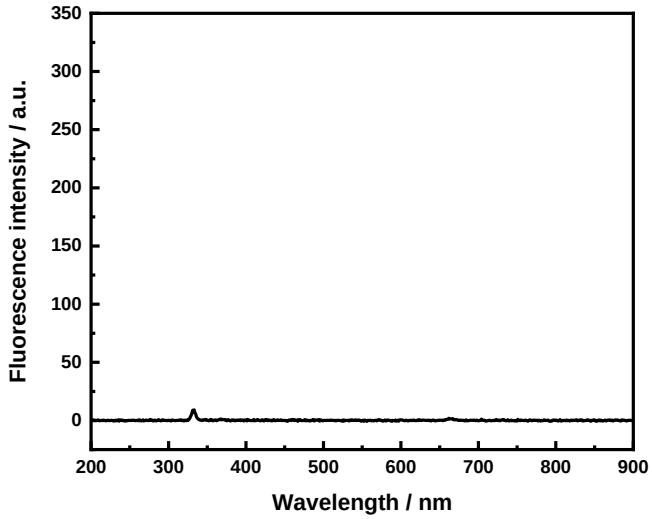

Figure S4.6. Fluorescence spectra of PEG (M_n = 300). The excitation wavelength was 332 nm.

No fluorescence emission (**Figure S4.6**) was observed, meaning that the clustering-triggered emission of PEG did not occur.

Reference(s)

(1) Bao, C. et al. *J. Polym. Sci. B: Polym. Phys.* **2014**, *52*, 1600–1619.

(2) Chen, W.-L. et al. *Macromolecules* **2017**, *50*, 4089−4113.

(3) Benetti, E. M. *Macromol. Rapid Commun.* **2018**, *39*, 1800189.

(4) Chen, C. et al. *Prog. Polym. Sci.* **2020,** *105*, 101241.

(5) Mocny, P.; Klok, H.-A. *Prog. Polym. Sci.* **2020**, *100*, 101185.

(6) Yan, J. et al. *Prog. Polym. Sci.* **2020**, *100*, 101180.

(7) Peng, W. et al. *Polym. Chem.* **2021**, *12*, 6198–6229.

(8) Ślusarczyk, K. et al. *Polymer* **2021**, *233*, 124212.

(9) Bhayo, A. M. et al. *Prog. Mater. Sci.* **2022**, *130*, 101000.

(10) Ding, Z. et al. *J. Mater. Chem. B* **2022**, *10*, 2430–2443.

(11) Poisson, J.; Hudson, Z. M. *Eur. J. Chem.* **2022**, *28*, e202200552.

(12) Wang, C.-G. et al. *J. Mater. Chem. B* **2022**, *10*, 9349–9368.

(13) Wang, R. et al. *Angew. Chem., Int. Ed.* **2023**, e202219312.

(14) Bhat, R. R. et al. *Adv. Polym. Sci.* **2006**, *198*, 51−124.

(15) Tsujii, Y. et al. *Adv. Polym. Sci.* **2006**, *197*, 1−45.

(16) Galvin, C. J.; Genzer, J. *Prog. Polym. Sci.* **2012**, *37*, 871−906.

(17) Krishnamoorthy, M. et al. *Chem. Rev.* **2014**, *114*, 10976−11026.

(18) Harris, B. P. et al. *Langmuir* **2006**, *22*, 4467–4471.

(19) Schuh, C. et al. *Adv. Mater.* **2009**, *21*, 4706–4710.

(20) Chen, T. et al. *Chem. Soc. Rev.* **2012**, *41*, 3280−3296.

(21) Zhao, H. et al. *Lab Chip* **2019**, *19*, 2651–2662.

(22) Yang, R. et al. *Prog. Polym. Sci.* **2021**, *118*, 101409.

(23) Ahn, S. J. et al. *Adv. Mater.* **2004**, *16*, 2141−2145.

(24) Schmelmer, U. et al. *Small* **2007**, *3*, 459–465.

(25) Adams, J. et al. *Langmuir* **2010**, *26*, 13600−13606.

(26) Carbonell, C. et al. *Nat. Commun.* **2020**, *11*, 1–8.

(27) Zhou, X. et al. *Angew. Chem. Int. Ed.* **2011**, *50*, 6506−6510.

(28) Chen, C. et al. *Small* **2015**, *11*, 6013–6017.

(29) Bog, U. et al. *ACS Appl. Mater. Interfaces* **2017**, *9*, 12109−12117.

(30) Zhou, F. et al. *J. Am. Chem. Soc.* **2006**, *128*, 16253−16258.

(31) Sheng, W. et al. *ACS Appl. Mater. Interfaces* **2020**, *12*, 9797–9805.

(32) Nie, Z.; Kumacheva, E. *Nat. Mater.* **2008**, *7*, 277−290.

(33) Hui, C. M. et al. *Chem. Mater.* **2014**, *26*, 745−762.

(34) Zoppe, J. O. et al. *Chem. Rev.* **2017**, *117*, 1105−1318.

(35) Goto, A. et al. *J. Am. Chem. Soc.* **2013,** *135*, 11131−11139.

(36) Ohtsuki, A. et al. *J. Am. Chem. Soc.* **2015,** *137*, 5610−5617.

(37) Wang, C.-G.; Goto, A. *J. Am. Chem. Soc.* **2017,** *139*, 10551−10560.

(38) Wang, C.-G. et al. *Macromolecules* **2019**, *52*, 2712−2718.

(39) Wang, C.-G. et al. *Polym. Chem.* **2020,** *11*, 5559−5571.

(40) Chen, Z.-H. et al. *Polym. Chem.* **2022**, *13*, 2402–2419.

(41) Wang, C.-G. et al. *Angew. Chem. Int. Ed.* **2018**, *57*, 13504−13508.

(42) Wang, C.-G. et al. *ACS Appl. Mater. Interfaces* **2019**, *11*, 14478–14484.

(43) Sim, X. M. et al. *ACS Appl. Mater. Interfaces* **2020**, *12*, 28711–28719.

(44) Sim, X. M. et al. *ACS Appl. Mater. Interfaces* **2021**, *13*, 24183–24193.

(45) Zhou, J. et al. *Chem. Rev.* **2015**, *115*, 395–465.

(46) Ostroverkhova, O. *Chem. Rev.* **2016**, *116*, 13279–13412.

(47) Gao, R. et al. *Chem. Soc. Rev.* **2021**, *50*, 5564–5589.

(48) Luo, J. et al. *Chem. Commun.* **2001**, 1740–1741.

(49) Hu, R. et al. *Prog. Polym. Sci.* **2020**, *100*, 101176.

(50) Cai, X.; Liu, B. *Angew. Chem., Int. Ed.* **2020**, *59*, 9868–9886.

(51) Fan, M. et al. *Appl. Phys. Rev.* **2021**, *8*, 041328.

(52) Chua, M. H. et al. *ACS Nano* **2023**, *17*, 1845–1878.

(53) Hu, R. et al. *Chem. Soc. Rev.* **2014**, *43*, 4494–4562.

(54) Qiu, L. et al. *ACS Appl. Mater. Interfaces* **2020**, *12*, 1348–1358.

(55) Jiang, Y.; Hadjichristidis, N. *Angew. Chem. Int. Ed.* **2021**, *60*, 331–337.

(56) Sharath Kumar, K. S. et al. *Coord. Chem. Rev.* **2021**, *447*, 214135.

(57) Kachwal, V.; Tan, J. C. *Adv. Sci.* **2022**, *10*, 2204848.

(58) Zhang, F. et al. *Polym. Chem.* **2022**, *13*, 8–43.

(59) Chen, Y. et al. *Biosens. Bioelectron.* **2018**, *111*, 124–130.

(60) Huo, Z. et al. *J. Colloid Interface Sci.* **2021**, *600*, 421–429.

(61) Kim, J. B. et al. *J. Polym. Sci. A Polym. Chem.* **2003**, *41*, 386−394.

(62) Marutani, E. et al. *Polymer* **2004**, *45*, 2231−2235.

(63) Genzer, J. *Macromolecules* **2006**, *39*, 7157−7169.

(64) Gorman, C. B. et al. *Macromolecules* **2008**, *41*, 4856−4865.

(65) Behling, R. E. et al. *Macromolecules* **2009**, 42, 1867−1872.

(66) Huang, C. et al. *Langmuir* **2009**, *25*, 13351−13360.

(67) Sunday, D. et al. *Macromolecules* **2010**, 43, 4871−4878.

(68) Turgman-Cohen, S.; Genzer, J. *Macromolecules* **2010**, *43*, 9567−9577.

(69) Turgman-Cohen, S.; Genzer, J. *J. Am. Chem. Soc.* **2011**, *133*, 17567−17569.

(70) Turgman-Cohen, S.; Genzer, J. *Macromolecules* **2012**, *45*, 2128−2137.

(71) Bain, E. D. et al. *Macromol. Theory Simul.* **2013**, *22*, 8−30.

Chapter 5 Conclusion and Outlook

This thesis described the fabrication of functional polymer brushes on surfaces prepared via an organocatalyzed living (reversible-deactivation) radical polymerization, termed reversible complexation mediated polymerization (RCMP) and its application to multi-stimuli responsive, rewritable, and luminescent polymeric materials.

Stimulus-responsive polymer brush on surfaces served as an efficient approach for creating smart surfaces possessing switchable functionalities and morphologies upon external stimulus. These materials find extensive applications in (bio)molecular adsorption/desorption, sensing, and so on. Reversibly crosslinked polymer brushes on surfaces, in this regard, present a useful method to control the mechanical, biological, and physicochemical properties of the surface via crosslinking and decrosslinking upon external stimuli. Yet, only sparse examples of reversibly crosslinked polymer brushes on surfaces have been reported. In Chapter 2, we described a multi-stimuli responsive reversible crosslinked polymer brush on the surface via RCMP and tailored the surface wettability by controlling the crosslinking and decrosslinking processes.

Chapter 2 described the synthesis of multi-stimuli responsive reversibly crosslinked polymer brushes on solid surfaces. While polymer brushes have been extensively studied, crosslinked polymer brushes (polymer brush gels) are less studied because of their challenging synthetic methodologies, even though crosslinked polymer brushes possess superior mechanical strength, solvent resistance, and durability compared to their uncrosslinked counterparts. Chapter 2 presents an efficient approach to prepare crosslinked polymer brushes that exhibit reversible crosslinking and decrosslinking upon external stimuli, which is unique. The significance is the ease of tuning the surface wettability by reversible crosslinking/decrosslinking without the need for elaborate chemical transformation of the

polymer backbones. The crosslinking and decrosslinking of the obtained crosslinked brushes are responsive to multiple stimuli i.e., thermal, photo, and chemical stimuli. The reversibility, proved by thermal stimulus, was repeatable for many cycles. Furthermore, by using photo-stimulus in conjunction with a photo mask, spatial control of the crosslinked/decrosslinked domains was achieved. This enables the subsequent selective functionalization of the surface, generating binary and patterned polymer brushes with dual physicochemical and optical properties, respectively. A unique feature of the obtained patterned polymer brushes is that the patterns are erasable, reverting to the original uniform uncrosslinked polymer brush on a single surface, accentuating the reversibility (and re-writability) of the crosslinked polymer brushes in the present work. Such multi-stimuli responsive reversibly crosslinked polymer brushes on a surface can be tailored to selectively capture (in the crosslinked conformation) or release (in the decrosslinked conformation) specific molecules upon various external stimuli. This capability could be harnessed for applications in the selective capture/release of target molecules in (bio)separation processes and/or sensing interfaces in which the polymer brushes can undergo crosslinking/decrosslinking in response to specific molecules or analytes, and these interactions can be detected by the changes in the surface wettability.

Future work concerns deeper analysis and experimental optimization to increase the extent of crosslinking of polymer brushes on surfaces by incorporating either electron-donating groups on the diene or electron-withdrawing groups on the dienophile to accelerate and improve the efficiency of the Diels–Alder process, and the validation of the proposed system capability for applications in adsorptive/desorptive interfaces, brush-gel/metal-nanoparticle nanoreactors, and molecular recognition and sensing interfaces, for example.

Surface functionalization has demonstrated remarkable efficacy in tailoring the physicochemical, optical, and mechanical properties of the surface. The use of reversible

surface functionalization techniques has been a driving force in the development of rewritable (write–erase–rewrite) surfaces. Various reversible chemical reactions, e.g., thiol-quinone methide click, disulfide exchange, and Diels–Alder reactions have been used to reversibly anchor small molecules and bio-(macro)molecules to the surface. The Diels–Alder reaction was also used to achieve the reversible attachment of synthetic polymers to a surface, generating a rewritable surface. However, the utilization of a thiol-terminated polymer (Polymer-SH) for generating a rewritable polymer brush on a surface through a disulfide exchange remains unexplored in the realm of synthetic polymers. Disulfide exchange offers the advantage to perform the reaction under a milder condition compared to the Diels–Alder reaction, particularly the retro-Diels-Alder reaction, which often requires an elevated temperature to proceed efficiently. In Chapter 3, we described a rewritable polymer brush on a surface using a hetero-disulfide exchange while, at the same time, tuning the surface wettability during the process of writing, erasing, and rewriting.

Chapter 3 described the first use of synthetic polymers to rewritable surfaces via hetero-disulfide exchange. The significance of using synthetic polymers to rewritable surfaces is in the versatility to attach (graft) a wide range of hydrophilic, hydrophobic, and super-hydrophobic synthetic polymers to solid surfaces in a rewritable manner, concomitantly tuning the surface wettability during the process of writing, erasing, and rewriting. Notably, the present study also attached (grafted) synthetic polymers onto soft polymer brushes on a solid surface, giving a rewritable block copolymer brush on the surface. Furthermore, by using photo-irradiation with a photo mask, a patterned rewritable surface was achieved. Scientifically, Chapter 3 presented a new, robust, and remarkably fast (10 min) approach to prepare Polymer-SH at room temperature. Chapter 3 demonstrated the hetero-coupling of Polymer-SH and pyridyl disulfide, establishing a reversible hetero-disulfide exchange pivotal to the creation of a rewritable surface in the present study. Metal-free synthetic procedures, mild conditions for

the chain end post-modification, and the versatility to tune the surface wettability through the writing–erasing–rewriting cycle are appealing aspects of the present method. As mentioned, the present approach uses a mild reaction condition for the hetero-disulfide exchange, rendering them suitable for biomedical applications involving bio-(macro)molecules, drugs, and cells. Such rewritable smart surfaces could serve as a versatile platform for rewritable microarray technologies and sensing interfaces to which the surface can be reversibly and repeatedly modified to adapt to the various analytical purposes without the need for new arrays and/or interfaces. The present method may offer greater flexibility and a cost-effective alternative to data acquisition and analysis.

Future work concerns deeper analysis and experimentation to study the morphological changes of an amphiphilic PPEGA–PBA block copolymer under different solvents, where PPEGA is poly(poly(ethylene glycol)methyl ether acrylate) and PBA is poly(butyl acrylate). Atomic force microscopy study of the PPEGA–PBA block copolymer may reveal different morphological features after treatment with acetone (a good solvent for PPEGA and PBA) and hexane (a non-solvent for PPEGA and a good solvent for PBA) because of the different solubilities of the two polymer segments in different solvents. In the presence of a good solvent, PPEGA–PBA block copolymer would be well-stretched. However, in the presence of hexane, a non-solvent for PPEGA, the hydrophobic PBA segment would remain well-stretched while the hydrophilic PPEGA segment may collapse, displaying reversible morphological transformations by simple solvent exchanges.

Luminescent polymer brushes, which contain luminophores at polymer chain ends or in the monomer units (main polymer chain), find applications in molecular sensing and optoelectronics. Aggregation-induced emission (AIE)-type luminogens (AIEgens) are weakly emissive as isolated molecular species but show strong photoemission when they are

aggregated. In Chapter 4, we took advantage of the AIE phenomenon and incorporated AIEgens into polymer brushes to create a novel patterned AIE polymer brush with different graft densities, designed for the size recognition of external molecules. The obtained fluorescent polymer brush offers a (potentially simple and faster) alternative to size exclusion chromatography.

Chapter 4 described the first experimental demonstration of a molecular size analyzer on a solid surface, stemming from a size exclusion effect influenced by graft density. Chapter 4 presented the polymerization of AIE monomer with pre-pattern of the initiators with different initiator densities on a surface and obtained a patterned fluorescent polymer brush with different graft densities domains. The significance of using a patterned AIE-bearing polymer brush with different graft density domains is that we can selectively capture external molecules of different sizes and detect the capture through the change in AIE intensities, thereby facilitating the size recognition of external molecules. As a proof-of-concept, the present study demonstrated the capture of small external molecules with molecular weights of 300 in the high-density domain via a more intense AIE. On the other hand, large external molecules with molecular weights of 1000 are excluded from the high-density domain giving a less intense AIE, therewith proving the viability of a new oligomeric molecular size analyzer driven by AIE. The present techniques can afford a wide range of tuneable graft densities for a wide range of analyzable molecular sizes. The present approach is straightforward and easy to implement, offering a (potentially simple, faster, and portable) alternative to size exclusion chromatography. AIE-bearing polymer brush may hold the potential to reshape the way in which the sizes of external molecules are recognized, particularly in trace amounts. AIE-bearing polymer brushes are highly regular ultra-thin films at the interface that are able to exhibit remarkable sensitivity to the presence of external molecules, even at low concentrations. This enhanced sensitivity allows for trace amounts of protein and/or bio-(macro)molecules to

be detected and recognized without requiring additional labelling or markers. AIE-bearing polymer brush may present a label-free approach that streamlines the detection process by simplifying the assay which opens up the possibilities for (bio)molecular recognition and sensing interfaces. However, it should be noted that analytes containing benzene rings that may interfere with the AIE fluorescence should be avoided.

Future work concerns enhancing the system to seamlessly integrate fluorescence change (increase) data from poly(ethylene glycol) with different molecular weights to construct a calibration curve that simplifies the identification of the sizes of unknown external molecules. Nevertheless, the fluorescence measurements using PEG (M_n = 300 and 1000) given in the present paper clearly demonstrated the size recognition capabilities of the AIE-based molecular size analyser. We believe that these measurements provided the essential proof of the present concept.